THREE ESSAYS ON RENEWABLE JET FUEL SUPPLY CHAIN NETWORK DESIGN AND TRAFFIC SAFETY

A Dissertation
Submitted to the Graduate Faculty
of the
North Dakota State University
of Agriculture and Applied Science

By

Sajad Ebrahimi

In Partial Fulfillment of the Requirements
for the Degree of
DOCTOR OF PHILOSOPHY

Major Department:
Transportation, Logistics, and Finance

May 2022

Fargo, North Dakota

North Dakota State University

Graduate School

Title

THREE ESSAYS ON RENEWABLE JET FUEL SUPPLY CHAIN NETWORK DESIGN AND TRAFFIC SAFETY

By

Sajad Ebrahimi

The Supervisory Committee certifies that this ***disquisition*** complies with North Dakota State University's regulations and meets the accepted standards for the degree of

DOCTOR OF PHILOSOPHY

SUPERVISORY COMMITTEE:

Dr. Joseph Szmerekovsky

Chair

Dr. Simone Ludwig

Dr. Alan Dybing

Dr. Stephanie Day

Approved:

5/25/2022

Date

Dr. Tim Peterson

Department Chair

ABSTRACT

Because of rising energy consumption, climate change, and environmental concerns about fossil fuels, finding alternative renewable energy sources is becoming increasingly crucial. With the non-advanced share of the U.S. Renewable Fuel Standard having been mainly met by corn ethanol, many states are considering cellulosic or non-edible oilseed crops as the next source of biofuels. This study seeks to design a supply chain to produce renewable jet fuel (RJF) within the Midwest region and southeastern U.S. This is accomplished through the use of optimization models (mixed-integer linear programming). Furthermore, because RJF manufacturing incurs higher expenses than conventional jet fuel, the use of various monetary incentives is being studied to establish their usefulness in commercializing the supply chain. The findings of this study can be used by energy policymakers, RJF producers, and investors to operate in a competitive market while safeguarding the environment.

In another study, we evaluate speeding crash risk in North Dakota counties. In the United States, one of the most common contributing factors to car crashes is speeding. Speeding impairs a driver's ability to control and steer properly, as well as respond to a dangerous situation in a timely manner. Speeding crashes account for one-third of fatal crashes in the United States and are one of the risks for drivers on U.S. highways. Speeding crash risk can vary among regions. When it comes to allocating road safety expenditures to regions in order to reduce speeding crashes, it's vital for road management to understand which areas are at higher risk and should be prioritized for safety measures. This study uses a failure mode effect analysis method to evaluate the speeding crash risk.

ACKNOWLEDGEMENTS

I would like to express my deepest gratitude to my advisor and chair of my committee, Dr. Joseph Szmerekovsky, for his professional guidance and invaluable support through every stage of this research. It was a great pleasure to conduct research under your supervision. My sincere thanks are also extended to my brilliant committee members, Dr. Alan Dybing, Dr. Stephanie Day, and Dr. Simone Ludwig for their time and insightful comments and suggestions.

This study would not have been possible without the assistance of several other essential contributors to my research. I would like to express my appreciation to Dr. Kimberly Vachal for providing significant support throughout the research project. Additionally, I am thankful to my dear friends Dr. Ali Haji Esmaeili and Dr. Ahmad Sobhani for their valuable suggestions on this research project. I would also like to thank Dr. Tim Peterson for being a great mentor to me, believing in me, and providing me with opportunities to expand my skills.

Several agencies contributed data and funding to part of this study. I wish to thank the Upper Great Plains Transportation Institute (UGPTI) and the Mountain-Plains Consortium (MPC) for their funding support through the project number FAR0031432. I also wish to acknowledge the North Dakota Department of Transportation (NDDOT) for providing the required data.

Lastly, I'd like to thank my parents, as well as my brothers and my wife for continuously believing in me and supporting me. Undoubtedly, your support kept me motivated throughout this journey.

DEDICATION

To my *Mom* and *Dad,* for their unconditional love and support.

To my *Brothers,* for inspiring me with their success.

To my *Wife*, for being such a wonderful companion on this journey.

TABLE OF CONTENTS

LIST OF TABLES

LIST OF FIGURES

LIST OF APPENDIX TABLES

1. INTRODUCTION

1.1. Background and motivation

1.1.1. Renewable jet fuel supply chain network design

The aviation industry is responsible for 2% of global carbon emissions (Claudia Gutiérrez-Antonio et al., 2013). However, the industry will continue to grow, and emissions are expected to increase respectively. Although electric and hydro-powered vehicles are replacing vehicles powered by fluid fuels such as fossil-based and biomass-based fluid fuels, there are not similar options for the aviation industry. The International Air Transport Aviation (IATA) has committed to reducing its net carbon footprint to below 50% of the volume by 2050 (referenced to 2005) (de Jong et al., 2017). To reach this goal, renewable jet fuel (RJF) has been proposed as a practical replacement that will effectively reduce the consumption rate of fossil-based jet fuels and environmental effects by jet fuel consumption (Wei et al., 2019). Finding greener energy sources is crucial for addressing energy security, food security, and environmental concerns. The problem has sparked a significant amount of research into developing biofuel supply chains based on biomass feedstock (Haji Esmaeili, Sobhani, Szmerekovsky, Dybing, & Pourhashem, 2020; E. Huang et al., 2019; Leila et al., 2018).

Fuel and energy products that can be produced directly/indirectly from biomass are called feedstocks. Biomass feedstock is an important component in biofuel supply chains, and its utilization as a source of supply should help reduce GHG emissions (Hendricks et al., 2016). Appropriate biomass to a biofuel supply chain needs to meet several requirements such as a high conversion rate to biofuels, causing no conflicts with food crops and livestock feeding, and causing no change in land use at croplands. This study investigates the application of two types of biomass

feedstock to produce RJF where winter carinata is used in the study provided in chapter 2 and corn stover supplies the RJF supply chain studied in chapter 3.

Geographically, biomass supply sites are not necessarily near airports. Because of the low energy density and dispersed nature of biomass, a biomass supply chain system needs a vast sourcing region to be able to cover any given demand for economic benefits. Hence, designing an optimized supply chain network for RJF has emerged as an issue. Additionally, implementing an RJF supply chain may not be economically competitive with fossil-based jet fuel. Government interventions and setting financial incentives can improve efficiency and sustainability of biofuel supply chains (Zheng et al., 2020). Government intervention through incentives for renewable energy is potentially advantageous in that they can encourage the expansion of renewable energy to benefit society, economy, and environment (Mohamed Abdul Ghani et al., 2018). Therefore, it has become increasingly important to learn about the different aspects of considering monetary incentives when producing RJF.

Recently, federal agencies such as the Department of Energy (DOE), US Department of Agriculture (USDA), and Department of Transportation (DOT) agreed to work together to develop strategies to scale up RJF production (DOE, 2022). RJF production can improve the economy of farmers, reduce greenhouse gas emissions (GHG), save energy sources for future generations, improve diversity of energy resources, and make industries more resilient to oil price changes and supply risks.

A biofuel supply chain requires a vast network of suppliers, manufacturers, transportation providers, and consumers, where sustainability should be considered in the network for not only maximizing profits but also for minimizing adverse environmental impacts from the network (Park, 2018). Several countries presented various carbon emission mitigation policies (Haji

Esmaeili, Sobhani, et al., 2020). These policies not only could assist in emission reduction but also might convey economic benefits to companies (Mohammed et al., 2017). Therefore, it would be important for policymakers and producers to find policies that can efficiently and effectively incentivize the RJF production.

1.1.2. Risk assessment of speeding crashes

Traffic crashes and their related consequences such as fatalities, injuries, and financial loss remain critical whereas safety road managers work relentlessly to realize approaches to reduce them. Speed is one of the most important contributing factors to a significant number of crashes as it can affect crash risk and severity (Castillo-Manzano et al., 2019). Speed not only increases the severity of a crash, it can also affect the risk of having other vehicles involved in a crash (Aarts & van Schagen, 2006). Almost a third of fatal crashes in the United States are related to speeding and can be considered speeding crashes (Fitzpatrick et al., 2017). Highway agencies have limited resources when it comes to executing road safety initiatives. As a result, they require a realistic evaluation approach for identifying crash-prone regions. Therefore, before taking safety actions to reduce speeding crash risks, it is important to determine which regions should be prioritized for receiving safety measures based on their speeding crash risk level.

1.2. Research objectives

Due to a considerable amount of investments for construction, high operational costs and related risks with new applied technologies, many advanced biorefineries have failed to maintain commercialization (Martinkus et al., 2019). Therefore, optimal designing of an RJF supply chain network that aims to improve economic, environmental, and social performance of a biofuel supply chain is of high importance (Ghaderi et al., 2016). However, implementing an RJF supply chain may not be economically competitive with fossil-based jet fuel. Government interventions and

setting financial incentives can improve efficiency and sustainability of biofuel supply chains (Zheng et al., 2020). However, due to the complexities in calculating possible impacts of the interventions, governments usually lack the guidance to formulate and acquire optimal strategies and policies to biofuel supply chains (Zhou et al., 2020; Tangtinthai, Heidrich, & Manning, 2019). Thus, in the first two topics in this essay, we design RJF supply chain and investigate the application of monetary incentives to answer the following questions:

- How much biomass feedstock is available to supply the RJF supply chain in the studied regions?
- Which supply and demand zones should be assigned to biorefineries to maximize profit and reduce carbon emissions?
- How many and what capacity of biorefineries would be needed to meet jet fuel demand?
- How do applications of different monetary incentives affect profitability of a RJF supply chain?

In chapter 4, using three risk factors including occurrence, severity, and detectability we assess speeding crash risk in North Dakota counties. The following essential questions will be explored to address the stated objectives of this study:

- Which ND counties have the highest occurrence risk of speeding crashes?
- Which counties have the highest risk of severe speeding crashes?
- How do ND counties compare on their detection risk of speeding crashes?
- How do the speeding crash risks compare among the ND counties?
- Which counties are prioritized for receiving funding to reduce speeding in their roadways?

1.3. Research methodologies and contributions

The following three studies will provide original contributions to address the questions.

Chapter 2 uses a mixed integer linear programming to design supply chain networks. Also, the impact of three incentive policies including producer credit program (PCP), biomass credit assistance program (BCAP), and biorefinery assistance program (BAP) are accounted for accelerating RJF production. This study considers southeastern US including Alabama, Florida, and Georgia as the study region while carinata is considered as the biomass feedstock for the supply chain. Our research aims to make strategic and operational decisions in an RJF supply chain such as selecting biomass sources, determining biorefinery locations and capacities, logistics of biomass and RJF between components of the supply chain. Further, impacts of considering monetary incentives are investigated. Findings from this study will inform policymakers and investors on the feasibility and effectiveness of each policy in accelerating the commercialization of RJF production.

Chapter 3 is devoted to the construction of a corn stover-based RJF supply chain network in the Midwest region, while four monetary/environmental incentives, including PCP, BCAP, BAP, and cap-and-trade carbon policy, are considered for subsidizing RJF production and accelerating its commercialization. This study is validated by applying the model on designing an RJF supply chain in the Midwest region. In the light of the results of this study, policy makers can develop policies that can accelerate commercialization of RJF production.

Finally, in Chapter 4, we use an integrated framework including failure mode and effect analysis (FMEA) and Delphi method to assess speeding crash risks in ND counties. According to the crash data from ND counties and experts' opinions, three risk factors are evaluated for each county, including the occurrence, severity, and detectability of speeding crashes. The approach

identifies counties with a higher risk of speeding crashes, so that they can be prioritized for safety measures to reduce speeding crash risks.

2. RENEWABLE JET FUEL SUPPLY CHAIN NETWORK DESIGN: APPLICATION OF DIRECT MONETARY INCENTIVES[1]

2.1. Abstract

Currently, the global aviation industry uses around 341 billion liters of jet fuel per year, with demand predicted to grow by 50% by the end of 2050. Renewable jet fuel (RJF) may cut greenhouse gas emissions (GHG), increase fuel diversity for the aviation industry, and promote rural economies. The commercialization of RJF has been delayed due to a shortage of sustainable biomass resources. This study recommends using winter carinata crops as a reliable biomass feedstock in the southeastern US states, where the availability of resources will be investigated in each agricultural zone. RJF production is more expensive than traditional jet fuel production. Investors and legislators need to learn more about prospective federal financial initiatives, such as subsidies and grants, to help with RJF supply chain implementation. In this paper, using a mathematical programming approach, we designed an RJF supply chain and then investigated the effects of three direct monetary incentive programs, including producer credit program (PCP), biomass crop assistance program (BCAP), and biorefinery assistance program (BAP), to accelerate the commercialization of RJF manufacturing. According to the findings, the amount of incentives through PCP needed to fulfill 50% of the RJF demand was assessed to cover 16.70% of the total costs, while the BCAP could reach the commercialization threshold by receiving incentives for 22.84% of the biomass purchasing cost. Furthermore, having the BAP covering 89.39% of the annual capital and operating costs could help commercialize RJF production. This study also

[1] The material in this chapter was co-authored by Sajad Ebrahimi, Seyed Ali Haji Esmaeili, Ahmad Sobhani, and Joseph Szmerekovsky. Sajad Ebrahimi had primary responsibility for collecting data and conducting the analysis. Sajad Ebrahimi was the primary developer of the concept, models, and conclusions that are advanced here. Sajad Ebrahimi also drafted and revised all versions of this chapter. This chapter appears in Applied Energy (Ebrahimi et al., 2022).

evaluated the effects of changes in renewable fuel prices, demand fulfillment rates, biomass yield rates, and the price of biomass feedstock and its resulting meal on the profitability of the supply chain. The study's findings will advise policymakers and investors on developing the RJF supply chain given various financial assistance programs and subsidies.

2.2. Introduction

According to the International Air Transport Association (IATA), by the end of 2036, the number of people utilizing air transport will have increased to 7.8 billion, which is more than double the number of users in 2017 (Alam & Dwivedi, 2019). Despite the relatively small contribution to emissions caused by the aviation sector, demand for jet fuel is predicted to rise by 50% by the end of 2050 (Alam & Dwivedi, 2019). Although commercial aviation currently emits approximately 859 million metric tons of carbon dioxide, accounting for approximately 2% of total man-made carbon dioxide emissions, this percentage is anticipated to rise to 20.2% by 2050 (Alam & Dwivedi, 2019). Although fuel alternatives for conventional gasoline-powered vehicles, such as low-carbon electricity or hydrogen, have been introduced, electrification of the aviation sector is still on a century time scale, and the industry will continue to rely on liquid fuels. With the rapid expansion of the fossil-fuel intensive aircraft transportation mode, renewable jet fuel (RJF) is gaining attention as a possible alternative to cut carbon emission (Wise et al., 2017). RJF can be produced from renewable biomass such as corn grain, oil seeds, algae, animal fats, agricultural residues, Forestry residues, and waste resources (FAA, 2021). RJF can perform as effectively as fossil-based jet fuel does, with a low carbon footprint compared to conventional jet fuel (DOE, 2021). The potential benefits of adopting RJF include increased energy security, diversification of energy sources, economic gains in rural regions with more job possibilities, and reduced greenhouse gas emissions (Bacenetti et al., 2017). The availability and sustainability of the

biomass feedstock are critical to replace fossil-based fuels with suitable renewable fuels that can be derived from biomass feedstock (Agusdinata et al., 2011). Appropriate biomass for a biofuel supply chain must meet a set of criteria, including a high conversion rate to biofuels, no conflicts with food crops or livestock feeding, and no change in land use at croplands (Alam & Dwivedi, 2019; Haji Esmaeili, Szmerekovsky, et al., 2020; Zemanek et al., 2020). Oilseeds have been identified as a potential source for producing RJF due to their chemical and economic performance as biomass.

However, producing RJF from oilseeds on a commercial scale would be difficult due to land limitations such as appropriateness and competition with primary crops. Even though winter crops have been proposed as a viable solution to the problem of supplying biomass feedstock and animal feed, investigating their sufficiency and practicality as feedstock have received little attention (Poiša et al., 2010; Blanco-Canqui et al., 2020). Winter cover crops can be planted after the summer planting season and prefer cooler temperatures to grow. In a pilot project, Seepaul et al. (2019) investigated cultivating carinata (Brassica carinata) during mild winters in the southeastern U.S. states of Alabama, Florida, and Georgia. Carinata, with its high oil content, low breaking rates, large seed size, and great heat and drought tolerance, is a suitable cover crop for areas with mild winters (R Seepaul et al., 2019; Kumar et al., 2020; Ramdeo Seepaul et al., 2021; Nóia Júnior et al., 2022; Alam & Dwivedi, 2019). Planting carinata as a cover crop has several advantages, including higher revenue for local farmers, reduced leaching and soil erosion, weed suppression, enhanced soil fertility, and providing a food supply for cattle (R Seepaul et al., 2019; Kumar et al., 2020; Ramdeo Seepaul et al., 2021). Additionally, carinata oil is unique in that it contains a high concentration of erucic and linoleic acids while containing less than 7% saturated

fatty acids, making it an attractive resource for use as biomass in RJF production (R Seepaul et al., 2019).

RJF can be produced using a variety of conversion processes depending on the biomass feedstock, including hydrothermal liquefaction (HTL) (Kargbo et al., 2021), Fischer Tropsch (FT) (Ail & Dasappa, 2016), alcohol to jet (ATJ) (W. C. Wang et al., 2016; Geleynse et al., 2018), and hydroprocessed esters and fatty acids (HEFA) (Mousavi-Avval & Shah, 2021). However, to replace fossil-based fuels with suitable renewable fuels that can be produced from biomass feedstock, production must be technically and economically feasible. HEFA is used to transform fats and oils (such as animal fats, used cooking oils, and seed oils) into RJF, renewable diesel fuel (RDF), liquefied petroleum gas (LPG), and naphtha. HEFA has received considerable research and investment and has been performing consistently on a commercial scale (Witcover & Williams, 2020; Gutiérrez-Antonio et al., 2017). In 2011, RJF derived through HEFA was certified by the American Society for Testing and Materials (ASTM). The blending rate with conventional jet fuel was allowed to be as much as 50% (Tao et al., 2017). Pearlson (2007) provides more extensive information regarding the production process under HEFA for interested readers. Several researchers employed techno-economic analysis (TEA) to explore the feasibility of using various conversion technologies to convert oilseed biomasses into RJF (Li et al., 2018; Tao et al., 2017). Chu et al. (2017) employed carinata as one of the prospective oilseed biomasses in a TEA study to analyze the financial viability of RJF production, with HEFA as the conversion pathway. Although the research investigated the economic feasibility of RJF production, it failed to take into account the intricacies of the RJF supply chain, such as the location of supply and demand nodes, the number of biorefineries needed, their location and capacities, the material flow between various components of the supply chain, and distances between the components. Determining these

configurations may be critical in understanding the realistic profits of RJF manufacturing (E. Huang et al., 2019), as many advanced biorefineries have failed to maintain commercialization due to significant construction investments and high operational costs that could be the result of an inefficient supply chain (Martinkus et al., 2019). Therefore, optimal design of a renewable fuel supply chain with the goal of improving economic performance of the network is critical (Ghaderi et al., 2016).

To design economically efficient biofuel supply chain networks, several researchers employed mathematical programming approach such as mixed integer linear programming (MILP) that could recommend optimal configurations for biofuel supply chains (Walther et al., 2012; Giarola et al., 2012; Schmidt et al., 2011). Furthermore, several studies, applying optimization models, designed RJF supply chain networks. Huang et al. (2019) used a multi-objective optimization model to explore the use of three pathways to convert corn stover to RJF. They developed a supply chain network with four tiers, including counties as supply nodes, centralized storage and preprocessing sites, biorefineries, and airports in major cities as demand nodes.

To become commercially feasible, the RJF price must be competitive with the price of fossil-based jet fuel. However, developing an RJF supply chain may not result in RJF being economically competitive with fossil-based jet fuel. Government actions and financial incentives can improve the efficiency and sustainability of biofuel supply networks (Zheng et al., 2020). In a comprehensive study on the literature of applying incentive mechanisms in biofuel supply chains, Noh, Benito, & Alonso (2016) presented several supportive programs in the U.S. provided by organizations such as the Environmental Protection Agency (EPA), Internal Revenue Service (IRS), Department of Agriculture (DOA), Department of Energy (DOE), US Customs and Border

Protection, and Department of Transportation (DOT). The monetary incentives are provided to different components in the production network and are offered through direct grants and subsidies or indirectly via loans or mortgages. Due to the difficulties in determining the potential impacts of intervention, governments frequently lack direction in developing and implementing effective strategies and regulations for renewable fuel supply chains (Zhou et al., 2020; Tangtinthai et al., 2019).

Few studies in biofuel supply chains have examined the effects of financial incentives on supply chain optimization. Leila et al. (2018) investigated the application of direct monetary incentives allocated to activated biorefineries. Haji Esmaeili et al. (2020) used MILPs to determine the financial incentives required to induce first-generation bioethanol producers to transition to second-generation biomass. Delving into the related literature, we could not find any study comparing the application of different direct monetary incentives to an RJF supply chain.

Inspired by previous research and to bridge the research gaps, our study uses MILPs to create an RJF supply chain network and explores the influence of three unique monetary incentives on supply chain profitability. To our knowledge, this is the first research to build an RJF supply chain network utilizing carinata as its biomass feedstock, and more specifically, as a winter crop. This study suggests direct federal initiatives, such as BCAP, BAP, and PCP, which can provide direct monetary incentives to encourage commercial-scale production of biofuels. BCAP, managed by the DOA, provides financial support for biomass crop adoption expenses, annual payments for biomass production, and payments to assist with biomass collection, harvest, storage, and transportation activities. In this study, we will investigate how the BCAP may improve supply chain profitability by lowering the costs associated with biomass provision, excluding the transportation costs. BAP is a program run by the Department of Agriculture (DOA) that offers

payments to assist in building and maintaining biorefineries to encourage the production of advanced biofuels. By considering the application of this program, we investigate how the program's cost coverage regarding manufacturing costs may affect the supply chain profits. PCP, a direct incentive program proposed by several studies (Mohamed Abdul Ghani et al., 2018; Haji Esmaeili, Szmerekovsky, et al., 2020; Haji Esmaeili, Sobhani, et al., 2020) provides monetary credits for each gallon of RJF produced. PCP covers all costs associated with RJF production, including supply purchasing, transportation, and capital and operational costs. Readers interested in learning more about potential federal monetary incentives for biofuel production might refer to Noh et al. (2016). The results from analyzing the policies' applications in the supply chain network will inform investors and decision-makers on the feasibility and effectiveness of each policy in accelerating the commercialization of RJF production.

This paper presents an integrated mathematical model that optimizes RJF supply chain in the US southeastern states. The research calculates the potential amount of carinata that can be planted in the region as a winter crop and the amount of RJF and byproducts that can be produced from the biomass. In addition, we compare the effects of three direct monetary incentives on profitability of the RJF supply chain and offer analysis on supply chain profit given varied coverage rates granted by the incentive programs. Finally, we provide a comprehensive analysis on the effect of changes in supply chain parameters such as biomass availability and cost, biomass yield rate, fuel price, and demand fulfillment rate.

2.3. Material and methods

2.3.1. Problem statement

In this study, using a MILP, we design an optimal RJF supply chain network including three echelons: croplands as supply nodes, biorefineries as manufacturing nodes, and airports as

demand nodes. The biomass feedstock flows from supplier nodes to biorefineries, where it is preprocessed (seed crushing) and processed (HEFA), and the outputs, including RJF, protein meal, LPG, RDF, and naphtha are transported to their demand nodes. While we explored a supply chain network setting in which preprocessing and biorefineries are co-located, it should be noted that preprocessing might be separated from biorefineries in other supply chain settings. Because road haulage (through trucks and tankers) is readily available, this study will focus only on road haulage for the delivery of biomass, protein meal, and the biofuels. Figure 2.1 displays the RJF supply chain network and its corresponding components and activities.

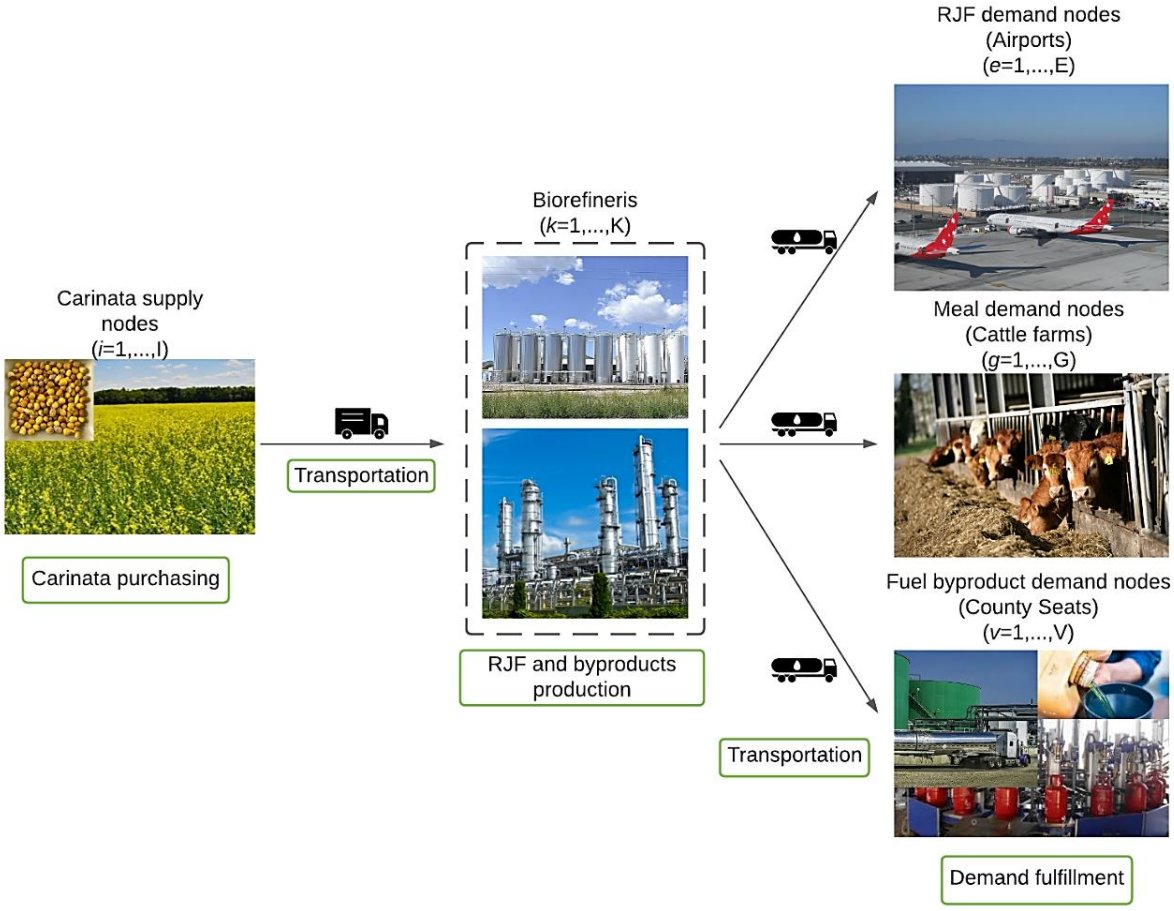

Figure 2.1. RJF supply chain network and the activities at each echelon

To validate our findings, we investigated decision-making aspects in a carinata-based RJF supply chain, such as the number, location, and capacity of required facilities and their establishment and operating costs, logistics related to supplies and final products, and mainly RJF required to meet demand in the southeastern United States. The supply nodes were spread across three states: Alabama (67 counties), Florida (67 counties), and Georgia (159 counties). To make the calculations scale consistent with the strategic level decision making of this study's topic, we grouped the counties into 19 Agricultural Statistical Districts (ASDs) (Gonela et al., 2015; Haji Esmaeili, Szmerekovsky, et al., 2020; Haji Esmaeili, Sobhani, et al., 2020). Assuming that each ASD is a supply zone for carinata (farms) and demand zone for carinata meal (cattle farms), the centroid of each ASD was chosen as the point from which carinata would be carried to biorefineries and carinata meal would be transported from biorefineries to cattle farms. Areas to obtain carinata as biomass in the RJF supply chain were chosen based on available lands in the southeastern United States, including Alabama, Florida, and Georgia, which were suitable for planting carinata after the regular planting season. Lands to plant cotton, corn, soybean, sorghum, and peanut were among the prospective croplands (Kumar et al., 2020). The available amount of carinata at each ASD was calculated using a yield rate of 2,802.70 kg/ha for carinata (Alam & Dwivedi, 2019). The aforementioned farmland area at each ASD was obtained from the National Agricultural Statistics Service (NASS) database (NASS, 2021). Table A2 in Appendix A shows the availability of carinata by each ASD in the three states.

For the biorefineries, three facility sizes were considered: small (350-700 M liter/year), medium (700-1,100 M liter/year), and large (1,100-1,500 M liter/year). Potential locations of biorefineries were considered at the center of each ASD. In the case of biorefineries located in an ASD, the transportation distance between the supply node from the same ASD and the biorefinery

was considered to be within 2/3 of the radius of that ASD, which was computed by the area of the ASD (E. Huang et al., 2019).

We considered 25, 35, and 45 required employees for small, medium, and large biorefineries, respectively. Furthermore, each employee's annual compensation was assumed $88,000 (M. Pearlson et al., 2013). We used Eq. (2.1) to compute the total capital cost (Q_r) of a biorefinery with capacity Z_r, where α was a scaling factor set to 0.6 (Haydary, 2019), Z_0 was a reference capacity, and Q_0 was the total cost of a biorefinery with capacity of Z_0 (Osmani & Zhang, 2013). The total capital cost for a biorefinery with the HEFA pathway and capacity of 398 million liters of liquid fuel annually (reference capacity), including RJF from carinata, was estimated to be $411.28 million (Chu et al., 2017).

$$Q_r = Q_0(Z_r/Z_0)^{\alpha} \quad \forall r \in R \tag{2.1}$$

The annualized fixed capital cost of building a biorefinery varies with capacity. Because we wanted to determine the annual profit of the supply chain, we looked at the capital cost of biorefineries on an annual basis and computed it for each capacity. Eq. (2.2) is used to annualize the initial investment of a biorefinery with an expected life of *n* years and an interest rate of q %. The expected life of the biorefineries was set at 20 years, with a 11.5% interest rate (Osmani & Zhang, 2014; Zetterholm et al., 2018). The biorefinery's annualized capital cost was $74.86 million, $98.19 million, and $118,27 million for small, medium, and large biorefineries, respectively.

$$Annualized\ cost = [q * (initial\ investment)]/[1 - (1 + q)^{-n}] \tag{2.2}$$

Airports in the region with jet fuel demand greater than 10,000 million gallons per year (MGPY) were identified as demand nodes. Airports with high demand shares were selected on the basis that airports with greater demand were assumed to be a more reliable market for RJF than

airports with low demand. However, since RJF produced by HEFA allows for up to 50% blending, only 50% of the annual demand for conventional jet fuel in the selected airports was expected to be met by RJF; hence Table 2.1 shows RJF demands at each airport.

Table 2.1. Demand for RJF at the selected airports (BTS, 2021)

Airports	Demand for RJF (MGPY)
Orlando International	139.61
Miami International	132.80
Tampa International	76.89
Southwest Florida International	33.11
Jacksonville International	31.72
Palm Beach International	26.10
Orlando Sanford International Airport	9.44
St. Pete–Clearwater International Airport	6.72
Pensacola International	11.86
Sarasota–Bradenton International Airport	6.32
Panama City, FL: Northwest Florida Beaches International	5.27
Tallahassee International	6.96
Hartsfield–Jackson Atlanta International	422.31
Savannah/Hilton Head International	16.01
Augusta Regional at Bush Field	5.05
Birmingham–Shuttles worth International	19.46
Huntsville International-Carl T Jones Field	10.02
Mobile Regional	6.60

The demand for carinata meal was considered proportional to the cattle inventory in the ASDs and were determined based on the carinata meal produced in biorefineries. The Cattle population in each ASD and their corresponding shares are provided in Table A3. It is assumed that the demand nodes for carinata meal are located on ASD's centroids and all demand for the meal will be fulfilled by the biorefineries.

The liquid byproducts including LPG, naphtha, and RDF are considered to be transported to their demand nodes in the three states. The demand nodes were chosen on the basis of having populations more than one million, which could assure a reliable demand rate for the products. It

turned out that five counties in Florida (Miami-Dade County, Broward County, Palm Beach County, Hillsborough County, Orange County) and one county in Georgia (Fulton County) could meet the condition. County Seats (administrative centers) in each county were considered as destinations. It is assumed that all the fuel byproducts produced by biorefineries would be consumed by their demand nodes. However, the amount of fuel byproducts to be supplied to each of the six demand nodes are proportional to their population resulting 10.67%, 19.21%, 26.59%, 13.85%, 14.90%, and 14.78% of the produced fuel byproducts to be allocated to Atlanta, Fort Lauderdale, Miami, Orlando, West Palm Beach, and Tampa, respectively. Figure 2.2 depicts the spatial distribution of supply chain components, including ASDs that can include the location of possible suppliers and manufacturers, as well as the location of the demand nodes to be serviced.

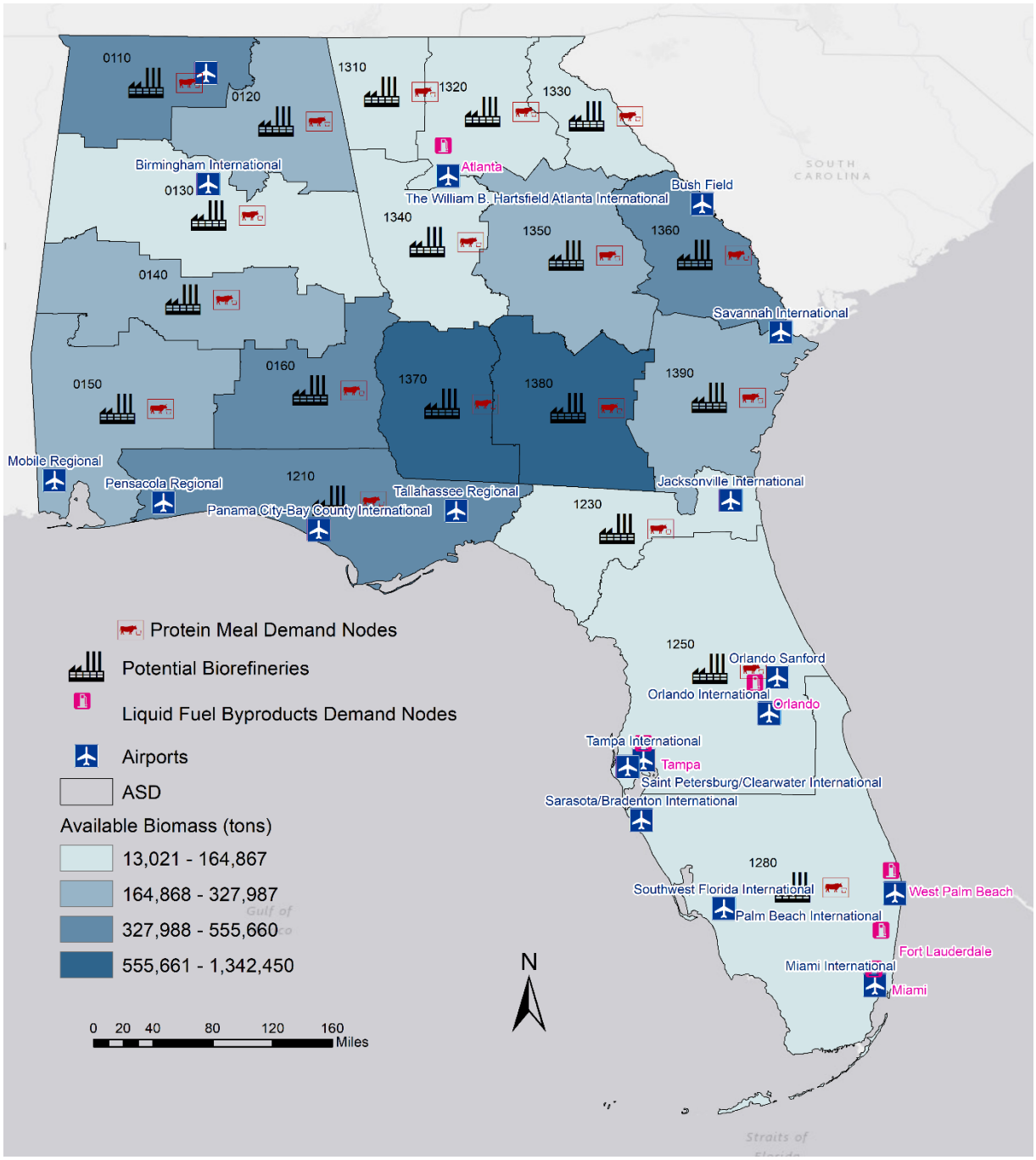

Figure 2.2. Spatial distribution of RJF supply chain components in the southeastern United States

2.3.2. Mathematical model

Optimization models were developed to optimally design a carinata-based RJF supply chain network and manage the logistics of RJF facilities. In this study, we developed four MILPs. The first MILP includes no monetary incentives, and the remaining three models consider three

distinct monetary incentives, PCP, BCAP, and BAP, to evaluate the impacts of employing monetary incentives on the supply chain's profitability. The developed models maximize the RJF supply chain profit. In addition, the MILPs calculate the number, location, and capacity of biorefineries required to meet the demand.

The supply chain's revenue included earnings from selling RJF and coproducts (protein meal, LPG, RDF, and naphtha). In contrast, costs included expenses associated with acquiring biomass feedstock from farms, transportation, establishing biorefineries, and fixed and variable operational costs. Constraints (2.4) – (2.18) outline the constraints of the model. Table 2.2 shows the notation used in the models. The MILPs are solved via Python 3.7 using the Gurobi 9.1.2 optimization engine.

Table 2.2. Sets, decision variables, and parameters

Notation	Description	Notation	Description
Sets		*Parameters*	
$\boldsymbol{I}$	Set of suppliers, indexed by *i*	γ^c	Transportation fixed cost of carinata/meal ($/ton)
$\boldsymbol{K}$	Set of biorefineries, indexed by *k*	η^c	Transportation variable cost of carinata/meal ($/ton-mile)
$\boldsymbol{E}$	Set of demand zones for RJF, indexed by *e*	γ^j	Transportation fixed cost of liquid fuel ($/gallon)
$\boldsymbol{S}$	Set of biorefinery sizes, indexed by *s*; small, medium, and large	η^j	Transportation variable cost of liquid fuel ($/gallon-mile)
$\boldsymbol{R}$	Set of fuel byproducts, indexed by *r*; LPG, naphtha, and RDF	ρ	Operational production cost of RJF from carinata at biorefinery ($/ton)
$\boldsymbol{G}$	Set of demand zones for carinata meal, indexed by *g*	∂^r	Fuel coproduct *r* conversion rate from carinata (gallon/ton)
V	Set of demand zones for fuel byproducts, indexed by *v*	ϑ	Contingency rate
Variables		θ	RJF conversion rate from carinata (gallon/ton)
$\boldsymbol{Y_k^s}$	1 if a biorefinery with size *s* is opened at location k; 0 otherwise	σ	Carinata meal conversion rate from carinata (ton/ton)
$\boldsymbol{Q_{ik}}$	Quantity of carinata transported from supply area *i* to biorefinery *k* (tons)	p^s	Capacity of biorefinery size *s* to produce RJF (MGPY)[2]
$\boldsymbol{Q_{kv}^m}$	Quantity of carinata meal transported from biorefinery *k* to cattle farm *v* (tons)	D_e	Demand for RJF at demand zone *e* (gallons)
$\boldsymbol{Q_{kg}^r}$	Quantity of biofuel coproduct *r* (naphtha, LPG, or RDF) transported from biorefinery *k* to county Seat *g* (gallons)	D_v^r	Demand for liquid fuel byproduct *r* (RDF, LPG, naphtha) at demand zone *v* (gallons)
$\boldsymbol{N_k}$	Number of employees required for biorefinery *k*	d_{ik}	Distance from supplier *i* to biorefinery *k* (mile)
Z	Profit ($)	d_{ke}	Distance from biorefinery *k* to demand zone *e* (miles)
Parameters		d_{kg}	Distance from biorefinery *k* to demand zone *g* (miles)
$\boldsymbol{a_i}$	The amount of carinata available at supply node *i*	d_{kv}	Distance from biorefinery *k* to demand zone *v* (miles)
$\boldsymbol{\pi}$	RJF selling price ($/gallon)	λ	RJF production credit under PCP ($/gallon)
$\boldsymbol{\varphi}$	Carinata meal selling price ($/ton)	β	Rate of carinata selling price reduction under BCAP (%)
$\boldsymbol{\psi^r}$	Fuel coproduct *r* selling price ($/ton)	ϕ	Rate of biorefinery capital and operational cost reduction under BAP (%)
$\boldsymbol{\alpha}$	Purchasing price of carinata ($/ton)	ξ	Aggregate rate of utility cost (overhead, maintenance, insurance, and taxes) ($)

[2] Million gallons per year.

Other data related to the parameters used in the RJF supply chain model is provided in Table A1 in Appendix A.

2.3.2.1. RJF supply chain with no monetary incentives

In this section, Eq. (2.3) presents the objective function used in the model for maximizing profits. The first three statements in Eq. (2.3) represent revenue to be earned from selling RJF, fuel coproducts including LPG, naphtha, and RDF, and protein meal produced from carinata. The remainder of the statement represents costs incurred as a result of purchasing biomass from suppliers, constructing biorefineries, annual payments to required staff, operational fixed and variable costs associated with producing RJF from carinata, transportation cost to transport feedstock from supplier nodes to biorefineries, transportation cost to deliver RJF, protein meal, and fuel byproducts from biorefineries to demand nodes.

Constraints (2.4) - (2.18) describe the model's limitations and constraints. Constraint (2.4) represents the supply constraint for carinata and ensures that the amount of carinata purchased does not exceed the maximum carinata available at supplier nodes. Constraint (2.5) depicts material flow in the supply chain and assures that the amount of RJF created from biomass in a biorefinery is equal to the amount of RJF leaving the biorefinery and reaching demand nodes. Eq. (2.6) guarantees that the amount of protein meal produced in a biorefinery is equal to the amount of the meal that leaves the biorefinery. Also, Eq. (2.7) assures the amount of each fuel byproducts such as LPG, naphtha, and RDF produced at a biorefinery is equal to the amount of the biofuel that leaves the biorefinery. Eq. (2.8) assures that the quantity of RJF and biofuel coproducts produced at each biorefinery (if activated) does not exceed the biorefinery capacity. Eq. (2.9) assigns the required number of employees to a biorefinery. Only one biorefinery can be activated in each ASD, as stipulated by constraint (2.10). Constraints (2.11), (2.12), and (2.13) ensure that

the RJF, fuel byproducts, and protein meal delivered from biorefineries to their demand nodes are sufficient to meet the demand. Eqs. (2.14) to (2.18) show the nature of the variables included in the model and their non-negativity.

$$Max\ Z = \pi \sum_{k\in K}\sum_{e\in E} Q_{ke} + \sum_{r\in R}\sum_{k\in K}\sum_{v\in V} \psi^r Q_{kv}^r + \varphi \sum_{k\in K}\sum_{g\in G} Q_{kg}^m - \alpha \sum_{i\in I}\sum_{k\in K} Q_{ik}$$
$$- \sum_{k\in K}\sum_{s\in S} f^s\, Y_k^s - \sum_{k\in K}\sum_{s\in S} N_k w Y_k^s - \xi(1+\vartheta) \sum_{k\in K}\sum_{s\in S} f^s\, Y_k^s$$
$$- \rho \sum_{i\in I}\sum_{k\in K} Q_{ik} - \sum_{i\in I}\sum_{k\in K} (\gamma^c + \eta^c\, d_{ik}) Q_{ik}$$
$$- \sum_{k\in K}\sum_{e\in E} \left(\gamma^j + \eta^j\, d_{ke}\right) Q_{ke} - \sum_{k\in K}\sum_{g\in G} \left(\gamma^c + \eta^c\, d_{kg}\right) Q_{kg}^m$$
$$- \sum_{r\in R}\sum_{k\in K}\sum_{v\in V} \left(\gamma^j + \eta^j\, d_{kv}\right) Q_{kv}^r \qquad (2.3)$$

Subject to:

$$\textstyle\sum_{k\in K} Q_{ik} \le a_i \quad \forall i \in I \qquad (2.4)$$

$$\theta\ \textstyle\sum_{i\in I} Q_{ik} = \sum_{e\in E} Q_{ke} \quad \forall k \in K \qquad (2.5)$$

$$\sigma \textstyle\sum_{i\in I} Q_{ik} = \sum_{g\in G} Q_{kg}^m \quad \forall k \in K \qquad (2.6)$$

$$\partial^r \textstyle\sum_{i\in I} Q_{ik} = \sum_{g\in G} Q_{kg}^r \quad \forall k \in K, \forall r \in R \qquad (2.7)$$

$$\textstyle\sum_{e\in E}\sum_{s\in S} Q_{ke} \le p^s \cdot Y_k^s \quad \forall k \in K \qquad (2.8)$$

$$N_k^s = 25Y_k^S + 35Y_k^M + 45Y_k^L \quad \forall k \in K \qquad (2.9)$$

$$\textstyle\sum_{s\in S} Y_k^s \le 1 \quad \forall k \in K \qquad (2.10)$$

$$\textstyle\sum_{k\in K} Q_{ke} \ge D_e \quad \forall e \in E \qquad (2.11)$$

$$\textstyle\sum_{k\in K} Q_{kv}^r \ge D_v^r \quad \forall v \in V, \forall r \in R \qquad (2.12)$$

$$\sum_{k\in K} Q_{kg}^{m} \geq D_g \quad \forall\, g \in G \tag{2.13}$$

$$Y_k^s = \{0,1\} \quad \forall k \in K, \forall s \in S \tag{2.14}$$

$$Q_{ik} \geq 0 \quad \forall i \in I, \forall k \in K \tag{2.15}$$

$$Q_{kv}^{r} \geq 0 \quad \forall k \in K, \forall r \in R, \forall v \in V \tag{2.16}$$

$$Q_{kg}^{m} \geq 0 \quad \forall k \in K, \forall g \in G \tag{2.17}$$

$$Q_{ke} \geq 0 \quad \forall k \in K, \forall e \in E \tag{2.18}$$

2.3.2.2. RJF supply chain incentivized with PCP

In this section, RJF produced by the supply chain will be incentivized with PCP which considers monetary incentives for each gallon of RJF produced by biorefineries. The objective function employed in this model to optimize supply chain profits is shown in Eq. (2.19). The first part of the equation represents the revenue from selling RJF, with a producer credit for the RJF produced. The rest of the elements are the same as in Eq. (2.3)

$$\begin{aligned} Max\, Z = {} & (\pi + \lambda) \sum_{k\in K}\sum_{e\in E} Q_{ke} + \sum_{r\in R}\sum_{k\in K}\sum_{v\in V} \psi^{r} Q_{kv}^{r} + \varphi \sum_{k\in K}\sum_{g\in G} Q_{kg}^{m} - \alpha \sum_{i\in I}\sum_{k\in K} Q_{ik} \\ & - \sum_{k\in K}\sum_{s\in S} f^{s}\, Y_k^s - \sum_{k\in K}\sum_{s\in S} N_k w Y_k^s - \xi(1+\vartheta) \sum_{k\in K}\sum_{s\in S} f^{s}\, Y_k^s \\ & - \rho \sum_{i\in I}\sum_{k\in K} Q_{ik} - \sum_{i\in I}\sum_{k\in K} (\gamma^{c} + \eta^{c}\, d_{ik}) Q_{ik} - \sum_{k\in K}\sum_{e\in E} \left(\gamma^{j} + \eta^{j}\, d_{ke}\right) Q_{ke} \\ & - \sum_{k\in K}\sum_{g\in G} \left(\gamma^{c} + \eta^{c}\, d_{kg}\right) Q_{kg}^{m} - \sum_{r\in R}\sum_{k\in K}\sum_{v\in V} \left(\gamma^{j} + \eta^{j}\, d_{kv}\right) Q_{kv}^{r} \end{aligned} \tag{2.19}$$

Similar to the preceding model, this objective function is subject to limitations (2.4) to (2.18).

2.3.2.3. RJF supply chain incentivized with BCAP

In this section, we use BCAP to incentivize the supply chain, with all components in Eq. (2. 20) being the same as in Eq. (2.3), except for monetary incentives for purchasing biomass crops (discounts on carinata selling prices) in the fourth component.

$$
\begin{aligned}
Max\ Z = \pi \sum_{k\in K}\sum_{e\in E} Q_{ke} + \sum_{r\in R}\sum_{k\in K}\sum_{v\in V} \psi^{r} Q_{kv}^{r} + \varphi \sum_{k\in K}\sum_{g\in G} Q_{kg}^{m} \\
- (1-\beta)\,\alpha \sum_{i\in I}\sum_{k\in K} Q_{ik} - \sum_{k\in K}\sum_{s\in S} f^{s}\, Y_{k}^{s} - \sum_{k\in K}\sum_{s\in S} N_{k} w Y_{k}^{s} \\
- \xi(1+\vartheta) \sum_{k\in K}\sum_{s\in S} f^{s}\, Y_{k}^{s} - \rho \sum_{i\in I}\sum_{k\in K} Q_{ik} \\
- \sum_{i\in I}\sum_{k\in K} (\gamma^{c} + \eta^{c}\, d_{ik}) Q_{ik} - \sum_{k\in K}\sum_{e\in E} \left(\gamma^{j} + \eta^{j}\, d_{ke}\right) Q_{ke} \\
- \sum_{k\in K}\sum_{g\in G} \left(\gamma^{c} + \eta^{c}\, d_{kg}\right) Q_{g}^{m} - \sum_{r\in R}\sum_{k\in K}\sum_{v\in V} \left(\gamma^{j} + \eta^{j}\, d_{kv}\right) Q_{kv}^{r}
\end{aligned}
\tag{2.20}
$$

This objective function, similar to the previous model, is subject to constraints (2.4) to (2.18).

2.3.2.4. RJF supply chain incentivized with the BAP

This section uses BAP to incentivize the supply chain, with all components in Eq. (2.21) identical to those in Eq. (2.3), except for the monetary incentives considered in the fifth composite component. This component takes into account discounts for production costs and capital costs at biorefineries.

$$Max\ Z = \pi \sum_{k\in K}\sum_{e\in E} Q_{ke} + \sum_{r\in R}\sum_{k\in K}\sum_{v\in V} \psi^r Q^r_{kv} + \varphi \sum_{k\in K}\sum_{g\in G} Q^m_{kg} - \alpha \sum_{i\in I}\sum_{k\in K} Q_{ik}$$

$$- (1-\phi)\left(\sum_{k\in K}\sum_{s\in S} f^s\, Y^s_k + \sum_{k\in K}\sum_{s\in S} N_k w Y^s_k + \xi(1+\vartheta)\sum_{k\in K}\sum_{s\in S} f^s\, Y^s_k\right.$$

$$\left. + \rho \sum_{i\in I}\sum_{k\in K} Q_{ik}\right) - \sum_{i\in I}\sum_{k\in K} (\gamma^c + \eta^c\, d_{ik}) Q_{ik}$$

$$- \sum_{k\in K}\sum_{e\in E} \left(\gamma^j + \eta^j\, d_{ke}\right) Q_{ke} - \sum_{k\in K}\sum_{g\in G} \left(\gamma^c + \eta^c\, d_{kg}\right) Q^m_{kg}$$

$$- \sum_{r\in R}\sum_{k\in K}\sum_{v\in V} \left(\gamma^j + \eta^j\, d_{kv}\right) Q^r_{kv} \qquad (2.21)$$

This objective function, similar to previous models, is subject to constraints (2.4) to (2.18).

2.4. Results and discussion

In this section, we first illustrate and discuss various optimized supply chain decisions with regard to supply management of the supply chain network, transportation management, location of biorefineries, capacity level for activated biorefineries, and material flow from supply nodes to activated biorefineries, and material flow from biorefineries to airports. Following that, the models' implementation of three direct incentive policies is considered, and the corresponding results are discussed. It is worth noting that the minimal incentive to commercialize RJF production is assumed to be the level that decreases profit loss to zero. Finally, optimal decisions for various market penetrations to meet their corresponding RJF demand are examined, and the impacts of various biofuel prices (RJF, RDF, LPG, and naphtha), carinata yield rate, and carinata and meal prices on the supply chain's profitability are evaluated.

2.4.1. Supply chain analysis with no monetary incentives

The results from the MILP show that the optimal number of biorefineries to be activated is three, including one small, one medium, and one large biorefinery with capacities of 185 MGPY,

291 MGPY, and 396 MGPY, respectively. Based on the available biomass feedstock to be converted to RJF and the demands for RJF at the selected airports, it could be concluded that the produced RJF from the available biomass could only supply 53.9% of the projected RJF demand ($520.83 MGPY). The base optimization model was solved when we assumed that the supply would be converted to RJF and would meet 50% of the jet fuel demand in the airports. Table 2.3 depicts the optimal supply allocations to activated biorefineries and optimal RJF assignment from activated biorefineries to the airports. To supply the biorefineries, 94% of the available farm fields had to be planted with Carinata.

Table 2.3. Optimal assignment of supply zones and demand nodes to activated biorefineries

Supplier district (share of supply assignment)	Activated biorefinery and its capacity	Demand node (share of demand fulfillment)
S[3]0110 (42.20%), S0120 (21.11%), S0130 (8.67%), S0140 (15.62%), S1310 (4.43%), S1320 (0.99%), S1340 (6.98%).	B[4]0120 (Small)	Pensacola International (5.79%), Hartsfield-Jackson Atlanta International (76.58%), Birmingham–Shuttlesworth International (9.51%), Huntsville (4.89%), Mobile Regional (3.22%).
S1230 (6.22%), S1250 (4.52%), S1350 (6.46%), S1360 (19.99%), S1380 (50.66%), S1390 (12.14%).	B1230 (Large)	Orlando International (33.88%), Orlando Sanford (2.29%), St. Pete–Clearwater, International Airport (1.63%), Sarasota–Bradenton International Airport (1.53%), Northwest Florida Beaches International (1.28%), Tallahassee International (1.69%), Hartsfield–Jackson Atlanta International (52.58%), Savannah/Hilton Head International (3.89%), Augusta Regional at Bush Field (1.23%).
S0160 (20.94%), S1210 (19.55%), S1350 (1.49%), S1370 (58.03%).	B1370 (Medium)	Miami International (38%), Tampa International (22%), Southwest Florida International (9.47%), Jacksonville International (9.08%), Palm Beach International (7.47%), Hartsfield–Jackson Atlanta International (13.98%).

[3] The letter "S" in the beginning of the biorefinery node indicates that the supply node is located at ASD 0110.
[4] The letter "B" in the beginning of the biorefinery node indicates that the biorefinery node is located at ASD 0120.

Figure 2.3(a) depicts the spatial aspect of the supply chain decisions on the activation of biorefineries with varying capacities and the provision of RJF from each of the activated biorefineries to the specified airports. To meet 50% of the RJF demand, three biorefineries must be established, as shown in Figure 2.3(a). The model determined the optimal locations where biorefineries would be built so that transportation costs for transporting carinata from farms to biorefineries, carinata meal from biorefineries to cattle farms, and RJF from biorefineries to the airports would be as low as possible while all the predefined demands for the outputs would be met. Due to the higher transportation costs required to transport each ton of biomass feedstock and carinata meal compared with the costs for transporting RJF and other fuel products, the model prioritized the distance between supply nodes and biorefineries and the distance between biorefineries and cattle farms above the distance between biorefineries and the airports and the demand nodes for the fuel byproducts (Leila et al., 2018). Thus, biorefineries are activated in ASDs closer to supply zones with a high rate of carinata available and also cattle farms with high rate of demand for carinata meal rather than being closer to the airports. It should be mentioned that the supply chain did not need to supply its activated biorefineries with carinata from three ASDs, including S0150, S1330, and S1280 (illustrated with hatched lines in Figure 2.3(a)). Additionally, only 62% of the supply in S1350 (illustrated with crosshatched lines in Figure 2.3(a)) was used to produce RJF in activated biorefineries. Figure 2.3(b) shows the optimal assignment of the airports to individual biorefineries. As depicted in this figure, there were airports that needed only one biorefinery to supply them, as well as airports that required numerous biorefineries to supply them.

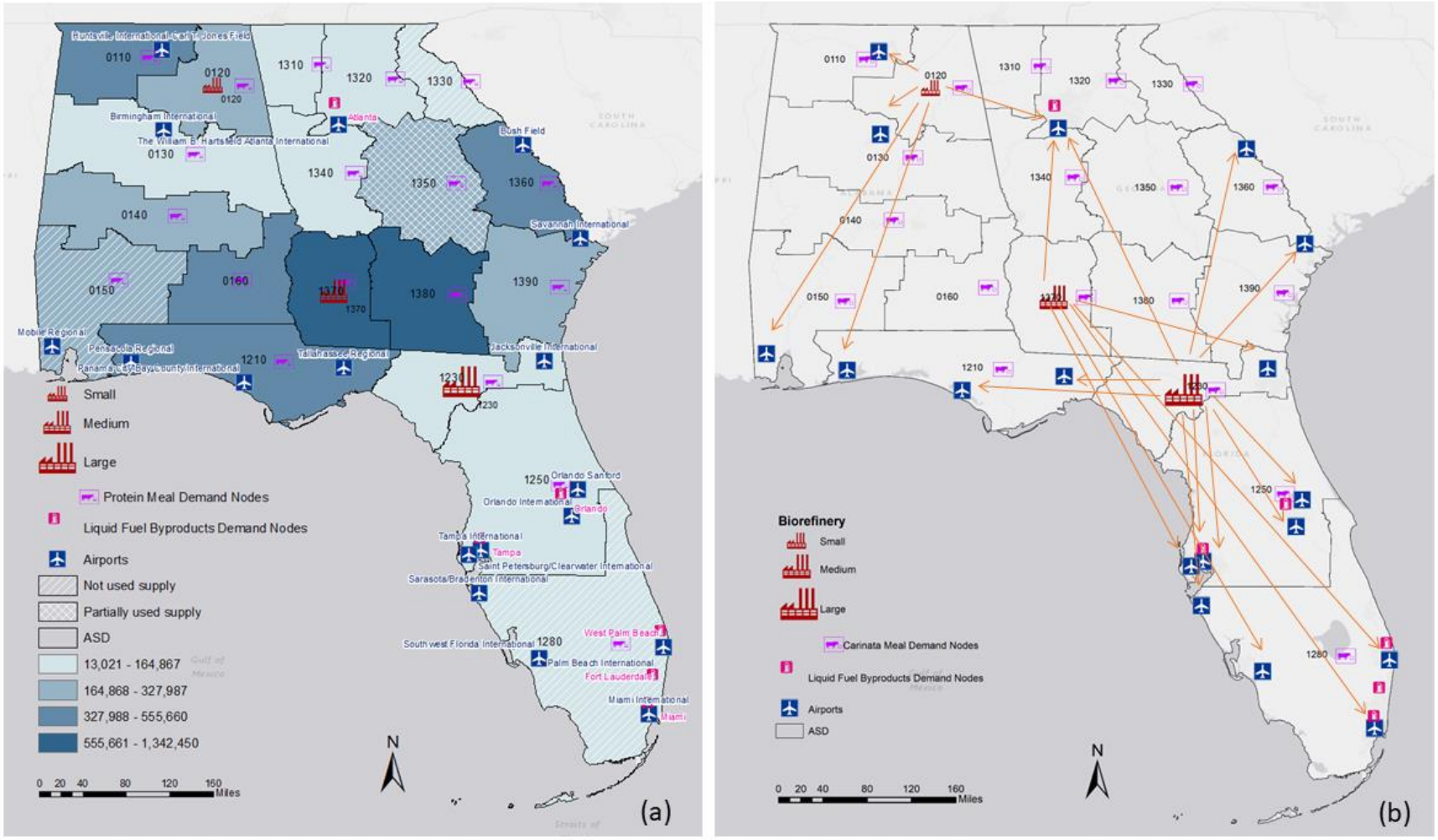

Figure 2.3. (a). Optimal decisions with regard to location allocation of biorefineries and their capacities and (b) material flow from activated biorefineries to the airports

Figure 2.4(a) provides the details of cost components in the supply chain. The total cost was $2,722 million, including biomass feedstock purchasing cost, transportation costs, capital costs, and operational costs. The majority of the cost (72.15%) is associated with supply purchasing expenses. As a result, changes in availability and the price of biomass feedstock are likely to have a significant impact on supply chain costs. These results agree with previous findings from studies that considered oilseeds as their biomass (Leila et al., 2018; Chu et al., 2017; Diniz et al., 2018). Nine percent of the entire cost was allocated to transportation.

Capital expenses (CAPEX) were tied to the overall annualized costs for constructing the needed biorefineries, which included 11% of the total cost resulting from the establishment of three biorefineries. It was projected that 105 employees were needed to operate the activated biorefineries. Furthermore, operating expenses (OPEX) accounted for 8.28% of total costs, with fixed operational costs (13.35%) attributed to employees, overhead, maintenance, insurance, taxes, and contingency, and variable operational costs (86.65%) associated with utility costs (thermal energy, electricity, water, and hydrogen gas). Regarding the high share of total capital and operational costs (19%), it was expected that providing subsidies for establishing biorefineries and their associated operating expenses would significantly lower operational costs. This is consistent with the conclusion from the study by Chu et al. (2017) which highlights the sensitivity of RJF production costs to its production costs at biorefineries.

The results in Figure 2.4(b) reveal that the revenue created by protein meal extracted from carinata (43.17%) outweighs the overall revenue from fuel coproducts, including RJF, LPG, and naphtha (20%) and the revenue generated by selling RJF (36.93%). It should also be noted that, while procuring biomass was the most expensive cost component of the supply chain, half of the costs ($979 M of a total of $1,973 M for purchasing the biomass feedstock) could be offset by

selling the protein meal produced from it. Furthermore, the revenue from coproducts (protein meal and biofuel coproducts combined) generated throughout the RJF production process was 63% of the total revenue, which confirms that selling coproducts from oilseed through HEFA have a significant impact on the supply chain's profitability (Chu et al., 2017).

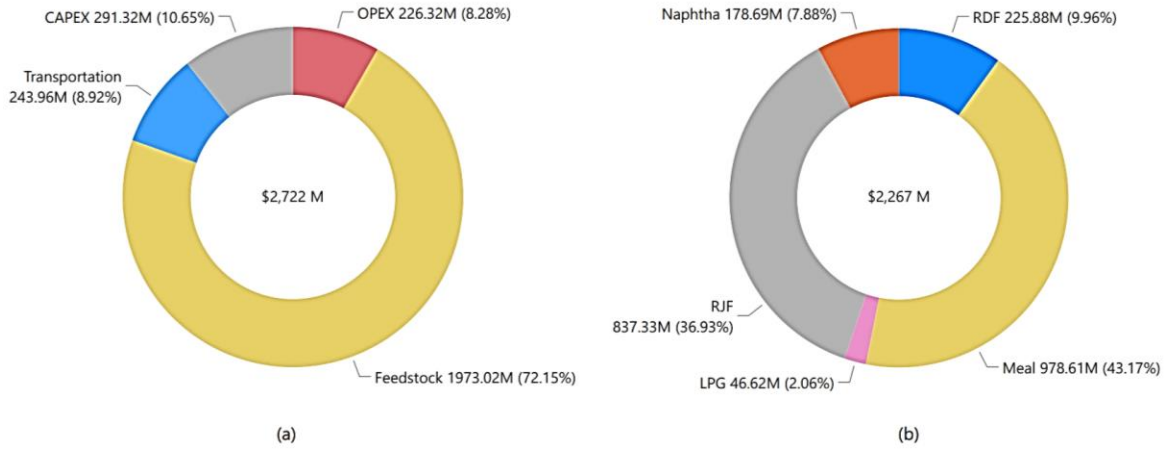

Figure 2.4. Total cost and revenue breakdowns: (a) cost breakdown of the supply chain ($ M), (b) revenue breakdown of the supply chain ($ M)

When the transportation expenses were broken down (Figure 2.5), 45.69% and 34.73% of the costs were associated with transporting feedstock and carinata meal respectively, while transporting fuel products altogether, including RJF, LPG, naphtha, and RDF, incurred 19.59% of the costs. These results could be attributed to the greater costs of transporting biomass and carinata meal (fixed and variable transportation costs) and their lower density compared to biofuels.

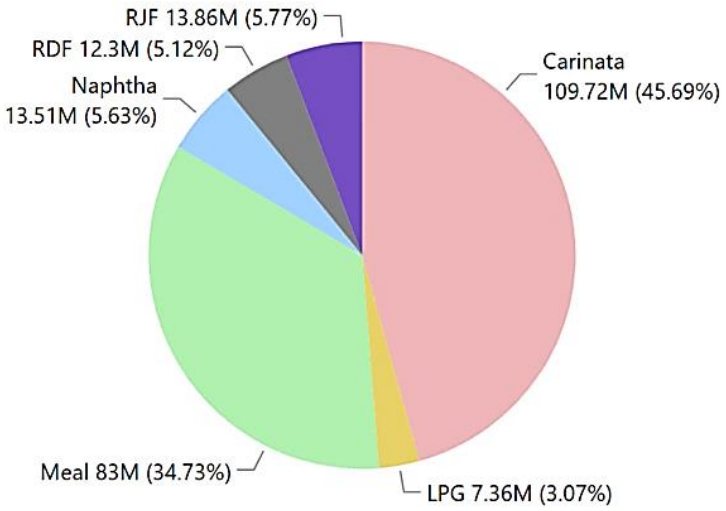

Figure 2.5. Transportation cost breakdown for the RJF supply chain

2.4.2. Supply chain analysis with application of different monetary incentives

2.4.2.1. Supply chain incentivized with PCP

The PCP monetary incentive was developed to determine the direct monetary incentives to bridge the gap between the profit loss per gallon of RJF produced and profit loss of zero for a gallon of RJF produced (the breakeven point). Because the incentives would cover a proportion of the total costs, PCP could be viewed as a comprehensive assistance program covering all forms of RJF production costs, such as capital, operating, carinata procurement, and transportation costs. According to the results shown in Figure 2.6, the optimized supply chain network needed to have 16.70% of its total cost compensated by PCP to start commercializing the RJF production. In other words, to reach profitability in the supply chain and cover the $0.94 cost per gallon of the RJF produced, at least 16.70% of the total cost had to be covered by the assistance program. In case of applying inclusive incentives, $0.57 incentive per gallon of biofuels was needed to commercialize RJF production.

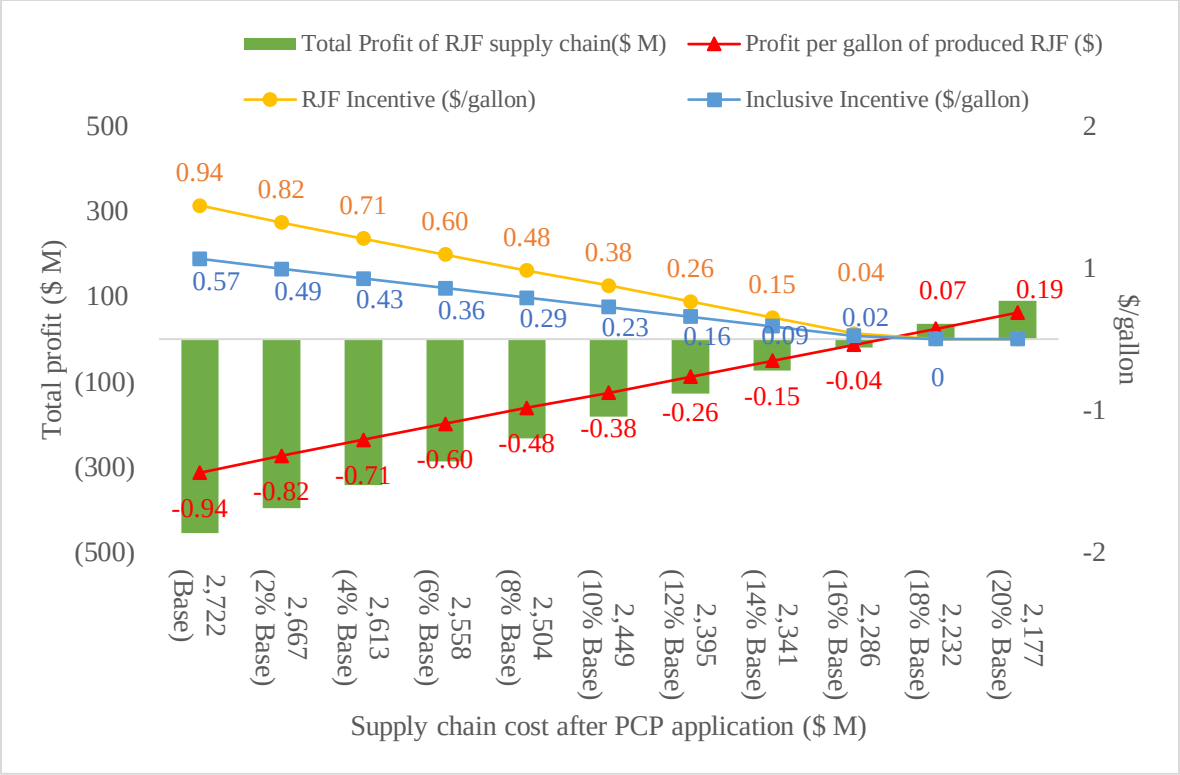

Figure 2.6. RJF production profit, with regard to various PCP incentive scenarios

2.4.2.2. Supply chain incentivized with BCAP

In this section, the BCAP incentive is incorporated into the supply chain model. BCAP allocates monetary incentives to manufacturers to buy biomass feedstock from farmers, as explained in section 2.2. As shown in Figure 2.7, as the share of BCAP incentives provided to the supply chain increases, profit per gallon of RJF in the supply chain gradually increases. When the assistance program covers 22.84% of the carinata price ($254.02 per ton of carinata), the graph approaches zero profit, indicating that the supply chain could produce RJF commercially. However, when the BCAP program covers the entire cost of the biomass feedstock, the maximum profit per gallon of RJF ($3.13) is achieved. Because supply provision accounted for 72% of the overall supply chain expenses, carinata buying prices significantly impacted the supply chain's total profit (Chu et al., 2017).

We also considered a case where an inclusive monetary incentive could be applied to all the produced liquid fuels. The results in Figure 2.7 shows that by spreading the incentives over all the produced liquid fuels, the RJF supply chain needs to get lower incentives per gallon of biofuels produced ($0.56 per gallon for the biofuels produced versus $0.93 per gallon for the RJF produced).

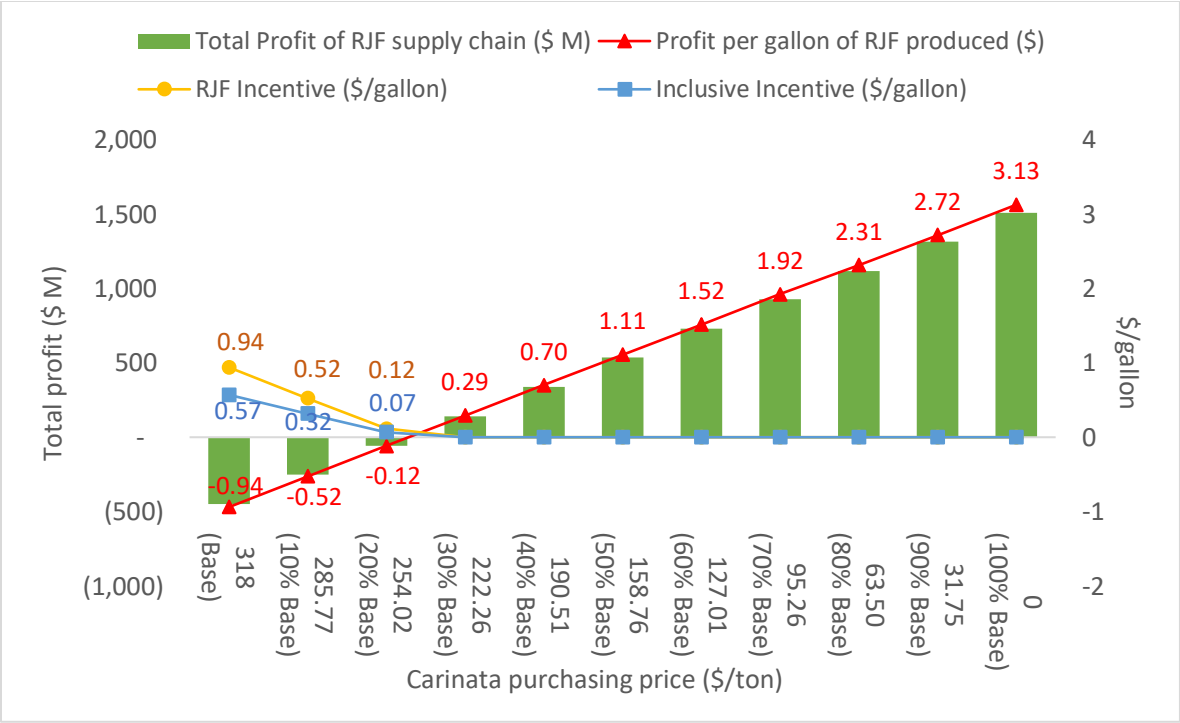

Figure 2.7. RJF production profit, with regard to various BCAP incentive scenarios

2.4.2.3. Supply chain incentivized with BAP

Under BAP, manufacturers (biorefineries) would be compensated for capital investments in biorefineries and operational costs for producing RJF. Figure 2.8 depicts the effects of different shares of BAP coverage of biorefinery expenses on the supply chain's profitability. As shown in Figure 2.8, the supply chain did not profit from RJF production until its capital and operational costs of the base case were covered by at least 89.39%. The large share of the BAP incentive

required to commercialize the supply chain is related to the low proportion of biorefinery-related costs in the total costs (19%).

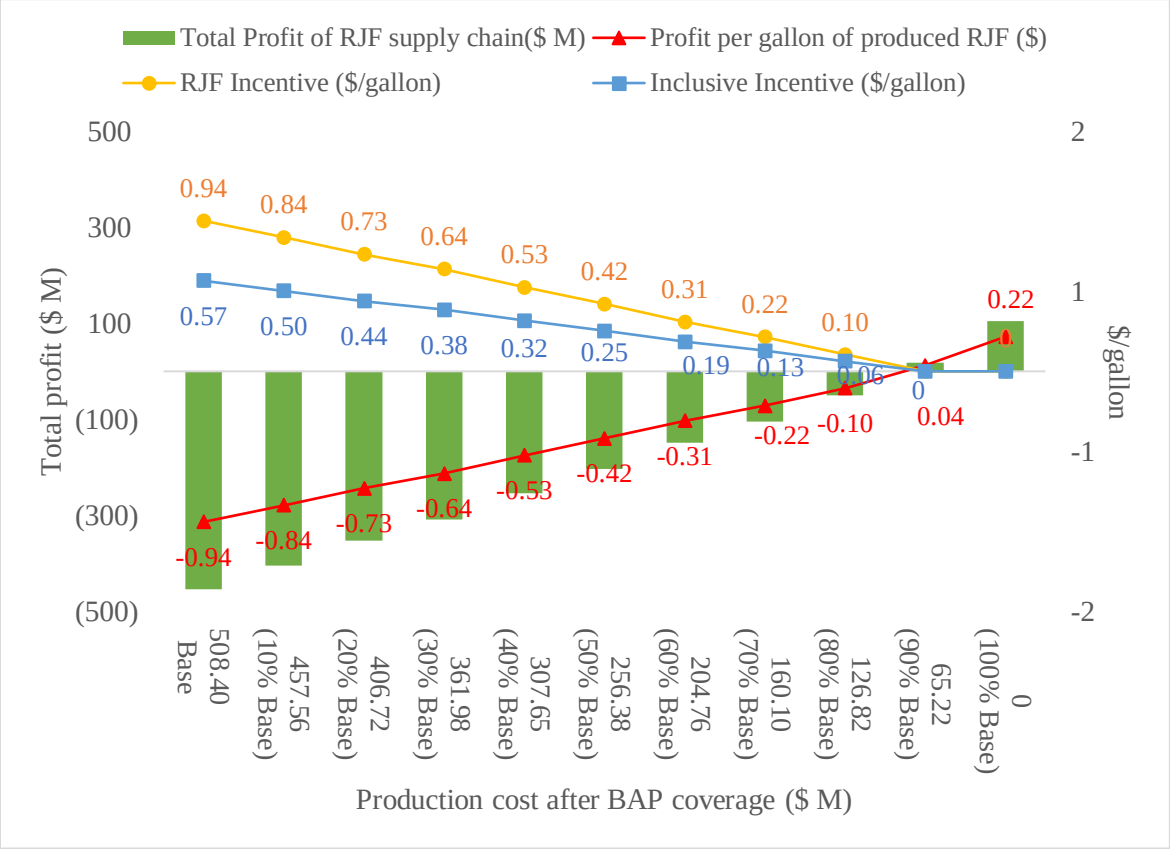

Figure 2.8. RJF production profit, with regard to various BAP incentive scenarios

We also examined the application of a combination of BCAP and BAP to cover the costs. The results are demonstrated in Table 2.4. As it can be observed from the results of the combined assistance programs, the supply chain could reach the commercialization level with lower rates of BCAP compared to the rates of BAP in the combinations. This results from the higher share of costs to be covered by BCAP (72.15%) compared with the costs to be covered by BAP (19%).

Table 2.4. Combination of BCAP and BAP to reach commercialization

Share of incentives			
BCAP (%)	BAP (%)	BCAP (%)	BAP (%)
2	80.57	14	34.17
4	72.84	16	26.44
6	65.11	18	18.7
8	57.37	20	10.97
10	49.64	22	3.24
12	41.9		

2.4.3. Supply chain analysis with regard to changes in parameters

To evaluate the effect of various demand fulfillment rates on the profitability of the RJF supply chain, we also examined the impact of various market penetration scenarios on the supply chain decisions and its economic dynamics. According to the results shown in Figure 2.9, meeting higher demands in the airports resulted in lower total profit. However, the increased cost of meeting higher demand rates was offset by producing more RJF and coproducts, resulting in a lower cost per gallon of RJF produced. This outcome was anticipated given the economies of scale realized by producing more RJF. It was revealed that the cost per gallon of RJF generated was lowest (0.90 $/gallon) when the RJF supply chain satisfied 35% of the jet fuel demand in the airports (70% of the demands in the base case, respectively). In a case where only 48.31 M gallons of demand fulfillment for RJF was projected, an RJF supply chain network with one small biorefinery was optimal (with a 43.45% utilization rate). The cost of producing RJF per gallon changed for various market shares. However, for the rates between 50% of the demand fulfillment (the base case) and 35% of the base case, the changes in cost per gallon of RJF stabilized, resulting in almost equal costs per gallon of RJF and biofuels produced. Even though establishing more biorefineries to meet more demand may result in higher costs for a given demand fulfillment rate until all the capacity of biorefineries is used, the supply chain was able to balance the needed

capacity based on existing demand and could use the capacity more efficiently thanks to the flexibility of capacities in each potential biorefinery location.

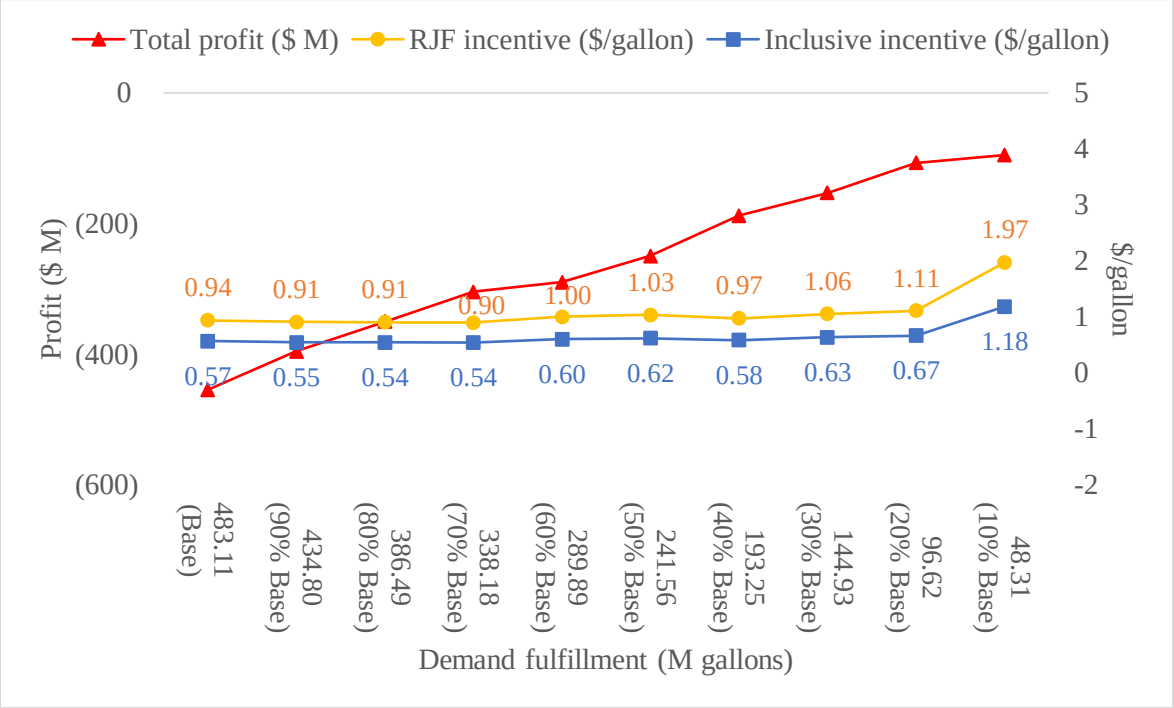

Figure 2.9. The effects of different demand fulfillments rates on the RJF supply chain profitability and incentive payments

We also studied the impact of low and high yield rates of carinata on the RJF demand fulfillment in the airports. As depicted in Table 2.5, for the low yield rate of 2,242.20 kg/ha (Alam & Dwivedi, 2019), the RJF supply chain could meet 43.12% of the RJF demand in the airports (86% of the demands in the base case). On the other hand, higher yield rate of 3,363.30 kg/ha (Alam & Dwivedi, 2019) resulted in a fulfillment rate of 64.69% of the RJF demand (128% of the demand in the base case). In the face of a low yield rate, we may need to consider other states as supply nodes in order to meet the established demands in airports (Alam & Dwivedi, 2019). On the other hand, higher carinata yield increases availability of the supplies that can lead to higher rate of RJF demand fulfillment which eventually benefits farmer's economy and reduces carbon emissions.

Table 2.5. Profit of RJF supply chain and incentive payments with regard to changes in carinata yield rate

Profit of RJF supply chain & incentive payments	Carinata yield rate (kg/ha)	
	Low (2,242.20)	High (3,363.30)
Total Profit of RJF supply chain ($ M)	-386.05	-553.61
Profit per gallon of produced RJF ($)	-0.93	-0.90
RJF Incentive ($/gallon)	0.93	0.90
Inclusive Incentive ($/gallon)	0.56	0.54

To better understand the impact of the produced biofuels' prices on the supply chain's profitability, we examined the price changes over a range from the lowest to the highest average of conventional jet fuel prices between 2011 and 2020 (10 years). According to EIA (2021), the lowest average of conventional jet fuel prices was assigned to 2020, with 1.293 $/gallon, while the highest average price was attributed to 2012, with 3.104 $/gallon. Because the base price for selling RJF (1.73 $/gallon) was based on the average of conventional jet fuel prices from 2016 to 2020, the lowest range for the threshold could be set to 30% less than the base price, while the maximum range for the threshold could be set to 80% higher. Figure 2.10 depicts the variations in the profitability of the supply chain as a result of changes in the prices of all the biofuels produced in the supply chain. Furthermore, the amount of incentives (RJF and inclusive incentives) required to offset the associated costs is depicted at each price adjustment level. As indicated in Figure 2.10, if the biofuels' prices dropped by 30%, the supply chain would experience its highest profit loss ($853.37 M) and would need to offset $1.77 per gallon of RJF produced via RJF incentives or $1.06 per gallon produced biofuels to reach the commercialization level. The graph shows that when the base fuel price increases by more than 30%, the supply chain may begin commercializing RJF, though profit per gallon of RJF produced may reach 1.19 $/gallon if the fuel price grows by

80%. This results confirms the findings from the study by Chu et al. (2017) that highlights the impact of fuel price on RJF commercialization.

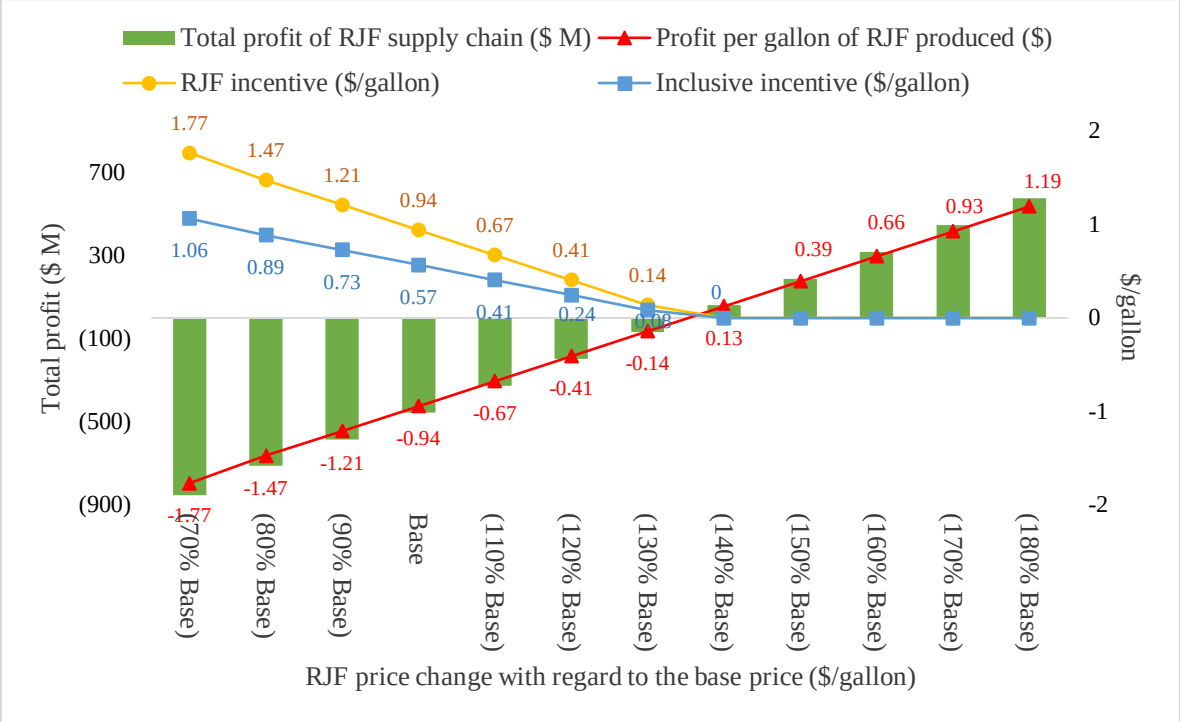

Figure 2.10. Profit of RJF supply chain and incentive payments under different fuel prices

We also investigated the impacts of changes in the carinata and meal prices on the profit of the RJF supply chain and found the incentive payments required to reach the commercialization level. The low price rate for purchasing carinata was considered at 254.01 $/ton while the highest range was set to 399.16 $/ton (Chu et al., 2017). Also, we considered 254.01 $/ton and 344.73 $/ton for the lowest and highest price range for selling carinata meal, respectively, while the prices corresponding to the base case were considered as the most likely prices expected (Chu et al., 2017).

According to the results indicated in Table 2.6, the supply chain with a low price for carinata and meal needs the lowest incentives ($0.32 per gallon from RJF incentives and $0.19 per gallon from inclusive incentives) to start commercialization. The resulting differences in the

supply chain's profits and incentive payments refers to the difference between carinata price and meal price in each price level. In the low-price range, the price of carinata and meal are assumed to be the same, however in the other two pricing scenarios, the price of carinata is greater than the price of meal, incurring higher supply chain costs. The analysis emphasizes the importance of carinata meal pricing and finding markets where we may sell them at prices higher than carinata price.

Table 2.6. Profit of RJF supply chain and incentive payments with regard to changes in the prices of carinata and meal

Profit of RJF supply chain & incentive payments	Carinata and Meal price ($/ton)		
	Low (254.01, 254.01)	Base (317.52, 281.23)	High (399.16, 344.73)
Total Profit of RJF supply chain ($ M)	-154.53	-454.45	-744.58
Profit per gallon of produced RJF ($)	-0.32	-0.94	-1.54
RJF incentive ($/gallon)	0.32	0.94	1.54
Inclusive incentive ($/gallon)	0.19	0.57	0.93

We also investigated the impact of soil erosion on the profitability of the supply chain. Leaving land bare and unprotected for a long time (during winter) can cause soil erosion in farm fields (DeLonge & Stillerman, 2020). Soil erosion can eventually incur costs to farmers and society. According to Duffy (2012), the range of cost per acre per year caused by erosion would be from $2.75 to $6.45 an acre. However, considering planting carinata during winter, we assumed that there will be no erosion in fields planted by winter carinata. Hence, the corresponding costs would be transformed to revenues by farm fields not experiencing erosion. The farm fields planted with carinata totaled 2,995 thousand acres and planting carinata during winter could result in reduced soil erosion which would save $13.61 million to $31.93 million annually. Adjusting the supply chain's profits by this cost savings from reduced soil erosion changed the $0.93 loss per gallon of RJF to a profit loss of no more than $0.9 and as low as $0.87 per gallon of RJF. Hence,

potential savings from soil erosion can have a substantial impact on the viability of an RJF supply chain.

2.5. Conclusion

Using a MILP, we identified an optimal supply chain design to meet 50% of the existing demand at airports in the southeastern United States. This study offered an optimal RJF supply chain configuration that could minimize costs, as well as assess the adoption of several existing and proposed direct monetary incentive programs to commercialize mass RJF production. We suggested employing carinata as a viable biomass alternative that could be grown throughout winter and was proven to be effective biomass to produce RJF. The study also determined the supply chain configurations required to manufacture RJF in the study region that could reflect a realistic network setting and enhance understanding of various aspects to implement the supply chain.

Considering the findings, more availability of carinata in the region would cut the cost of generating RJF per gallon. According to the findings almost 43% of the revenue in the RJF supply chain could be earned by selling the protein meal. As a result, finding local or international markets for protein meals that can guarantee a profit from selling them is critical to the supply chain's profitability.

This research analyzed the application of three distinct incentive policies, PCP, BCAP, and BAP, on the RJF supply chain profitability. From these results, it could be concluded that the supply chain's profitability was highly sensitive to changes in PCP and BCAP coverage shares. The reason is that high proportion of cost consist of biomass feedstock costs (72%), which makes the costs to be covered by the two programs close. It is likely that after planting carinata on a massive scale in the region, its farming costs will decline, resulting in a lower coverage rate

needed from the BCAP program. It is projected that once RJF production from carinata is commercialized, the costs associated with the manufacturing, such as costs related to biomass feedstock, preprocessing, and conversion, will gradually decrease due to technological developments in those areas (Leila et al., 2018; J. Zhang et al., 2013). As Gutiérrez-Antonio et al. (2017) suggested, there would be potentials to create hydro-processing technology that may effectively cut operational and capital costs, resulting in lower RJF prices. Even if none of the aforementioned changes occur, the supply chain may become profitable if the biofuels prices increase by more than 35.26%. Furthermore, the results indicated that planting carinata with greater yield rates might improve supply chain sustainability, and that could be obtained by adopting high yielding varieties with optimum oil content and fatty acid profile (Ramdeo Seepaul et al., 2021). It can be concluded that there are several opportunities to make the supply chain profitable, and if financially supported earlier by federal agencies, the RJF supply chain can start its journey toward maturity and cutting costs and GHG emissions in the coming years.

This study investigated the effects of various monetary incentives that would be directly supplied to RJF producers. However, there are numerous financial incentives that can be provided to producers indirectly, such as tax credits or loans, as highlighted by Noh et al. (2016). Recently, under a collaborative plan, called sustainable aviation fuel grand challenge, DOE, USDA, and DOT set a goal of delivering enough RJF to cover all aviation fuel needs by 2050 (DOE, 2022). Therefore, the RJF production is expected to be incentivized until it reaches the commercialization level with innovative conversion technologies and the implementation of optimized supply chains with the lowest possible cost. However, there might be issues such as drought, floods, or even pandemics that could impair the profitability of supply chains. Therefore, it would be also important to consider risk mitigation strategies that can offset the related risks. According to Sajid

(2021), uncertainties in the biomass supply chain, such as biomass production, biomass harvesting, transportation, labor availability, and high preprocessing costs caused by the Covid-19, have harmed biofuel supply chains. There have been recommended strategies to mitigate the risks including providing temporary biofuel sales tax reductions and extending the debt repayment schedules of refiners, which could also be applied to RJF production (Nocera Alves Junior et al., 2021).

Although this study was conducted for the southeastern United States case study, the decision-making approach in this research could be applied to any place with similar environmental conditions, provided sufficient farming lands would be available. Furthermore, the approach appears to be feasible for places with extensive fallow lands and favorable meteorological conditions for carinata throughout the summer planting season (Kumar et al., 2020).

The availability of feedstock for biofuel, which can consequently impact biofuel production can be affected by precipitation, biomass pricing, and fuel price. Thus, another analysis is proposed that considers the stochastic character of components that contribute to the RJF supply chains. In the future, it may be feasible to do a more comprehensive study of the supply with particular farm sites, as well as include more freight options such as rail and pipeline. Furthermore, future research can incorporate geographic information system (GIS) tools into optimization models to analyze geographical features of potential locations for constructing biorefineries in the supply chain.

3. RENEWABLE JET FUEL SUPPLY CHAIN NETWORK DESIGN: THE APPLICATION OF INCENTIVES TO ACCELERATE COMMERCIALIZATION

3.1. Abstract

The manufacture of renewable jet fuel (RJF) has been recognized as a promising approach for reducing the aviation sector's carbon footprint. Over the last decade, commercial production of RJF has piqued the interest of airlines and governments around the world. However, RJF production can be challenging due to its disperse supply resources. Furthermore, the production of RJF is more costly compared to producing conventional jet fuel. In this study, using a mixed integer linear programming, we design an RJF supply chain network in which we obtain an optimized configuration of the supply chain and determine operational decisions required to meet RJF demand in airports. To accelerate commercialization of the RJF production, we considered four different monetary incentive programs, which could cover the supply chain's costs. This study is validated by employing the model on designing an RJF supply chain in the Midwest region, US. Results from this study is promising as it shows that the supply chain could reach the commercialization level via partial financial coverage from the incentive programs. Based on the findings of this study, policymakers can devise policies to commercialize RJF production and accelerate its adoption by the industry.

3.2. Introduction

Finding cleaner sources of energy is critical to addressing concerns about energy security, food, and the environment. The aviation industry is responsible for 2% of the global carbon emissions (Claudia Gutiérrez-Antonio et al., 2013). However, the industry will continue to expand, and emissions will rise accordingly. Although electric and hydro-powered vehicles are replacing vehicles powered by fluid fuels such as fossil-based and biomass-based fluid fuels, there are not

similar options for the aviation industry. In 2005, the International Aviation industry committed to cut its net carbon footprint to less than half of its volume by 2050 (Chu et al., 2017). To achieve this goal, renewable jet fuel (RJF) has been proposed as a viable replacement that will effectively reduce the consumption rate of fossil-based jet fuels as well as the environmental effects of jet fuel consumption (Wei et al., 2019). RJF production can improve the economy of farmers, reduce greenhouse gas emissions (GHG), save energy sources for future generations, improve diversity of energy resources, and make industries more resilient to oil price changes and supply risks.

Several types of feedstocks can be considered as biomass for producing RJF. However, feedstock derived from food crops is contentious because it can also be used as food (Stelle & Pearce, 2011). Most of the expected sustainability impacts of RJF stem from feedstock choice and its associated characteristics (Diniz et al., 2018). To address these concerns and improve sustainability in producing RJF, the aviation industry has committed to using second-generation feedstock that does not compromise food security, requires low energy to produce, uses minimal land with high yield, and improves socio-economic values to local areas where biomass is planted. Second-generation biomass comprises crop residues (e.g., corn stover, wheat straw, rice straw, rice hull, etc.), forestry residues (e.g., wood pulp, wood chips, and sawdust), waste products (e.g., used cooking oils), or crops cultivated in perennial fields as biomass that does not induce food conflicts (e.g., switchgrass, camelina, and carinata). As Perkis & Tyner (2018) stated, after meeting the U.S. Renewable Fuel Standard (RFS) requirements by first-generation corn ethanol, many states are now looking for other generations of biomass feedstock such as cellulosic crops. According to the U.S. Billion-Ton Update, there are sufficient biomass resources to meet the advanced biofuel standards of the RFS (U.S. Department of Energy, 2011). The Midwest region in the United States

entails regions where corn is widely cultivated, and its residues seem to be a reliable resource for the RJF production.

W. C. Wang et al. (2016) provided a comprehensive review of the pathways (process technologies) applied to RJF production. Pathways such as alcohol-to-jet (ATJ), Fischer Tropsch (FT), hydrothermal liquefaction (HTL), and hydroprocessed esters and fatty acids (HEFA) are considered to convert biomass to RJF (de Jong et al., 2015). The pathways are certified or under review by the American Society for Testing and Materials (ASTM). Many studies known as techno-economic analysis (TEA) compared the feasibility of using the conversion technologies (Wang, 2016; de Jong et al., 2015; Natelson, Wang, Roberts, & Zering, 2015; Pearlson, Wollersheim, & Hileman, 2013; Pham, Holtzapple, & El-Halwagi, 2010). In a study comparing the feasibility of technologies such as FT, ATJ, and HTL, de Jong et al. (2015) discovered RJF price ranges higher than conventional jet fuel prices. Furthermore, several studies known as life-cycle analyses (LCA) have been conducted to estimate GHG emissions caused by the implementation of various pathway technologies (de Jong et al., 2017; Agusdinata, Zhao, Ileleji, & Delaurentis, 2011).

Despite rigorous assessment on the application of TEA and LCA approaches in the literature, the related studies fail to consider the complexity of RJF supply chains. These studies do not take into consideration optimized number and location of biorefineries that could potentially affect the supply chain costs. Due to the dispersed nature of biomass supply sources and their low energy density, a biofuel supply chain requires a large sourcing area that can meet demands and make the supply chain profitable (Castillo-Manzano et al., 2019; Malladi & Sowlati, 2018). To achieve this goal, it is critical to locate biorefineries optimally to reduce transportation costs and emissions while also ensuring feedstock availability.

To become commercially feasible, RJF production cost must become competitive with the production cost of fossil-based jet fuel. The costs incurred by the RJF production needs to be covered by government assistance and subsidies (Zheng et al., 2020). Noh et al. (2016) conducted a comprehensive study in which they discussed multiple existing incentive policies that are already in use in US agencies and could be considered for RJF production. In another study, Ebrahimi et al. (2022) investigated the application of three monetary incentives to cover the costs of RJF supply chain. They considered three different incentive programs including biomass crop assistance program (BCAP), producer credit program (PCP), and biorefinery assistance program (BAP). In BCAP, governments and agencies cover the costs related to supplying biomass feedstock for producing the biofuel. This program has been provided by the US department of Agriculture (USDA). BAP has provided financial support to cover the production costs in biorefineries. This assistance program has been provided by USDA. PCP provides comprehensive support to cover all costs associated with RJF production in the supply chain, including costs associated with biomass supply, production, and transportation. Furthermore, the use of carbon trading has been considered in several studies that could help renewable energy production compete with the cost of conventional fossil-based fuel production (Haji Esmaeili et al., 2020; Waltho et al., 2019). Cap-and-trade is one of the carbon policies that has been applied to restrict carbon emissions by fuel industries. Since the biofuel production could incur lower carbon emissions compared to the production of fossil-based fuels, application of carbon policies that capacitate carbon generation through the production process and allow the producers to trade and sell the unused amount of carbon emissions could be considered as an incentive program.

While many studies have examined the economic and environmental aspects of RJF production, a few have investigated how various monetary incentives could be employed to cover

costs related to RJF production (Ebrahimi et al., 2022; Haji Esmaeili et al., 2020). In this study, after designing an optimized RJF supply chain network in the Midwest region, we study the impact of four various monetary incentives to commercialize RJF production. The monetary incentives include programs such as PCP, BCAP, BAP, and cap-and-trade carbon policy.

The contributions of this study are

- Collecting associated data regarding amount of second-generation biomass feedstock (corn stover) in the Midwest and finding the optimal locations to establish biorefineries.
- Designing a corn stover based RJF supply chain with the application of FT pathway.
- Comparing the impacts of various incentive policies on profitability of the supply chain.
- Providing managerial implications of the results related to the application of monetary incentives.

3.3. Material and methods

3.3.1. The RJF supply chain configuration

Corn is widely planted in the Midwest and its residues are considered good feedstock resource for producing second-generation biofuels. In this study, we developed models that could be used to design an RJF supply chain using corn stover. The models determined the supply chain's profit through producing RJF. FT is considered as the conversion pathway to produce RJF from corn stover. The outputs from the production process include RJF, renewable diesel fuel (RDF), naphtha, and electricity (Pereira et al., 2017).

We assumed the supply chain network has three tiers: supplier nodes, biorefineries, and demand nodes. The biomass feedstock flows from supplier nodes to biorefineries where after being preprocessed and going through conversion process, produced RJF in biorefineries is disseminated to demand nodes (airports). Transporting raw materials to biorefineries and RJF to demand nodes is conducted by trucks. It was assumed that selling RDF and naphtha took place at biorefineries, and that customers were responsible for the transportation costs. We also assumed that preprocessing of corn stover is performed at the activated biorefineries. Figure 3.1 illustrates the three echelons of the RJF supply chain and its including components.

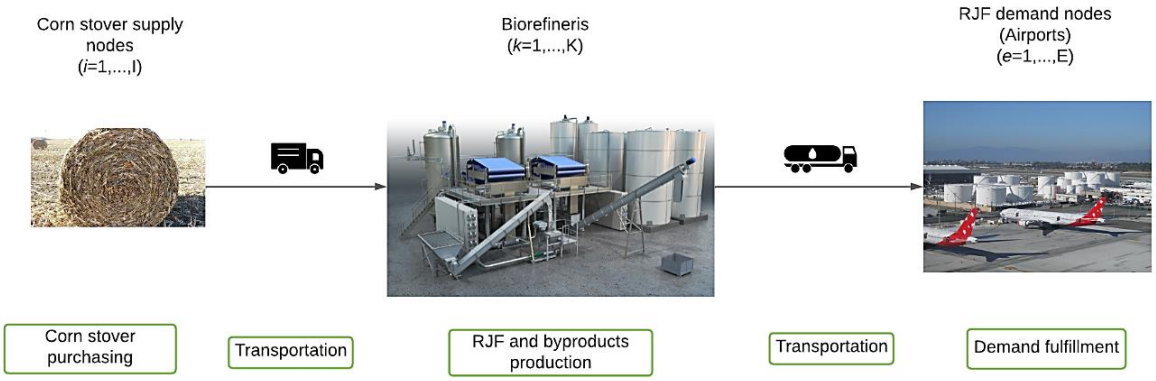

Figure 3.1. RJF supply chain network and the activities at each echelon

To validate our study, we considered the Midwest region in the United States. The Midwest region comprises of the states Illinois, Indiana, Iowa, Kansas, Michigan, Minnesota, Missouri, Nebraska, North Dakota, Ohio, South Dakota, and Wisconsin. For supplier nodes, we consider each agricultural statistical district (ASD) as a supply node (Ebrahimi et al., 2022; Haji Esmaeili et al., 2020). Supply for each ASD includes supply from all farms planting corn in the corresponding ASDs. However, to consider the extractable corn stover from farm, we excluded 50% of the available corn stover and assumed only 35% of farmers in the studied region would be interested to sell their corn stover (Guo et al., 2022). The quantity of biomass feedstock was calculated based on the planted areas with corn (NASS, 2021) in the region multiplied by the yield

rate of corn stover (3.099 tonnes per acre) that could be extracted from them. Figure 3.2 shows the spatial placement of the RJF supply chain including the supply areas as well as potential biorefinery locations and airports. The biorefineries can be supplied by 2,000 million tonnes of corn stover annually (E. Huang et al., 2019). It is assumed that both preprocessing of the corn stover and producing RJF are performed at biorefineries.

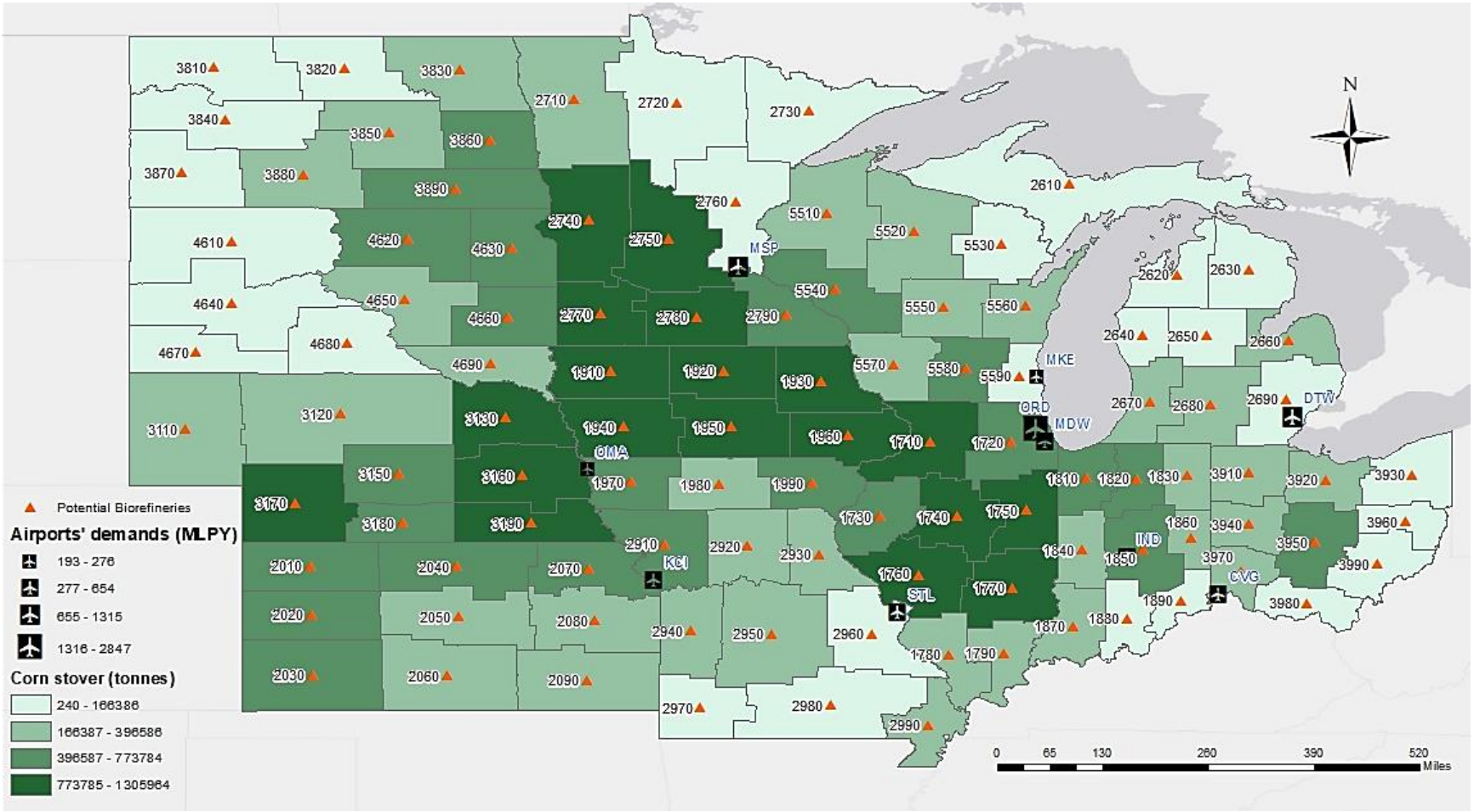

Figure 3.2. Spatial distribution of the RJF supply chain components in the Midwest region

For transportation purposes, each supply node at an ASD is considered to originate from the center of the ASD unless the destination biorefinery is in the originating ASD. In which case, the transportation distance is assumed 2/3 of the radius of that ASD which is calculated by the area of each ASD (E. Huang et al., 2019). Demand nodes are airports in the region with annual RJF demands greater than 100 million gallons. Due to a 50% maximum blending limit of RJF produced via FT pathway, only 50 percent of the required jet fuel in the airports was projected to be fulfilled by RJF. The airports with their corresponding demands are depicted in Table 3.1.

Table 3.1. The estimated RJF demand in the airports

Airports	Jet fuel demand (MLPY)	Estimated RJF demand (MLPY)
O'Hare International Airport (ORD)	2,846.51	1,423.25
Minneapolis-Saint Paul International Airport (MSP)	1,301.50	650.75
Detroit Metropolitan Wayne County Airport (DTW)	1,314.88	657.44
Chicago Midway International Airport (MDW)	653.79	326.90
St. Louis Lambert International Airport (STL)	618.58	309.29
Kansas City International Airport (KCI)	415.03	207.51
Indianapolis International Airport (IND)	375.96	187.98
Cincinnati/Northern Kentucky International Airport (CVG)	365.37	182.69
General Mitchell International Airport (MKE)	276.33	138.16
Eppley Airfield (OMA)	192.90	96.45
Total	8,360.84	4,180.42

Other data related to the parameters used in the RJF supply chain model is provided in Table B1.

3.3.2. Model formulation

We developed five MILP models: a base model with no monetary incentives and four alternative models, each with an assistance program. The models were designed to maximize the total profit of the RJF supply chain while accounting for the use of incentive programs. Moreover,

the models find the optimal number and location of biorefineries to be established in the study region.

3.3.2.1. RJF supply chain with no monetary incentives

In this section, no carbon policy is considered in the supply chain. Eq. (3.1) presents the objective function used in this model to maximize profits through using FT conversion technology. The first two components of the statement represent revenue from selling RJF and coproducts including RDF, naphtha, and electricity. The remainder of the statement represents costs incurred by purchasing biomass feedstock from suppliers, establishing biorefineries, production, transportation. Coproducts are assumed to be sold to customers at the location of biorefineries, and costs related to transporting them are not considered in the model. Table 3.2 demonstrates the notations used in the models.

Table 3.2. Sets, decision variables, and parameters

Indices	Description	Indices	Description
Sets		*Parameters*	
I	Set of suppliers, indexed by *i*	γ^b	Transportation fixed cost of corn stover via truck (*$/tonne*)
K	Set of biorefineries, indexed by *k*	η^b	Transportation variable cost of corn stover via truck (*$/tonne-km*)
E	Set of demand zones, indexed by *e*	γ^m	Transportation fixed cost of RJF via truck (*$/liter*)
J	Set of byproducts, indexed by *j*; naphtha, RDF, and electricity	η^m	Transportation variable cost of RJF via truck (*$/liter-km*)
Variables		ω_j	Selling price of byproduct *j* (*$/liter*)
Y^k	1 if a biorefinery is activated at location k; 0 otherwise	D_e	Annual RJF demand level at demand node *e* (*liter*)
Q_{ik}	Quantity of biomass transported from supply area *i* to biorefinery *k* (*tonne*)	ρ	Production cost of RJF at biorefinery (*$/liter*)
Q_{ke}	Quantity of RJF transported from biorefinery *k* to demand zone *e* (*liter*)	p^+	Buying price of one kg of carbon (CO_2e) in the carbon market ($)
Q_k^j	Quantity of byproduct *j* produced at biorefinery *k* (*liter*)	p^-	Selling price of one kg of carbon (CO_2e) in the carbon market ($)
e^+	Number of carbon credits purchased	e_b	Emission factor of transporting corn stover (*kg CO_2e /tonne-km*)
e^-	Number of carbon credits sold	e_j	Emission factor of transporting RJF (*kg CO_2e /liter-km*)
Parameters		C^{cap}	Carbon capacity allowed for the RJF supply chain (*kg CO_2e*)
π	RJF selling price (*$/liter*)	$e^{acquisition}$	Emission factor of corn stover acquisition (*kg CO_2e /tonne*)
φ	BAP discount rate	$e^{production}$	Emission factor of producing RJF from corn stover (*kg CO_2e /liter*)
β	BCAP discount rate	d_{ik}	Distance from supplier *i* to biorefinery *k* (*km*)
λ	Monetary incentive for PCP program (*$/liter*)	d_{ke}	Distance from biorefinery *k* to demand zone *e* (*km*)
α	Selling price of corn stover (*$/tonne*)	T	Capacity of biorefinery (*tonne*)
a_i	Quantity of corn stover available at supply node *i*	f	Annualized fixed cost of biorefinery (*$*)
θ	RJF conversion rate from corn stover (*liter/tonne*)	V	Annualized variable cost of biorefinery (*$*)
σ^j	Conversion rate of fuel byproduct *j* from corn stover (*liter/tonne*)		

$$\text{Max } Z = \pi \sum_{k\in K}\sum_{e\in E} Q_{ke} + \sum_{j\in J}\sum_{k\in K} \omega_j Q_k^j - \alpha \sum_{i\in I}\sum_{k\in K} Q_{ik} - f\sum_{k\in K} Y^k$$
$$- \rho \sum_{k\in K}\sum_{e\in E} Q_{ke} - \sum_{i\in I}\sum_{k\in K} (\gamma^b + \eta^b d_{ik}) Q_{ik}$$
$$- \sum_{k\in K}\sum_{e\in E} (\gamma^m + \eta^m d_{ke}) Q_{ke} \quad (3.1)$$

Subject to:

$$\textstyle\sum_{k\in K} Q_{ik} \le a^i \quad \forall i \in I \quad (3.2)$$

$$\theta \textstyle\sum_{i\in I} Q_{ik} = Q_{ke} \quad \forall k \in K \quad (3.3)$$

$$Q^j \textstyle\sum_{i\in I} Q_{ik} = Q_k^j \quad \forall k \in K, \forall j \in J \quad (3.4)$$

$$\textstyle\sum_{k\in K} Q_{ke} \ge D_e \quad \forall e \in E \quad (3.5)$$

$$\textstyle\sum_{i\in I}\sum_{k\in K} Q_{ik} \le TY^k \quad \forall k \in K \quad (3.6)$$

$$Y^k = \{0,1\} \quad \forall k \in K \quad (3.7)$$

$$Y^k \ge 0 \quad \forall k \in K \quad (3.8)$$

$$Q_{ik} \ge 0 \quad \forall i \in I, \forall k \in K \quad (3.9)$$

$$Q_{ke} \ge 0 \quad \forall k \in K, \forall e \in E \quad (3.10)$$

Eqs. (3.2) to (3.10) represent the constraints for the RJF supply chain. Constraint (3.2) is a supply constraint for the feedstock availability and ensures the amount of corn stover purchased does not exceed the maximum biomass feedstock available in supplier nodes. Constraint (3.3) presents material flow in the supply chain and ensures the quantity of RJF converted from biomass in a biorefinery is equal to the quantity of RJF leaving the biorefinery to demand nodes. Eq. (3.4) shows the quantity of generated coproducts at each established biorefinery. Constraint (3.5) guarantees the RJF transported from biorefineries to an airport will meet the RJF demand in the

airport. Based on Eq. (3.6), a biorefinery located at location k cannot exceed the designated capacity for the biorefinery. Eqs. (3.7) – (3.10) display the nature and non-negativity of variables applied to the model.

3.3.2.2. RJF supply chain incentivized with PCP

This part provides PCP incentives to the supply chain for each liter of RJF produced by biorefineries. In order to apply the PCP incentives into the model, we added parameter λ to the first component of the objective function in Eq. (3.11). However, the rest of the equation is identical to Eq. (3.1).

$$\begin{aligned}\text{Max } Z = (\pi + \lambda) \sum_{k\in K}\sum_{e\in E} Q_{ke} + \sum_{j\in J}\sum_{k\in K} \omega_j Q_k^j - \alpha \sum_{i\in I}\sum_{k\in K} Q_{ik} - f \sum_{k\in K} Y^k \\ - \rho \sum_{k\in K}\sum_{e\in E} Q_{ke} - \sum_{i\in I}\sum_{k\in K} (\gamma^b + \eta^b d_{ik}) Q_{ik} \\ - \sum_{k\in K}\sum_{e\in E} (\gamma^m + \eta^m d_{ke}) Q_{ke}\end{aligned} \tag{3.11}$$

Subject to constraints (3.2) to (3.10).

3.3.2.3. RJF supply chain incentivized with BCAP

This section employs BCAP to incentivize the supply chain, with all components in Eq. (3.12) identical to those in Eq. (3.1), except for the monetary incentives to purchase corn stover (discounts on corn stover pricing) in the third component.

$$\begin{aligned}\text{Max } Z = \pi \sum_{k\in K}\sum_{e\in E} Q_{ke} + \sum_{j\in J}\sum_{k\in K} \omega_j Q_k^j - (1-\beta)\alpha \sum_{i\in I}\sum_{k\in K} Q_{ik} - f \sum_{k\in K} Y^k \\ - \rho \sum_{k\in K}\sum_{e\in E} Q_{ke} - \sum_{i\in I}\sum_{k\in K} (\gamma^b + \eta^b d_{ik}) Q_{ik} \\ - \sum_{k\in K}\sum_{e\in E} (\gamma^m + \eta^m d_{ke}) Q_{ke}\end{aligned} \tag{3.12}$$

Subject to constraints (3.2) to (3.10).

3.3.2.4. RJF supply chain incentivized with BAP

In this section, the supply chain is incentivized using BAP, with each component in Eq. (3.12) being identical to those in Eq. (3.1), except for monetary incentives that are factored into the fourth composite component, including costs related to capital and operational costs at biorefineries.

$$\begin{aligned}\text{Max } Z = \pi \sum_{k\in K}\sum_{e\in E} Q_{ke} + \sum_{j\in J}\sum_{k\in K} \omega_j Q_k^j - \alpha \sum_{i\in I}\sum_{k\in K} Q_{ik} \\ - (1-\varphi)\left(f\sum_{k\in K} Y^k + \rho \sum_{k\in K}\sum_{e\in E} Q_{ke}\right) \\ - \sum_{i\in I}\sum_{k\in K} (\gamma^b + \eta^b d_{ik}) Q_{ik} - \sum_{k\in K}\sum_{e\in E} (\gamma^m + \eta^m d_{ke}) Q_{ke}\end{aligned} \tag{3.13}$$

Subject to constraints (3.2) to (3.10).

3.3.2.5. RJF supply chain incentivized with cap-and-trade policy

This section considers cap-and-trade carbon policy for emissions created by the RJF supply chain. Cap-and-trade policy considers a carbon capacity for the supply chain, while it also allows trading unused carbon credits. In other words, with a capacitated emission level in a supply chain, the network might either sell unused carbon emissions or purchase more carbon credits to successfully satisfy its demands. In the objective function presented in Eq. (3.14), e^+ and e^- are defined as the quantity of carbon credits purchased and sold, respectively. Eq. (3.15) ensures the carbon generated throughout the supply chain does not exceed the carbon cap considered for the supply chain. However, if needed, the capacity could be increased by purchasing carbon credits.

$$Max\ Z = \pi \sum_{k\in K}\sum_{e\in E} Q_{ke} + \sum_{j\in J}\sum_{k\in K} \omega_j Q_k^j - \alpha \sum_{i\in I}\sum_{k\in K} Q_{ik} - f\sum_{k\in K} Y^k$$
$$- \rho \sum_{k\in K}\sum_{e\in E} Q_{ke} - \sum_{i\in I}\sum_{k\in K} (\gamma^b + \eta^b d_{ik}) Q_{ik}$$
$$- \sum_{k\in K}\sum_{e\in E} (\gamma^m + \eta^m d_{ke}) Q_{ke} - [p^+ e^+ - p^- e^-] \quad (3.14)$$

Subject to constraints (3.2) to (3.10) and

$$e^{acquizition} \sum_{i\in I}\sum_{k\in K} Q_{ik} + e^{production} \sum_{k\in K}\sum_{e\in E} Q_{ke} + \sum_{i\in I}\sum_{k\in K} e_b d_{ik} Q_{ik}$$
$$+ \sum_{k\in K}\sum_{e\in E} e_j d_{ke} Q_{ke} + e^- \leq C^{cap} + e^+ \quad (3.15)$$

3.4. Results and discussion

In this section, we first define the optimal structure of the RJF supply chain network, including the number and location of biorefineries (strategic decisions), as well as the material flow between the various supply chain components (tactical decisions). Afterwards, application of the four incentive policies on profitability of the supply chain is discussed. We assume the minimal incentive to commercialize RJF production is the level that reduces profit losses to zero. Finally, the impacts of changes in various parameters of the supply chain on its profitability are discussed.

3.4.1. Supply chain analysis with no monetary incentives

The results showed that 10 biorefineries in ASDs 1710, 1720, 1750, 1850, 2690, 2750, 2790, 2910, 2960, 5590 were required to be established to meet the demand in the airports. In terms of the biomass feedstock necessary to supply the biorefineries, 28.96 million tonnes of corn stover were required to create the desired RJF. However, the region's potential biomass might result in 44.44 million tonnes of feedstock, which could provide 6,417 million liters per year (MLPY) of RJF. Due to the blending limitations, the airports could only refill their airplanes with

up to 50% of their capacity. Therefore, only 4,180.42 million liters RJF was projected to be supplied to the airports in the region. The optimal assignments of the supply and demand nodes to the activated biorefineries are shown in Table B2.

According to the findings, the supply chain resulted in a profit loss of $481.65 million, which equates to a profit loss of $0.12 per liter. As shown in Figure 3.3, the majority of supply chain revenue (46%) could be attributed to the selling of RJF, while the lowest revenue share (15%) could be attributed to the sale of power generated during the manufacturing process.

Supply chain costs include operational costs (OPEX), capital costs (CAPEX), transportation costs, and purchasing cost of biomass feedstock, where operational costs constitute the largest portion of overall costs. In terms of transportation costs, 25.53% and 41.48 % of the total transportation cost was allocated to fixed and variable transportation costs for transporting corn stover, while 0.22% and 32.78% of the total transportation cost was allocated to fixed and variable transportation costs for transporting RJF from biorefineries to airports.

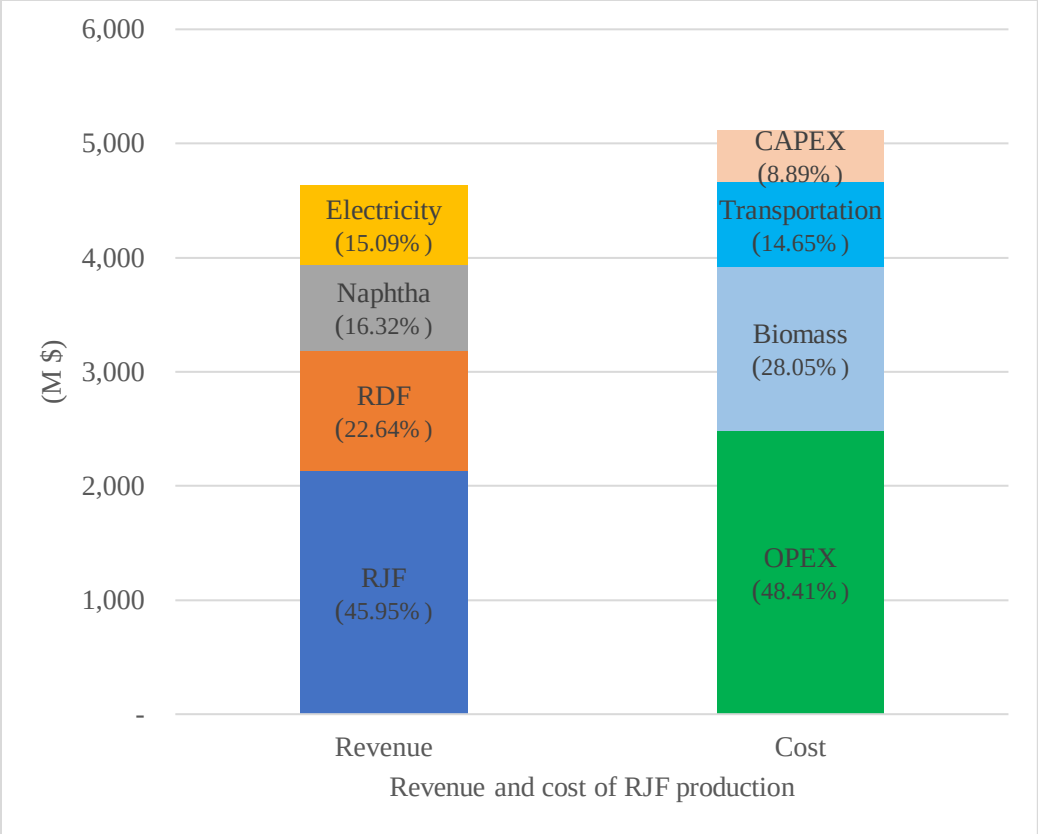

Figure 3.3. Total revenue and cost breakdowns for producing RJF

Also Figure 3.4 shows the spatial configuration of the optimized RJF supply chain network including the location of farms and their potential to supply the supply chain with available corn stover, location of activated biorefineries, and location of the supported airports. According to the results, the 10 activated biorefineries wished to be located in ASDs where there was a balanced distance between biorefineries and airports, as well as between farms and refineries. Thus, the model allocated biorefineries to ASDs where biomass feedstock was abundant in their vicinity, while simultaneously reducing transportation costs between biorefineries and supported airports. It should be noted that due to the higher transportation costs to transport biomass feedstock from western part of the region, the model decided not to supply the activated biorefineries with corn stover from ASDs in those regions. The ASDs that did not supply the biorefineries are differentiated from supplying ASDs with hatched lines. It should also be stated that only 18% of

the available corn stover in ASD 4630 was utilized to supply the RJF production in the supply chain (illustrated with crosshatched lines in Figure 3.4).

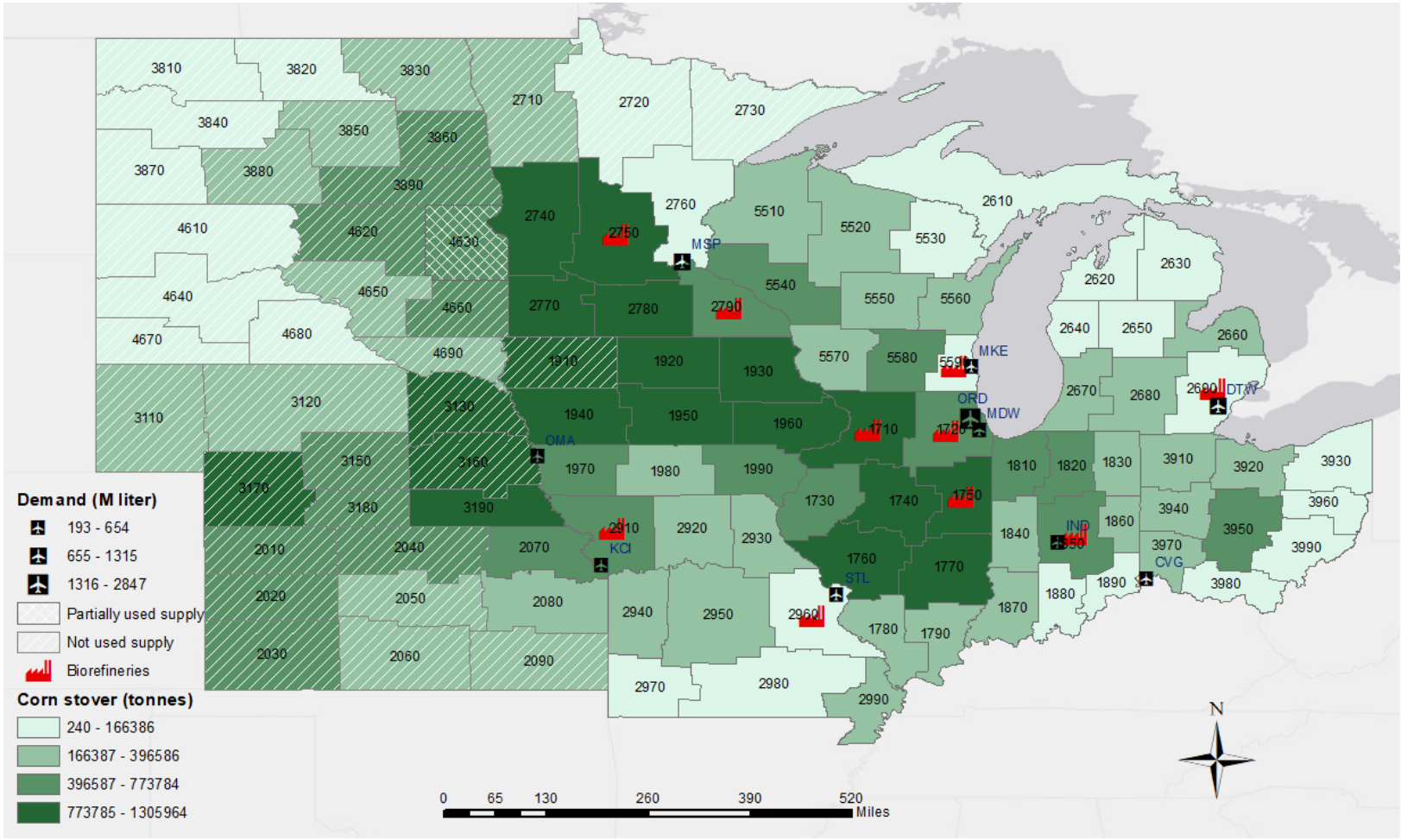

Figure 3.4. Configuration of the RJF supply chain for the base model

3.4.2. Supply chain analysis with application of different monetary incentives

In this section, we provide the results regarding the application of various monetary incentives, including PCP, BCAP, BAP, and cap-and-trade carbon policy, on the RJF supply chain profitability.

3.4.2.1. Supply chain incentivized with PCP

PCP could allocate direct monetary incentives to each liter of produced RJF. PCP incentives were considered to cover all kinds of costs in the supply chain including purchasing costs of the biomass feedstock, transportation cost, and capital and operational costs. Figure 3.5 shows the impact of PCP incentive programs on reducing supply chain costs. By having PCP incentive programs cover 9.04% of its total costs, the supply chain could achieve breakeven. The point where the supply chain revenue starts to exceed the costs is called the breakeven point.

Since monetary incentives could also be employed to other biofuels produced along RJF, including RDF and naphtha, we calculated the quantity of monetary incentives that could be applied to the total amount of biofuel produced. The required incentive is referred to as the inclusive incentive (Ebrahimi et al., 2022). According to the results illustrated in Figure 3.5, the supply chain needed $0.12 incentive per liter of RJF produced, while the quantity of inclusive monetary incentives to obtain profitability was $0.06.

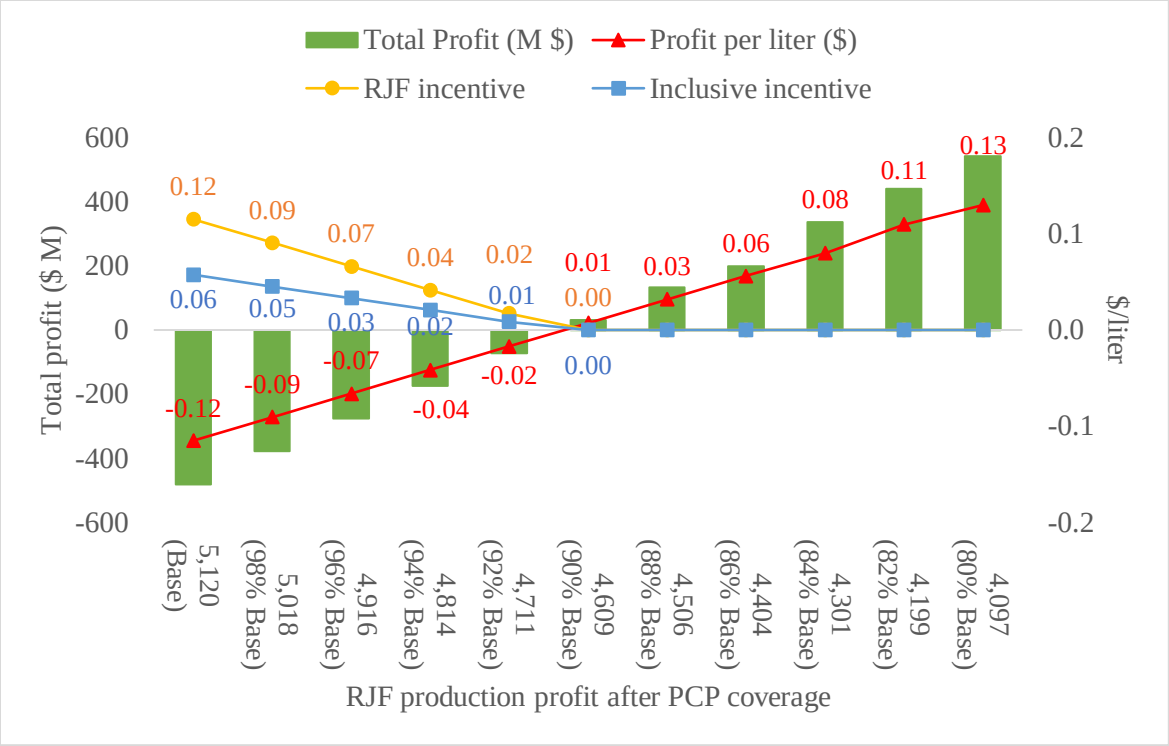

Figure 3.5. RJF supply chain profit, with regard to various PCP incentive scenarios

3.4.2.2. Supply chain incentivized with BCAP

In this section, we included a BCAP monetary incentive that could be applied to costs associated with purchasing corn stover from farmers. The results related to applying BCAP to the RJF supply chain profits are illustrated in Figure 3.6. The results showed that the RJF supply chain could achieve the commercialization level where 33.53% of the costs related to purchasing corn stover was covered by the incentive program. A greater percentage of the costs covered by the incentive program compared to the PCP program is due to a lower share of the costs associated with the purchase of biomass feedstock compared to the total costs in the supply chain.

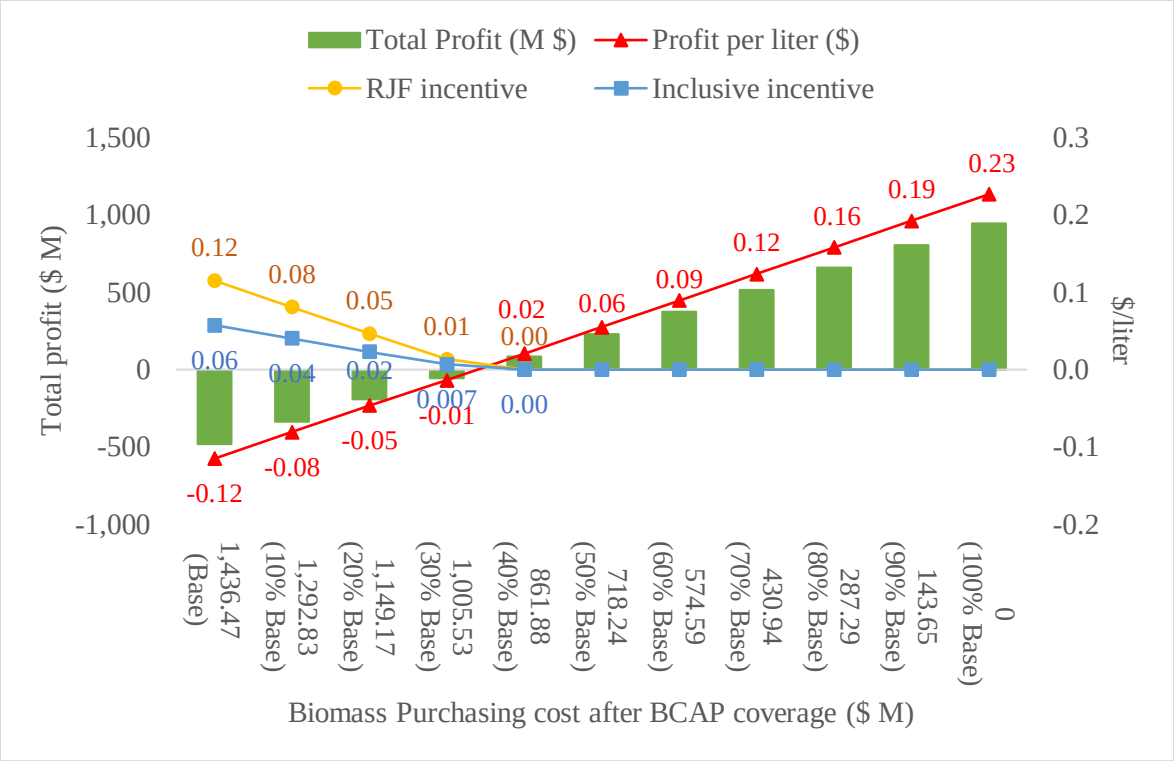

Figure 3.6. RJF production profit, with regard to various BCAP incentive scenarios

3.4.2.3. Supply chain incentivized with BAP

The costs associated with the manufacturing aspect of the supply chain could be compensated by BAP as an incentive program. The costs include fixed capital costs and operational costs to produce RJF. According to the results, presented in Figure 3.7, the BAP incentive program could potentially reduce the profit loss to the commercialization level by covering at least 16.64% of the capital and operational costs in the supply chain. The high percentage of capital and operating costs (57.3%) in the supply chain is the cause for the BAP program's low coverage rate in reaching commercialization. We also considered the PCP incentives as a complementary incentive program to cover the remaining costs of the supply chain.

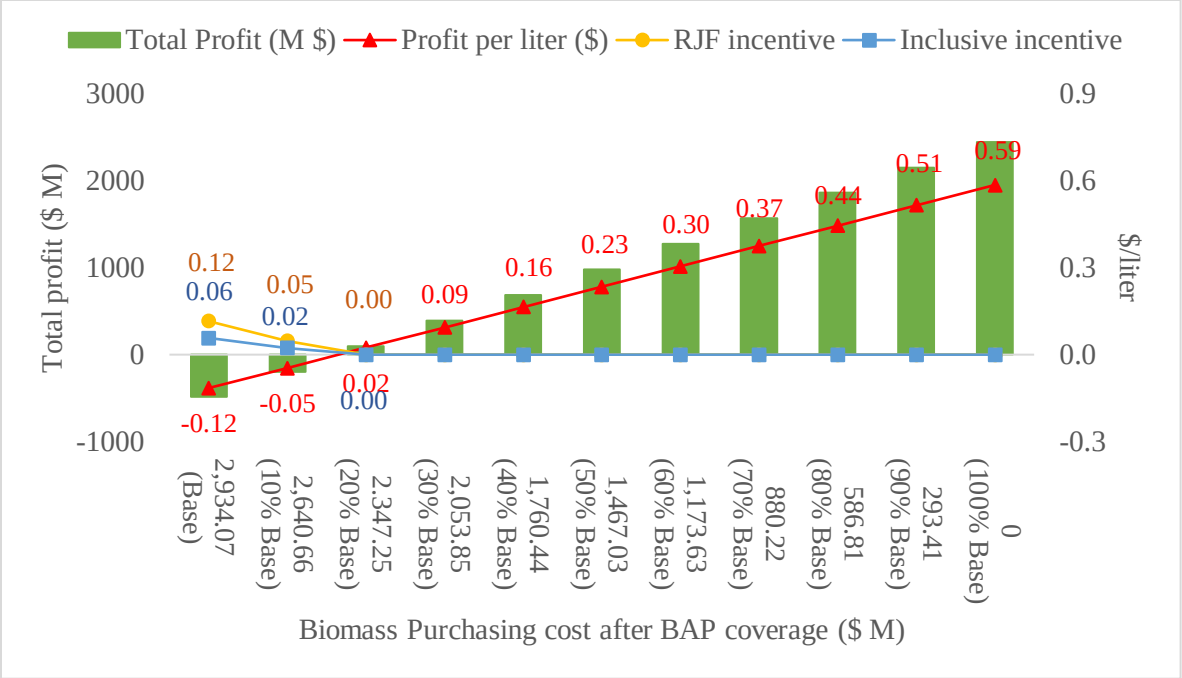

Figure 3.7. RJF supply chain profit, with regard to various BAP incentive scenarios

3.4.2.4. Supply chain incentivized with cap-and-trade

Via implementing a cap-and-trade policy, we consider a carbon capacity for the carbon generated through the supply chain. The supply chain players can sell the unused amount of carbon emissions or buy additional carbon emission credits. Since RJF production is expected to generate less carbon emissions compared to the production of conventional jet fuel, we expect that the RJF supply chain would have unused amount of carbon emissions to be sold. This could ensure that the carbon policy is an efficient mechanism for incentivizing RJF production and assisting it in achieving commercialization.

After implanting the carbon policy, it could be concluded that the 10 biorefineries were needed to fulfill the demand in airports. We considered the purchasing and selling price to be $0.22 per kg of CO_2 produced (H. Huang et al., 2016). The amount of CO_2 generated throughout the supply chain's activities was 446,909.58 tonnes. We established the baseline capacity for carbon emission generation based on the quantity of CO2 that might be produced by producing the same

amount of traditional jet fuel. For the production of fossil-based jet fuel, we considered an emission rate of 3.08 kg CO2 per liter (de Jong et al., 2017). Additionally, we assumed that by reducing one additional kg of CO_2, the supply chain could earn $0.22 (J. Huang et al., 2020). We examined the policy under four different scenarios where the carbon allowance by the RJF supply chain was capacitated to various levels with regard to the carbon generation for producing the same amount of conventional jet fuel. The carbon allowance levels were set to 100%, 75%, 50%, and 25% of the level of carbon generation in conventional jet fuel production. The results are illustrated in Table 3.3. Findings showed that if carbon emissions were capacitated at least by the level of 20% of the carbon emission generated from conventional jet fuel production, the RJF supply chain might become profitable.

If the supply chain could set the carbon cap in the supply chain to the capacity of total carbon emissions made by generating conventional jet fuel, it might end up with a profit of $0.5 per liter of RJF produced. Comparing the results related to the profit loss concluded from the base model with cases having monetary incentives from cap-and-trade policy employed, one could verify the significant impact of implementing the policy on incentivizing RJF production. Table 3.3 depicts the effects of implementing a carbon cap policy on supply chain profitability, demonstrating that the policy has the potential to increase supply chain profitability by 65% (from -$0.12 to $0.53 per liter).

Table 3.3. Supply chain performance under cap-and-trade policy

	Carbon cap with regard to emission created by fossil-based jet fuel				
	Base	25%	50%	75%	100%
Total profit ($ M)	-481.65	126.59	826.27	1,526.82	2,210.26
Sold carbon credit (Mg)	0	2,795	6,013	9,236	12,442
Profit per liter ($)	-0.12	0.03	0.19	0.37	0.53

3.4.3. Supply chain analysis with regard to changes in parameters

In this section, we evaluated the effect of changing various model parameters on supply chain profitability. Figure 3.8 indicated that lowering the demand fulfillment rate could necessitate relatively lower monetary incentives to commercialize RJF manufacturing. However, given the social costs of using conventional jet fuel, creating more RJF and its associated social and environmental advantages may balance the impact of additional monetary incentives required for greater demand fulfillment rates.

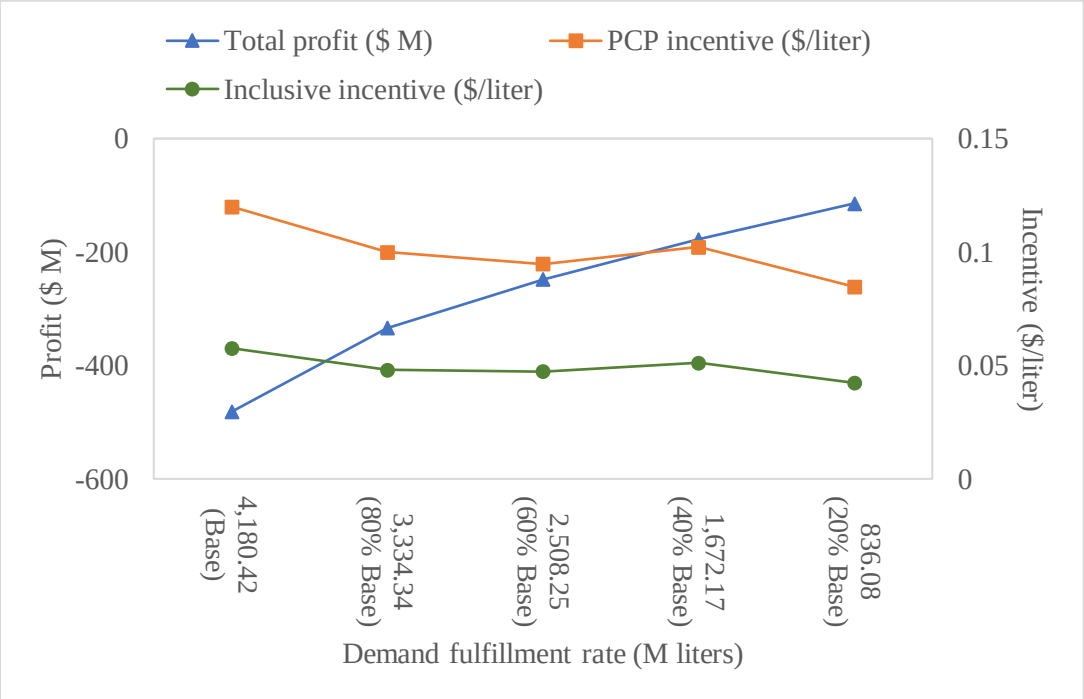

Figure 3.8. The effects of different demand fulfillments rates on the RJF supply chain profitability and incentive payments

We also investigated the impact of changing biofuel prices on profitability of the RJF supply chain. Based on the data from EIA (EIA, 2021), the lowest average price for conventional jet fuel was attributed to 2020, at 1.293 $/gallon, while the highest average price was assigned to 2012, at 3.104 $/gallon. Comparing the base price ($0.51 per liter) with the maximum and minimum prices experienced through recent years, it could be concluded that the jet fuel price fluctuated between 30% less and 60% higher than the base price. If biofuel prices rise by 60% above the basis price, the supply chain could become profitable, resulting in a profit of $0.45 per liter of RJF produced, whereas biofuel prices fall by 30% below the base price, resulting in a profit loss of $0.40 per liter of RJF produced. It could also be concluded that if biofuel prices (RJF, RDF, and naphtha prices) increased by 12% over the base case, the supply chain could become profitable.

3.5. Conclusion

Commercialization of RJF can be highly dependent on the lower cost of the supply chains that can efficiently produce the required RJF to meet the demand in airports. Using proper biomass that is abundantly available and does not put a threat on food and feed production is essential. Furthermore, RJF production can cost higher compared to the production of fossil-based jet fuel. In this study, using MILP, we designed a supply chain that had access to large resource of biomass feedstock (corn stover) that did not compete with any food resources. The study investigated the application of four different monetary incentives on profitability of the supply chain. From the results, we could conclude that all the studied incentives could make the supply chain profitable. It is worth mentioning that while the three monetary incentives of PCP, BCAP, and BAP were purely aimed to incentivize the supply chain with covering various costs, the cap-and-trade policy offered monetary incentives that could be earned over selling unused carbon credits (with regard

to carbon capacity allowed). It could also be concluded that a lower coverage share of PCP (9.04 percent) was required to attain the commercialization threshold when compared to other analyzed monetary incentives. Other monetary incentives in terms of their minimum coverage share to become profitable could be listed as BAP with 16.64%, cap-and-trade capacitated on 20% of the carbon generated through producing conventional jet fuel, and BCAP with covering 33.53% of the costs related to purchasing corn stover. It should be noted that all the incentive programs were aimed at covering the same amount of costs of the supply chain. However, they differed based on the types of costs they covered (total costs, biomass purchasing costs, operational costs).

From policy and managerial standpoint, results from this study could help producers find out the potential of each incentive program to commercialize the production. Furthermore, the discussed commercialization potential may inspire policymakers to provide assistive programs, which may result in increased interest in generating RJF and accelerate RJF production. Furthermore, due to the high sensitivity of the RJF supply chain's profitability to changes in the biofuel price and considering the increase in the oil price (which can affect biofuel price), it is expected that price increase will result in a profitable RJF supply chain, even without application of the offered monetary incentives.

Future studies can be related to the consideration of multiple biomass feedstock for producing RJF in the Midwest region. Considering uncertainties of the supply chain parameters in the model through using stochastic programming could also be a way to proceed this study.

4. A DECISION SUPPORT FRAMEWORK TO ASSESS SPEEDING CRASH RISK

4.1. Abstract

Speeding is a common contributing factor to traffic crashes. It contributes to a third of fatal crashes in the United States and is a critical risky behavior for drivers. Due to the limited budgets received by states to improve traffic safety, they must identify high-risk regions that can be prioritized to receive safety-related funding. Speeding crash risk can vary among regions. Therefore, identifying regions with the highest speeding crash risk enables road managers to balance and arrange corresponding budget allocations. Failure modes and effects analysis (FMEA) was used to assess speeding crash risk. A localized risk assessment of the speeding crashes was demonstrated for North Dakota counties. Local experts' opinions determined thresholds to calculate risk priority number (RPN). Additionally, an innovative preference approach was employed to rank the duplicate RPN values. A comparison study was conducted to validate the effectiveness of incorporating detectability risk and localized degrees of risk parameters in evaluating the speeding crash risks. The findings equip decisionmakers and road managers with an effective tool to prioritize high-risk counties in receiving safety budgets. Due to its generality, the new framework can be adapted for a wide range of applications in evaluating risks of various crash types.

4.2. Introduction and literature review

Traffic crashes and their related consequences, such as fatalities, injuries, and economic loss, remain critical. Road managers work relentlessly to find approaches to reduce them. Speed is one of the most important contributing factors to many crashes as it can affect crash risk and severity (Castillo-Manzano et al., 2019). Speeding not only increases the severity of a crash but can also affect the risk of having other vehicles involved (Aarts & van Schagen, 2006). It also

reduces a driver's ability to control safely and react quickly to a dangerous situation. Almost a third of US fatal crashes are considered speeding-induced crashes (Fitzpatrick et al., 2017). Speeding is defined as an attribute related to driving behaviors that refers to two modes of speeding: driving too fast for conditions and exceeding posted speed limits (Bagdade et al., 2012). According to the National Safety Highway Traffic Safety Administration (NHTSA), speeding can result in consequences such as a higher probability of losing control of a vehicle, reduced effectiveness of occupants' protection equipment, increased fuel consumption, more severe injuries and fatalities, and increased stopping distance after detecting a danger. Speeding is a complicated issue, involving driver behavior, vehicle performance, roadway characteristics and design, posted speed limits, and enforcement activities.

A primary objective of a road safety management study is determining crash risk within the covered area (Shah & Ahmad, 2020). In the United States, an interdisciplinary approach termed speed management planning involving engineering, enforcement, education, and emergency services is incorporated to counteract speeding-related crashes (Bagdade et al., 2012). Bagdade et al. (2012) introduced four steps for the speed management process, which initiated with identifying locations of speeding issues.

Addressing safety issues such as speeding can be very challenging to transportation agencies because they face tight budgets and few tools in implementing road safety assessments (Bagdade et al., 2012). Road agencies prioritize high-risk regions to best direct funding to serve safety needs. Thus, they would benefit from a systematic assessment tool that reliably identifies areas with the highest priority based on speeding crash risk. The results from this demonstration of a holistic risk assessment approach can be used as a starting point for more detailed studies.

Frequency, severity, and detectability before occurrence are the risk parameters that can be used to compare various crash risks. Numerous attempts have explored the frequency and severity of crashes (Delen, Sharda, & Bessonov, 2006; Alkheder, Taamneh, & Taamneh, 2017; Abdulhafedh, 2016; Xie, Lord, & Zhang, 2007; Geedipally, Gates, Stapleton, Ingle, & Avelar, 2019; Delen, Tomak, Topuz, & Eryarsoy, 2017; Behbahani, Amiri, Imaninasab, & Alizamir, 2018). However, most studies focused on finding the frequency and severity of different types of crashes in very limited areas such as a specific length of a route, by studying the potential attributing factors in crashes such as road characteristics, drivers, vehicle type, or environment (microscopic level crash studies).

Hotspot identification methods have also been used to determine the locations with high crash risk. Ryder, Gahr, Egolf, Dahlinger, & Wortmann (2017) used a decision support system (DSS) that informed drivers about high-risk crash hotspots. Al-Kaisy, Ewan, & Hossain (2019) used an index to find the highest crash risk sites. The index identified hazardous locations utilizing highway geometry, traffic exposure, roadway features, and crash occurrence in a case study in Oregon. Applying an empirical Bayes sliding window technique in a geographic information system (GIS) environment, Qin & Wellner (2011) identified the high crash risk locations in South Dakota. Chen, Chen, & Anderson (2013) used the same method to find locations with a high risk of crashes.

Several studies were aimed to find regions with the highest crash risk. Shen, Hermans, Brijs, Wets, & Vanhoof (2012) used data envelopment analysis (DEA) to evaluate traffic safety in 27 European countries. Applying clustering analysis, they determined best-performing and under-performing countries with regard to traffic safety outcomes. Shah et al. (2018) used a similar

approach in assessing road safety risk where they used DEA to calculate and rank the road safety risk levels in Asian countries.

Even though previous studies have investigated crash risk through various methods, they only incorporated the occurrence probability of events and the severity of the consequences. According to Wan et al. (2019), reliance on only two risk parameters (occurrence and severity) would inevitably result in misleading information from the risk analysis. Additionally, distinguishing various risks based on their safety levels suffers from loss of useful information if other important risk parameters are not considered in evaluating the risks (Wan et al., 2019). Wan et al. (2019) used FMEA to analyze the associated risks where visibility of the system was added to the aforementioned risk parameters in the assessment. Since the impacts of detecting speeding crash risk and the risks' visibility in reducing the number of crashes and speeding behavior had already been highlighted by transportation agencies, the application of the method to achieve a more realistic crash risk analysis seemed promising.

FMEA is well-known as a structured, systematic, and proactive approach to analyzing system failures (Xu et al., 2020). FMEA ranks risks according to RPN, a multiplication of three risk parameters (namely, failure occurrence likelihood (O), consequence severity (S), and the likelihood of the failure being undetected (D)) (Alyami et al., 2019). The method identifies and ranks the failure modes (potential or existing risks) in a system to allocate scarce resources to the most severe risk items (Liu et al., 2013).

Despite the popularity of the method in analyzing risks, FMEA is not without shortcomings. One shortfall is related to the duplicate RPNs produced by different risk parameters that can hinder the ranking process and provide misleading results to decisionmakers (Wan et al., 2019; Ciani et al., 2019; Mandal and Maiti, 2014). Furthermore, the scale defined to assess risk

parameters for different types of risks and in various regions can be different, which requires the application of local estimations to analyze the risks (Alyami et al., 2019), while predefined risk degrees in FMEA to evaluate risk parameters may not exactly reflect risk parameters' severities in a system.

This study introduces a novel framework to facilitate FMEA application in speeding crash risk analysis. It incorporates the Delphi method to reach consensus on the evaluation levels of the risk parameters in FMEA and employs an innovative preference approach to effectively rank the risks. Using this analysis, limited resources can be reallocated and rebalanced more effectively. In addition to discovering the overall speeding crash risk for the studied regions, the proposed approach results in important information regarding risks related to the occurrence, severity, and detectability of speeding-related crashes. Additionally, to reach a localized consensus on the evaluation levels of risk parameters in FMEA and obtain a realistic risk analysis, the Delphi method was employed. To validate the framework's practicality, the model was applied to assess the risk of speeding-related crashes in 53 counties in North Dakota. The results will allow road safety managers to systematically identify areas with the highest speeding crash risk.

The expected contributions from this research, compared to the previous work, primarily lie in that:

- For the first time, a holistic risk assessment approach is used, incorporating the three risk factors of occurrence, severity, and detectability to rank speeding crash risk.
- It uses the Delphi method to obtain localized severity levels of risk parameters to be used in calculating RPN.
- It develops a new preference algorithm to effectively rank risks with equal values.

Methodologically, this approach can be employed to analyze safety big data and identify regions with the highest risk to prioritize scarce resource allocations. The remainder of this paper proceeds as follows: 1) Section two introduces the framework and the theoretical dimensions of the research in detail, 2) Section three presents the results, 3) Section four provides a comprehensive discussion of the results, and 4) Section five provides a conclusion of the research including a concise summary and critique of the findings.

4.3. Methodology

This study uses FMEA to evaluate speeding crash risk. However, to incorporate experts' opinions into the ranking process, the Delphi method is employed within FMEA. Finally, utilizing a newly developed preference algorithm, the final ranking for each risk is obtained. The three analytical phases of the framework are explained in the following subsections.

4.3.1. Quantification of risk factors for each risk using FMEA

FMEA is a widely used technique, usually applied to identify and eliminate/reduce known or potential risks. The method can enhance the reliability and safety of complicated systems, providing managers with information to make effective decisions (Liu et al., 2013). The first step in implementing this method is identifying the failure modes (risks) in the system. This study defined the various risks as speeding crash risk in each ND county. After the risks have been defined, evaluating the severity level of risk parameters corresponding to each risk is the next step. The risk parameters include occurrence risk, severity risk, and detectability risk. A high occurrence level means a high probability of a risk happening, a high value of severity risk implies the heightened effect of the risk, and a high value of detectability risk refers to a high probability of the risk being undetected before occurrence. As presented in Eq. (4.1), the risk priority number (RPN), which includes the overall risk values, results from multiplying the risk factors. The main

goal of FMEA is to measure and prioritize the risks with respect to the RPN values, where the results can lead managers to a more effective assignment of limited resources. The RPN is expressed as:

$$\mathrm{RPN}_i = O_i \times S_i \times D_i \tag{4.1}$$

where O_i is the probability of failure *i*, S_i is the severity of failure *i*, D_i is the detectability of failure *i*, and *i* refers to the county for which we are evaluating the crash risk.

As a risk factor, each county's occurrence risk is calculated by dividing the number of speeding crashes in the county by the county's vehicle miles travelled (VMT). The severity of crashes in each county was obtained from a crash database for 2015 through 2018 (inclusive). Eq. (4.2) calculates the results for the severity of crashes.

$$O_i = \frac{CR_i}{V_i} \tag{4.2}$$

In Eq. (4.2), CR_i denotes the number of crashes due to speeding in county i and V_i refers to the annual average vehicle miles travelled (VMT) in county *i*.

The severity risk of speeding crashes is a function of various types of losses caused by the crashes. Eq. (4.3) is used to calculate the severity risk of the crashes where the coefficients are defined as the average of estimated costs related to each type of loss.

$$S_i = \frac{\sum_j a_j X_{ji}}{V_i} \tag{4.3}$$

where a_j is the weight (comprehensive equivalent cost) defined for severity of injury type *j*, and X_{ji} is the number of type *j* injuries in county *i* from 2015 through 2018. The losses correspond to injuries in several ranges, such as death, disabling injury, evident injury, possible injury, and no injury observed (property damage only). The average comprehensive cost of each injury type, including a measure of the economic cost components and lost quality of life, is illustrated in Table 4.1 (National Safety Council & ANSI, 2017).

Table 4.1. Average comprehensive cost of injuries with respect to their intensity

Injury intensity	Cost
Death	$10,855,000
Disabling	$1,187,000
Evident	$327,000
Possible injury	$151,000
No injury observed	$50,000

Detectability of risks is a significant risk factor that informs managers about the probability of a risk being realized by determining its likelihood of being undetected before a crash happens. Using an innovative index, we calculate the detectability risk. The index is presented in Eq. (4.4):

$$D_i = \frac{CR_i}{C_i} \tag{4.4}$$

where CR_i denotes the number of crashes due to speeding in county i and C_i denotes the number of citations related to speeding in county i, including citations resulting from either speeding crashes or speeding violations with no associated crashes. It is assumed that the speeding crashes are cited by the police at the crash scene, while the number of citations (C_i) refers to the total number of citations spotted by police, either leading to a crash or not. Therefore, the D_i values range between zero and one. The closer to zero, the higher the likelihood of the crash risk being detected. In other words, the equation implies that if the total number of citations in a county approaches the number of crash-involved citations, the risk of speeding crashes becomes less likely to be detected.

4.3.2. Incorporation of the Delphi method to FMEA

After the three risk factors' values have been determined for each county, we have to calculate the RPN for each county. To determine RPNs, values for the risk factors between 1 to 10 associated with the linguistic variables presented in Table 4.2 are needed. Even though the risk levels provided in the table are self-explanatory, some implications from the provided risk level

conversions are explained here. Regarding the occurrence risk, "extremely high" level of the risk relates to a high probability of speeding crashes while "nearly impossible" level conveys a very low possibility. Regarding the severity risk of speeding crashes, the "hazardous" risk level refers to the high costs resulting from a large number of crashes and/or a high ratio of the crashes associated with severe injuries and/ fatalities that result in higher costs.

Conversely, the "none" risk level for severity risk factor implies that the costs associated with the risk in a given county are negligible. Regarding detectability risk, "absolute uncertainty" relates to a situation where speed violations are not detected by police and the likelihood of speeding behavior being detected by the police is very low. On the other hand, the "almost certain" risk level indicates situations where police will certainly detect speed violations.

Table 4.2. Ratings for the occurrence, severity, and detectability risks of speeding crashes

Occurrence risk	Severity risk	Detectability risk	Score
Extremely high	Hazardous	Absolute uncertainty	10
Very high	Serious	Very remote detectability	9
Repeated failure	Extreme	Remote detectability	8
High	Major	Very low detectability	7
Moderately high	Significant	Low detectability	6
Moderate	Moderate	Moderate detectability	5
Relatively low	Low	Moderately high detectability	4
Low	Minor	High detectability	3
Remote	Very minor	Very high detectability	2
Nearly impossible	None	Almost certain	1

However, rescaling the actual values from each risk factor to values between 1 to 10 without considering their local risk degrees may not result in a realistic risk assessment. In other words, the ranking could not necessarily mirror the locally perceived risk levels in the study region. To resolve the issue, this research uses the Delphi method to determine the localized risk degrees of actual values that can be mapped into linguistic variables associated with each risk factor.

The Delphi method is an influential tool that has been widely used to achieve consensus on topics where empirical evidence is insufficient or contentious (Okoli & Pawlowski, 2004). Here, we used the Delphi method to collect experts' estimations of risk degree regarding linguistic variables defined for each risk factor. Specifically, they are asked to share their estimations of high and low levels of the occurrence risk, severity risk, and detectability risk of speeding crashes in ND counties. After having results from the first survey, the average of the responses regarding each risk factor were shared with the survey participants and they were asked to complete the survey again. The participants were questioned about the risk of each risk factor for two risk levels, including the highest and lowest risk degree levels for the risk factors. The average values obtained from the second round of the survey were compared with the average from the first round. Differences less than 10% indicate that consensus has been reached on the value for the risk level while obtaining differences larger than 10% indicates the need for another round of the survey, until consensus is met. A sample of the questionnaire appears in Appendix C.1 and Appendix C.2.

After having the highest and lowest values for each risk factor from the survey, we also needed to have other internal risk degrees between the extremes. The values were determined by considering eight equal intervals between the highest and lowest risk degree levels. Then, each of the ten values extracted from the survey was rescaled into values 1 to 10.

Having the model equipped with the conversion process, the results from actual values for the risk factors could be rescaled to risk degrees ranging from 1 to 10, where one corresponded to the lowest risk level, and ten referred to the highest. After rescaling the risk factors' values, the results were inserted into Eq. (4.1) to calculate RPN. Finally, RPNs represented the speeding crash risk in each county. The higher the RPN for a county, the higher the county's speeding crash risk. Figure 4.1 illustrates how the framework assesses speeding crash risks.

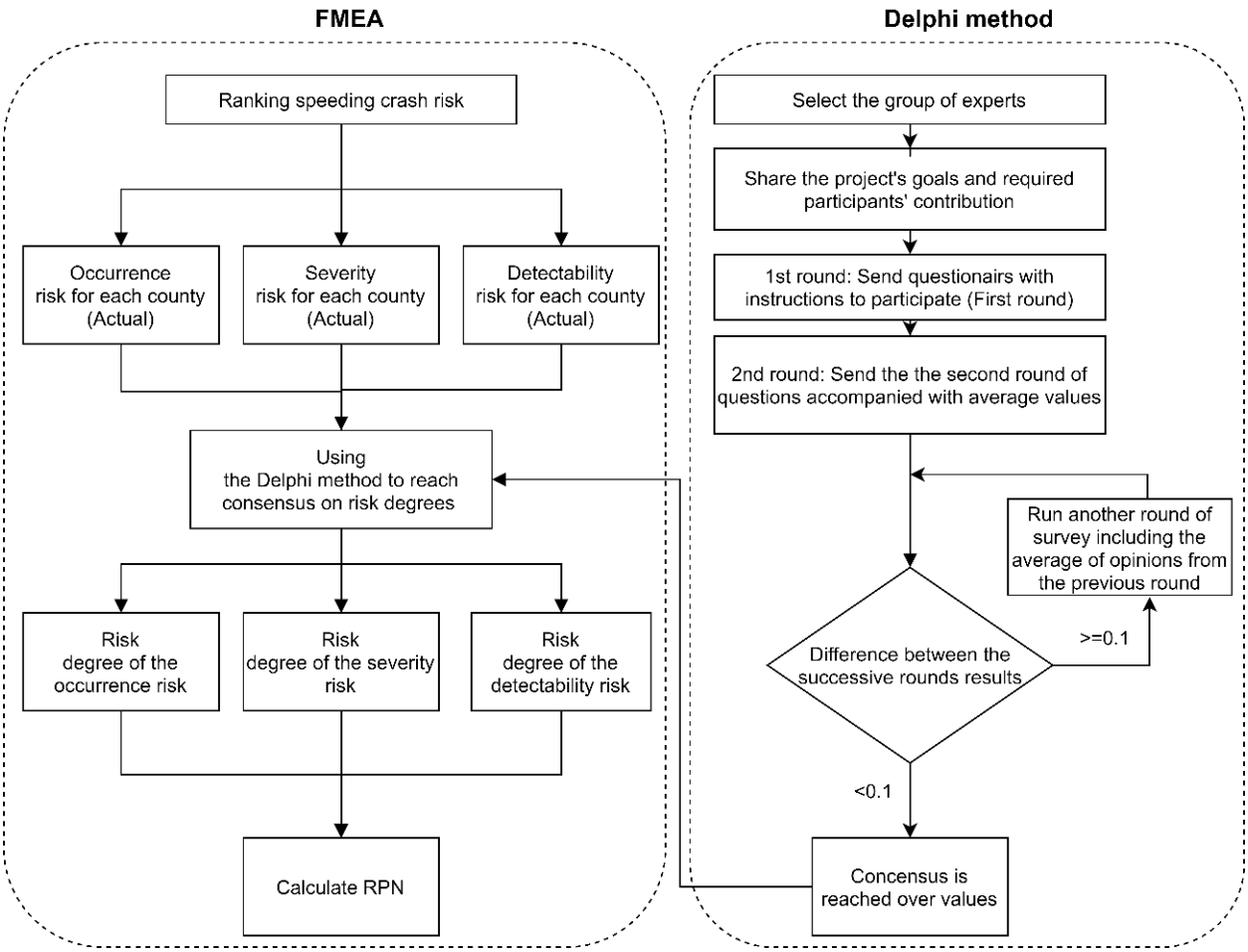

Figure 4.1. The flowchart of the proposed framework

4.3.3. The application of the preference algorithm

As discussed before, FMEA can generate several RPNs with equal values, resulting in multiple ties when ranking by RPN. To address the issue of duplicate RPN values, the model considered an extra procedure that prioritized the risks with regard to higher severity risk, occurrence risk, and lower VMT, respectively. In other words, to rank risks with equal RPNs, first, they would be compared based on their severity risks. We assume that severity risk is the most crucial risk parameter among the three because it reflects the social and financial impacts of the crashes. If one of the risks had a higher severity risk, it would be prioritized with a higher ranking. If the counties also had equal values for their severity risk, they would be compared based on

occurrence risk. The county with a higher occurrence risk would receive priority with a higher ranking. We preferred occurrence risk to the detectability risk as the comparative risk parameter because the occurrence risk would reflect a likelihood directly resulting from historical speeding crashes, while the detectability would refer to the likelihood of speeding behavior that might not necessarily lead to crashes. Finally, there would be other cases for duplicate RPNs in which all the risk factors would be equal. To rank those risks, they would be compared based on their associated VMTs. It is assumed that if two counties with equal risk values also had similar risk parameter values, the risk in the county with smaller VMT would be ranked higher. The logic behind this ranking refers to the fact that, for two counties with equal risk values, the multitude of a given risk value per VMT will be higher for the county with lower VMT. Figure 4.2 illustrates the procedure to rank two given risks with equal RPN values. In this figure, it is assumed that two equally assessed risks are being re-ranked.

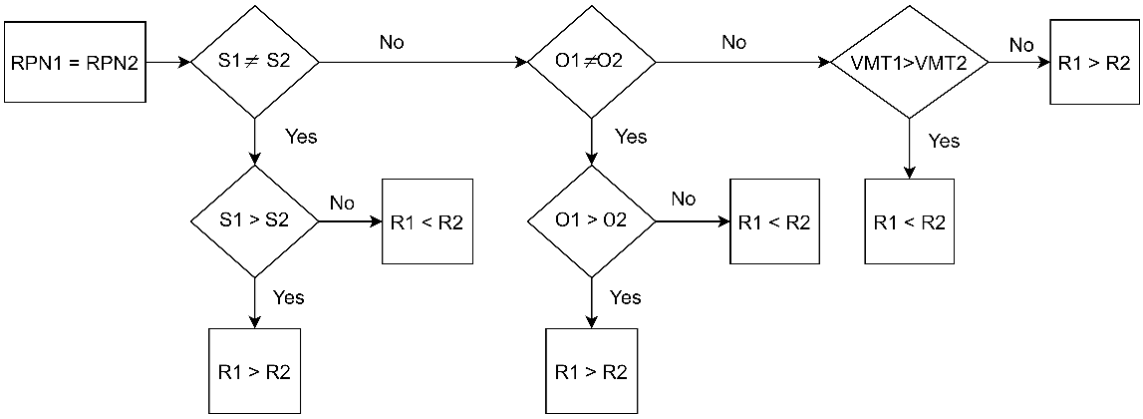

Figure 4.2. The flowchart for ranking duplicate risk values (the preference algorithm)

4.4. Data and study scope

The crash records between the years 2015 and 2018 were obtained from the North Dakota Department of Transportation (NDDOT) in a limited use agreement and aggregated by county. To calculate the occurrence risk, the model incorporated data concerning speeding crashes in ND

counties. Speeding crashes, exceeding the posted speed limit, and being too fast for conditions were recognized as identifying factors to quantify speeding crashes (Fitzpatrick, Rakasi, & Knodler, 2017). Also, to find the severity of crashes and their related injuries, the authors explored occupant injury records for observations between 2015 and 2018, considering crash outcomes that included fatal injuries, other injuries, property damage only, or no injury. The observations used to calculate detectability risk were obtained from the NDDOT citation records for the same period. For the number of speeding crashes used in calculating the detectability risk, the observations identified with speeding as one of the contributing factors or as the major contributing factor were considered.

According to the speed management plan that was developed jointly by the National Highway Traffic Safety Administration (NHTSA), the Federal Highway Administration (FHWA), and the Federal Motor Carrier Safety Administration (FMCSA) in 2014, the accurate role of speeding in crashes can be difficult to determine, and judgment of the investigating law enforcement officer plays an important role in determining the major contributing factor to crashes (Speed Management Program Plan, 2014). Therefore, to counteract the impact of possible misjudgments and underreporting in speeding crashes, all observations for which speeding was identified as a contributing factor to the crash have been counted as speeding crashes, even if speeding was not indicated as the major contributing factor. Data analysis was conducted using SAS Studio 3.8.

To find the severity level of the risk parameters, this research used experts' opinions through a Delphi survey. The survey was conducted in two rounds by sending emails to a group of local speeding/aggressive driving subject matter experts. Three experts participated in the survey. A consensus was reached in two rounds of the survey, finding the risk parameters' degrees.

4.5. Results

FMEA was used to find speeding crash risk in each ND county. To calculate RPNs, the occurrence, severity, and detectability risks were obtained. Subsections (4.5.1 - 4.5.3) present the results related to each of the risk factors. In section 4.5.4, the results from the previous sections are converted to values between 1 and 10 on the basis of the risk levels from the Delphi method. Finally, the overall risk value and ranking for each county, considering the preference algorithm, are provided.

4.5.1. Occurrence risk

Each county's frequency of speeding crashes is standardized by considering the VMT in that county. The number of crashes calculated in each county in the last column of Table 4.3 is based on the number of speeding crashes per 100 million VMT.

Table 4.3. Occurrence risk of speeding crashes in ND counties

County	Frequency	Frequency per 100 million VMT	County	Frequency	Frequency per 100M VMT
Burleigh	2,836	253	Emmons	34	14
Cass	2,232	112	Pierce	30	13
Ward	1,216	78	Dunn	90	13
Grand Forks	994	68	Hettinger	18	12
Stark	747	68	Slope	11	12
Williams	998	52	Cavalier	29	12
Stutsman	469	45	Mountrail	128	12
Morton	533	44	Logan	12	12
Ramsey	127	29	Nelson	32	12
Mercer	101	27	Dickey	26	12
McKenzie	498	26	McHenry	57	12
Barnes	201	25	Billings	41	10
Renville	35	23	Kidder	54	10
Bottineau	79	22	Pembina	49	10
Ransom	46	21	Golden Valley	19	9
Walsh	124	20	Eddy	11	9
McIntosh	22	19	Grant	12	9
Burke	43	18	Griggs	10	9
Richland	192	18	Divide	20	8
Sheridan	19	18	Steele	12	7
Adams	20	17	Benson	28	7
LaMoure	38	16	Towner	10	7
McLean	134	16	Bowman	11	6
Wells	43	15	Oliver	9	6
Traill	125	15	Rolette	20	5
Foster	28	15	Sioux	8	5
Sargent	33	14			

According to Table 4.3, Burleigh had the highest occurrence risk with 253 crashes annually per 100 million VMT, followed by Cass, Ward, Grand Forks, Stark, and Williams. In contrast, Rolette had the lowest occurrence risk.

4.5.2. Severity risk

The severity of speeding crashes was calculated by applying Eq. (4.3), where the costs related to different injury types caused by speeding crashes were calculated based on their associated estimated total costs. The severity of speeding crashes in ND counties from 2015 to 2018 appears in cost per crash in Table 4.4.

Table 4.4. Severity risk of speeding crashes in each ND county

County	No-injury	Fatal	Disabling	Not-disabling (Evident)	Possible/ claimed	Cost per crash ($)
Sioux	5	2	1	2	1	$2,177,455
Oliver	7	1	1	2	2	$1,026,769
Benson	28	2	1	9	1	$668,073
Golden Valley	18	1	4	2	2	$646,630
McHenry	52	3	12	17	6	$620,822
Renville	31	2	6	14	6	$607,898
Billings	47	2	8	4	4	$545,662
McLean	140	7	14	28	23	$529,396
Divide	27	1	5	3	3	$501,897
Rolette	22	1	3	7	9	$456,286
Dunn	128	4	16	17	9	$435,230
Mountrail	163	5	13	28	24	$388,996
LaMoure	36	1	4	12	5	$380,724
Pierce	39	1	1	6	3	$328,140
McKenzie	647	12	55	121	60	$308,963
Kidder	64	1	5	9	7	$278,953
Sargent	25	-	6	14	4	$276,612
Griggs	8	-	2	2	1	$275,308
Slope	7	-	2	3	4	$269,313
Pembina	58	1	2	10	10	$258,136
Mercer	124	2	4	23	18	$250,860
Emmons	38	-	6	10	3	$223,596
Richland	269	3	11	35	34	$214,918
Barnes	295	3	16	31	40	$214,244
Logan	11	-	1	5	1	$195,722
Cavalier	29	-	4	4	7	$194,614
Towner	8	-	1	1	4	$179,857
Steele	11	-	1	3	2	$177,647
Traill	163	1	6	24	14	$173,505
Grant	11	-	1	3	8	$170,696

Table 4.4. Severity risk of speeding crashes in each ND county (continued)

County	No-injury	Fatal	Disabling	Not-disabling (Evident)	Possible/ claimed	Cost per crash ($)
Bottineau	84	-	6	20	15	$161,016
Burke	58	-	5	7	4	$158,486
Wells	63	-	6	2	9	$153,563
Hettinger	16	-	-	9	1	$149,769
McIntosh	22	-	1	5	5	$141,727
Williams	1,579	5	52	168	104	$139,198
Walsh	168	-	10	18	19	$135,000
Ward	1,991	8	44	165	240	$134,319
Nelson	45	-	2	8	2	$132,316
Morton	883	3	15	76	87	$124,539
Dickey	28	-	-	10	1	$123,615
Grand Forks	1,749	6	26	127	155	$120,396
Adams	22	-	-	7	2	$119,065
Stutsman	816	2	14	36	68	$108,085
Stark	1,272	3	14	77	69	$103,401
Ransom	63	-	1	8	7	$101,392
Ramsey	198	-	4	13	27	$94,942
Foster	34	-	-	5	5	$92,955
Bowman	16	-	-	2	3	$90,810
Sheridan	26	-	-	4	1	$89,000
Cass	3,522	2	38	221	295	$88,212
Burleigh	5,150	4	33	188	472	$80,869
Eddy	14	-	-	-	2	$62,625

As depicted in Table 4.4, the highest severity based on estimated costs was for Sioux county, with $2,177,455 per speeding crash. Following Sioux, Oliver's average speeding crash cost is about $1,026,769, which is also considerably higher than that for other ND counties. The lowest average cost was for Eddy county, with an average estimated cost of about $62,625 per speeding crash. Further, the associated average costs for counties Burleigh, Cass, Sheridan, Bowman, Foster, and Ramsey were less than $100,000 per speeding crash.

4.5.3. Detectability risk

According to Eq. (4.4), each county's detectability risk level is calculated by dividing the number of speeding citations issued at crash scenes by the total number of citations. Table 4.5 presents the corresponding results.

Table 4.5. Detectability risk of speeding crashes in ND counties

County	Speeding citations at crash scene	Total speeding citations	Detectability Risk (%)	County	Speeding citations at crash scene	Total speeding citations	Detectability Risk (%)
Billings	22	96	22.92	Bottineau	50	826	6.05
Burleigh	2,047	9,678	21.15	Pierce	19	318	5.97
Stutsman	331	1793	18.46	Bowman	10	179	5.59
McKenzie	338	1946	17.37	Renville	16	292	5.48
Slope	8	47	17.02	Walsh	77	1,485	5.19
Stark	558	3,893	14.33	Foster	15	310	4.84
Barnes	125	897	13.94	Ransom	32	667	4.80
Kidder	27	194	13.92	Mountrail	77	1,618	4.76
Williams	780	5,836	13.37	Eddy	9	195	4.62
Grand Forks	644	5,452	11.81	Hettinger	10	232	4.31
Sheridan	15	138	10.87	Cavalier	20	501	3.99
Burke	33	305	10.82	Sargent	15	399	3.76
McLean	93	896	10.38	Divide	10	281	3.56
Wells	37	375	9.87	LaMoure	16	464	3.45
Richland	104	1,126	9.24	Logan	9	269	3.35
Golden Valley	8	89	8.99	McHenry	25	753	3.32
Dunn	51	592	8.61	Dickey	14	450	3.11
Ramsey	79	925	8.54	Towner	6	211	2.84
Ward	888	10,449	8.50	Griggs	5	176	2.84
Traill	63	801	7.87	Pembina	18	737	2.44
Morton	333	4,283	7.77	Grant	6	264	2.27
Emmons	25	332	7.53	Benson	9	492	1.83
Nelson	18	272	6.62	Steele	3	237	1.27
Cass	1,094	16,809	6.51	Oliver	3	249	1.20
Adams	12	191	6.28	Rolette	8	1,176	0.68
Mercer	70	1,131	6.19	Sioux	1	269	0.37
McIntosh	18	297	6.06				

According to the results, Billings receives the highest detectability risk, where nearly 23% of the total speeding-related citations are associated with crashes. In other words, about 77% of

total speeding citations in Billings are not associated with crashes. This indicates that the likelihood of speeding crashes being detected before their occurrence in Billings was lower than in other ND counties. Sioux and Rolette experienced likelihood levels higher than 99%.

4.5.4. The Delphi method

To calculate the final speeding crash risk, RPNs had to be calculated, where the results would represent the speeding crash risk for each county. However, to determine a localized risk assessment of the risk factors, the Delphi method was conducted. Running two rounds of surveys, the method reached a consensus on the risk levels for each risk factor. Next, the agreed risk level values for the lowest and the highest risk levels of each risk factor were rescaled to values between 1 and 10. The highest surveyed value from the two-round Delphi method for a specific risk factor was set to 10, and the lowest was converted to 1. The averages of the highest and lowest estimated values for each risk factor from the second-round survey are provided in Table 4.6. It should be noted that the internal risk level values between 1 and 10 (2, 3, …,9) were allocated based on the eight equal intervals considered between the lowest and the highest risk values.

Table 4.6. Experts' opinions on the level of risk factors in FMEA

Occurrence risk of speeding crashes	Frequency of speeding crashes per 100M VMT
Highest occurrence risk level	75
Lowest occurrence risk level	5
Severity risk of speeding crashes	Average cost per crash ($)
Highest severity risk level	700,000
Lowest severity risk level	50,000
Detectability risk of speeding crashes	$\frac{\text{Speeding citations at the crash scene}}{\text{Total number of speeding citations}}\%$
Highest detectability risk level	25
Lowest detectability risk level	5

4.5.5. Risk priority number, considering the preference algorithm

Using the values from the Delphi method regarding risk factors, Eq. (4.1) was used to calculate the RPN for each risk. Table 4.7 illustrates the rescaled risk factor values for each county and their associated RPNs and risk rankings. Comparing speeding crash risks among counties, Burleigh followed by Billings and McKenzie were ranked with the highest speeding crash risk, while counties Dickey and Eddy were found to have the lowest speeding crash risk. As expected, the model resulted in multiple duplicates of RPNs that made it necessary to compare the risks with regard to their RPN component risk levels (severity and occurrence) and VMTs. For example, the RPNs calculated for Ward and Stark were 90, putting them in the same ranking. To rank the risks effectively, they were compared according to the guidelines explained by the preference algorithm. First, they were compared based on severity risk. Since the counties had different severity risks and Ward County had the higher severity risk (three versus two), Ward was ranked higher than Stark.

Table 4.7. Risk assessment of speeding crashes in ND counties

County	VMT	RPN	Rank	County	VMT	RPN	Rank	County	VMT	RPN	Rank
Burleigh	280	160	1	Burke	58	36	19	Sargent	59	12	37
Billings	98	144	2	Morton	300	36	20	Nelson	69	12	38
McKenzie	477	120	3	Mercer	95	32	21	Adams	29	12	39
Williams	478	105	4	Wells	71	27	22	Sioux	41	10	40
Ward	275	90	5	Traill	214	27	23	Griggs	28	8	41
Stark	391	90	6	Ramsey	111	24	24	Pembina	124	8	42
McLean	213	84	7	Sheridan	26	24	25	Bowman	45	8	43
Stutsman	263	84	8	Oliver	39	20	26	Logan	26	6	44
Barnes	205	80	9	Pierce	56	20	27	Grant	34	6	45
Grand Forks	364	72	10	Benson	100	18	28	Hettinger	37	6	46
Renville	39	64	11	McHenry	123	18	29	Towner	38	6	47
Golden Valley	51	54	12	LaMoure	58	18	30	Steele	41	6	48
Slope	23	48	13	McIntosh	29	18	31	Cavalier	61	6	49
Kidder	129	40	14	Bottineau	89	18	32	Foster	48	6	50
Cass	499	40	15	Walsh	158	18	33	Ransom	55	6	51
Dunn	173	36	16	Divide	63	14	34	Eddy	30	4	52
Emmons	61	36	17	Rolette	96	14	35	Dickey	56	4	53
Richland	261	36	18	Mountrail	270	12	36				

4.6. Discussion

4.6.1. Distribution of risk parameters and speeding crash risk in ND counties

Regarding the frequency of speeding crashes (occurrence risk), the results indicated that the number of speeding crashes in Burleigh was considerably higher than the number in other counties, while its VMT was almost half of the VMT in the second high-risk county in the list (Cass County). This finding was unexpected and suggested that future studies would be beneficial to investigate the underlying reasons behind the low rate of speeding crashes while having high VMT rates in such counties. Discovering the relationship between the number and severity of speeding crashes, speed limits, speeding behavior, roadway geometry, demographics, and the acquisition rate of safety measurements could also help road managers in high-risk counties

determine the contributing factors in road segments that cause a higher frequency of speeding crashes (Islam & Mannering, 2021).

It was observed that the highest occurrence risk resulted from the most populated ND counties such as Cass, Burleigh, Grand Forks, Ward, Morton, Stark, Williams, and Stutsman. Counties such as Sioux, Rolette, Oliver, and Bowman experienced the lowest frequency of speeding crashes, indicating their speed management strategies for reducing speeding crashes could be investigated as alternatives for counties experiencing a high frequency of crashes. Figure 4.3(a)-3(c) depict occurrence, severity, and detectability risk mapped based on their risk values from 1 to 10 when values 1-3 are labeled low, values 4-6 are labeled moderate, and values 7-10 are labeled high. The results concerning the occurrence risk of speeding crashes are visualized in Figure 4.3(a). It was observed that counties with a high frequency of speeding crashes created semi-clusters in the east, north, west, and center of the state which could be resulted from a spatial correlation between the speeding crash risk in the corresponding counties. Further research might explore the effective speed management strategies in low-risk counties and examine their application to counties with similar geometries, demographics, and infrastructural characteristics, that were identified as high-risk counties.

As mentioned before, the results from this approach can be considered input for regulating the speed management strategy plan in ND counties. More specifically, results from the occurrence risk of speeding crashes can be used to reconsider engineering features in the roadways, such as re-establishing speed limits that balance mobility and safety for all road users, designing roads that enforce desired vehicle speed, and creating self-regulating roadways by adding physical countermeasures. The frequency of the crashes in different counties also informs law enforcement about the places that need more monitoring to ensure drivers' compliance with posted speed limits.

Furthermore, the frequency results could be a starting point for reallocating emergency medical services to affected areas regarding the various occurrence risks in different counties. However, more detailed studies such as assignment problems would be needed to allocate enough resources to the regions at a detailed level (Chen et al., 2013).

The severity of speeding crashes was calculated using the cost estimations for each type of consequence caused by the speeding crashes. Based on the results, it can be concluded that the cost per speeding crash in Sioux and Oliver counties was much higher than in other counties ($2,177,455 and $1,026,769 versus 90th percentile value of $615,653 per speeding crash). The high severity of the crashes could be caused by the two and one fatal crashes in the counties, respectively, while the total number of crashes in those counties was not as high as the number of crashes in other counties. A likely explanation for the results is that the road conditions on some routes in the counties elevate the severity risk of speeding. In contrast, Eddy, Burleigh, Cass, Sheridan, Bowman, Foster, and Ramsey maintained the lowest severity risk of speeding crashes among ND counties with a cost per speeding crash less than $100,000. Despite suffering from a considerably higher number of speeding crashes than other counties, Burleigh and Cass had low severity of speeding crashes. This finding relates to the small number of fatalities and disabling injuries in those counties that can burden high costs on a transportation system. Therefore, it would be reasonable for other counties to follow speed management strategies implemented in counties with lower severity risk, such as Burleigh and Cass. Figure 4.3(b) illustrates a map of ND counties ranked with regard to the severity of speeding crashes. It can be observed that clusters of counties in the northern and western parts encountered higher costs than other counties. The severity risk results suggest considering more detailed studies for counties at high risk to determine if redesigning road features or reallocating emergency services is required.

Considering that speeding citations and control activities play a preventive role in speeding crashes, counties such as Billings, Burleigh, Stutsman, McKenzie, and Slope are experiencing high detectability risk (higher than 17%). A likely explanation for this result is the lack of adequate law enforcement or speed violation detection facilities in those counties. Figure 4.3(c) depicts the distribution of detectability risk in ND counties. The map shows clusters of counties with moderate/high detectability risk of speeding crashes in central and western regions. The results from the detectability risk can inform law enforcement about the effectiveness of their enforcement countermeasures to curtail speeding crashes. Therefore, they could effectively rebalance their personnel and resources to the affected regions with different detectability risk values.

Finally, considering the three risk factors of occurrence, severity, and detectability, Burleigh was identified with the highest speeding crash risk. One recommendation to reduce the speeding crash risks is to identify effective strategies for lowering speeding crashes in counties with low risk of speeding crashes and applying them to counties with similar characteristics. As depicted in Figure 4.3(d), the high-ranking quartile of the speeding crashes consisted of two clusters; one extended from Barnes in the east to Renville in the northwest, and the other included six counties in the west. The clustered structure of the speeding crashes in the high-risk counties can accelerate the implementation of risk mitigation strategies. The FMEA tool for speeding crash risk informs decisionmakers about a data-driven prioritization to be considered in subsequent actions to reduce speeding crash risk.

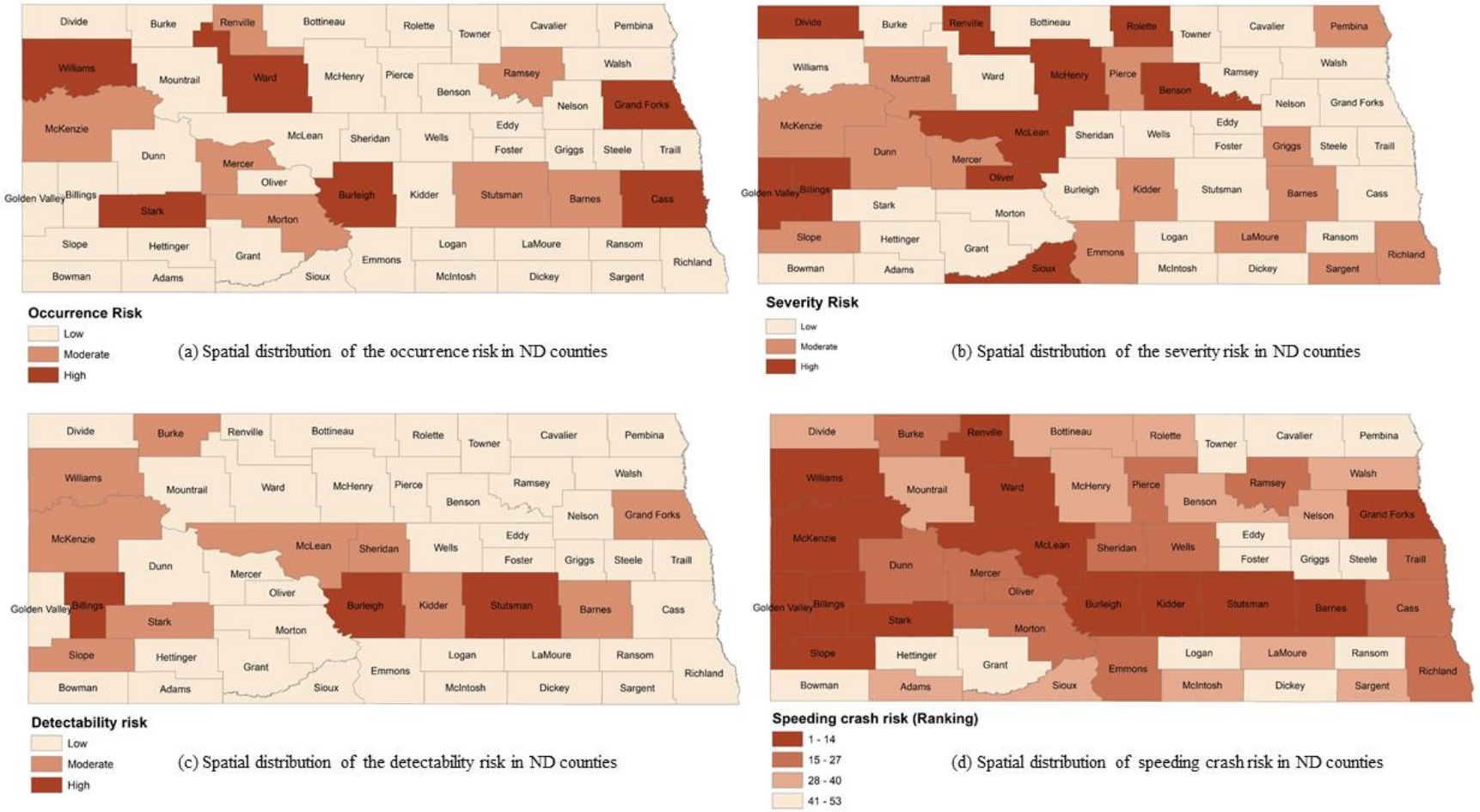

Figure 4.3. Spatial distribution of the risk parameters and risk values in ND counties

4.6.2. Exploring the effect of detectability in the risk assessment results

To illustrate the importance of incorporating detectability in the speeding crash risk assessment model, the results obtained using RPN are compared with the results obtained using the criticality index (Czernakowski & Müller, 1993) which uses only the product of occurrence risk and severity risk. A graph comparing the results from criticality analysis and RPN appears in Figure 4.4. The graph shows the criticality risk values (O×S) in ascending order for ND counties when their corresponding RPN values are also graphed along with the criticality values. As can be observed, adding detectability to the risk assessment method caused changes in risk values and final risk rankings. The observed changes in risk values by RPN show how a high or low detectability risk can affect speeding crash risk rankings for a given county. The highest increases calculated by RPN compared to criticality values were in Oliver with a change of 21 in ranking (from 5 to 26), and Benson, McHenry, and LaMoure with changes of 18 in rankings (from 10 to 28, from 11 to 29, and from 12 to 30).

On the other hand, low detectability risk in some counties caused decreases in the total risk value for some counties when the criticality index was used. The most significant reductions in rankings were observed in Kidder with a change of 24 in ranking (from 38 to 14) and Slope and Sheridan with changes of 22 in rankings (from 35 to 13 and from 47 to 25, respectively). From the results, it can be seen how significant the inclusion of detectability risk is to proper assessment of speeding crash risk. The changes become more important when the budget to be allocated for implementing the risk management programs is very limited and the ranking process will qualify a few high-risk counties to be funded.

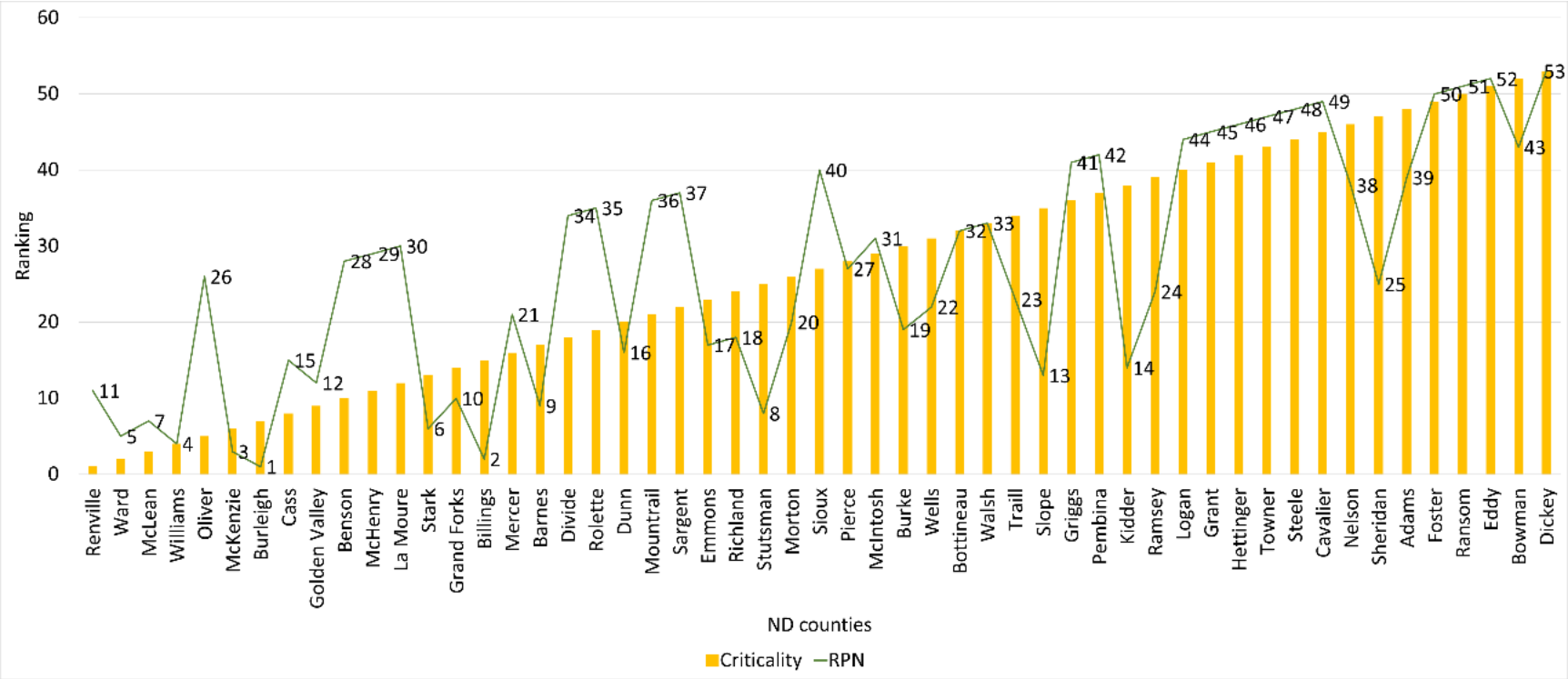

Figure 4.4. Comparing rankings evaluated by RPN and criticality

4.6.3. Exploring the effect of experts' opinions on ranking the risks

Figure 4.5 indicates the rankings resulting from a traditional FMEA method (without using the Delphi method) and the rankings from the modified FMEA method proposed by this study (RPN1 is the method used in this research while RPN2 is from an FMEA approach without incorporating expert opinions through the Delphi method). The comparison is provided to verify the importance of incorporating experts' opinions in the process of speeding crash risk assessment. To calculate the rankings with the traditional FMEA, the 10^{th} percentile of the data corresponding to each risk parameter was mapped to a value of 1 and the 90^{th} percentile of each risk parameter's results was mapped to a value of 10. The internal intervals were set by assigning equal intervals to risk scores from 2 to 9, between the lowest and highest defined thresholds.

According to the following Figure 4.5, the rankings obtained from the two approaches are highly different for some counties. For example, Adams, Cavalier, Bottineau, Foster Dickey, and Eddy were ranked considerably higher (differing by more than 20 ranks) when expert opinion was incorporated than their ranking obtained from the traditional RPN. On the other hand, the rankings for Oliver, Renville, and Traill were significantly lower (differing by more than 20 ranks) compared to the rankings obtained from the traditional RPN. The considerable differences in the rankings from the two FMEA approaches show how important experts' opinions are to speeding crash risk assessment.

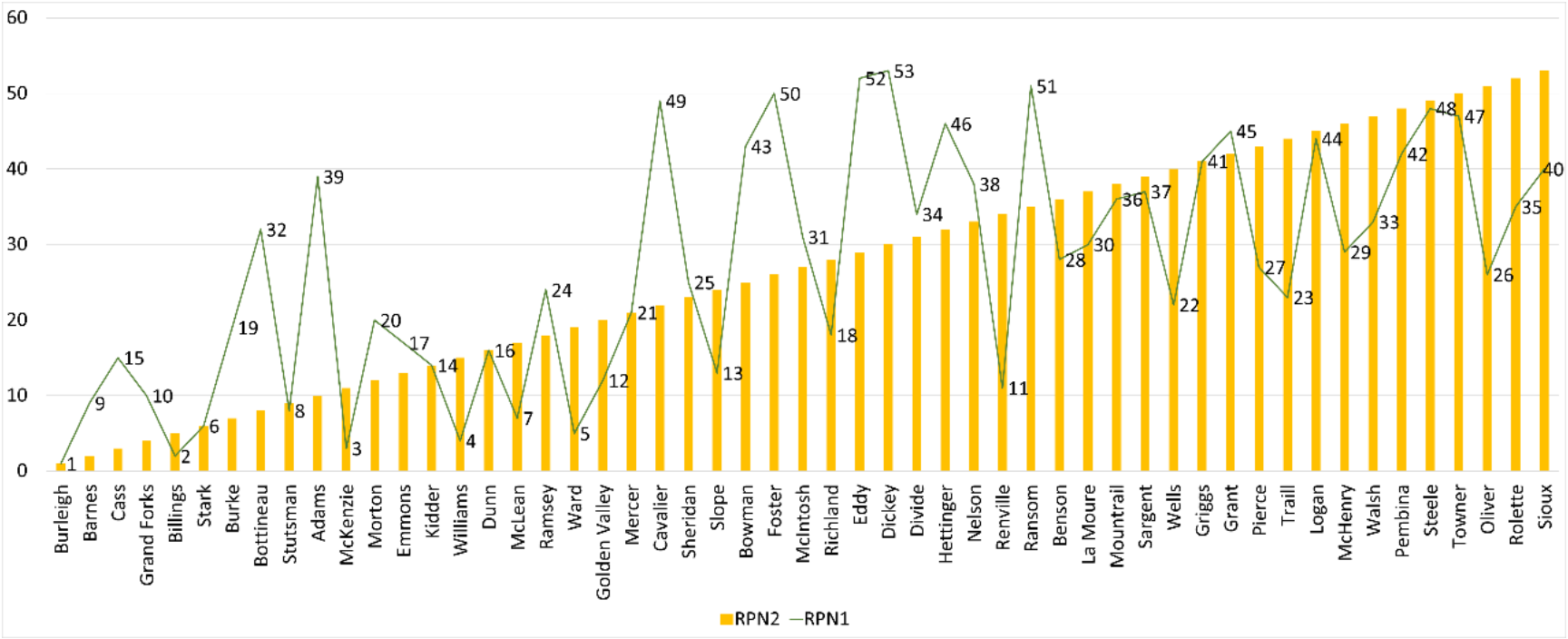

Figure 4.5. Comparing rankings evaluated with and without expert opinion

4.7. Conclusion

This study aimed to assess speeding crash risk among ND counties. A mix of empirical data (speeding crashes, injuries, and citation counts) and linguistic insights (experts' opinions of risk levels) were incorporated to evaluate the speeding crash risk. Using detectability as a risk factor is a novel approach to appraising speeding crash risk. Previous literature primarily used frequency and severity to measure crash risks while neglecting detectability. In addition, FMEA has been previously used to find the risk of failures in manufacturing or service companies, while the transportation sector has rarely applied this approach to evaluate failure risks. The evaluation of the speeding crash risk was conducted for a macroscopic scale of the region (county-level) with aggregate level data on speeding crashes.

Further, to establish the risk level for risk factors of occurrence, severity, and detectability, the Delphi method was used. This method evaluated the risk parameters based on local experts' perceptions of each risk factor. Finally, the findings could provide policymakers with an efficient and practical approach to differentiating between risky and safe regions regarding speeding behavior and speeding crashes. Several clusters of counties affected by various risks such as occurrence, severity, and detectability were identified. The declaration of the clusters can help provide the affected counties in each cluster the opportunity to collaborate regarding implementing more consistent safety policies.

This study provides road managers with helpful information to evaluate the speeding crash risk in ND counties and can inform them about their current speed management strategies' effectiveness in reducing speeding crash risk. In addition, the results can help road managers rebalance budget allocations to areas with a critical need for safety improvements. Having speeding crash risk broken down into three risk factors, safety practitioners can better identify the

origin of high speeding crash risk in a county. By doing so, they can address the areas that need development with appropriate safety improvement activities.

The findings in this study were subject to several limitations. First, there could be underreporting of the crashes in counties such as Sioux and Rollette that encompass Indian Nations. According to Iragavarapu et al. (2015), in tribal regions, crash data reporting and collection might not be accurate enough to capture all the traffic violations and crashes. Second, speeding-related crashes are identified by law enforcement officers who respond to a crash and complete a subsequent crash report where they must select one or more factors contributing to the crash. Since the crash reports can result from the discretionary decisions of different individuals completing the crash report, the data related to speeding-related crashes could be subject to misjudgments (Monsere et al., 2006).

Further studies that take into account potential contributing factors to speeding crashes and forecast occurrence, severity, and detectability of the crashes in high-risk counties are recommended. In addition, the performance of the proposed framework was not compared with other state of practice models and would be a worthy research direction. This study aimed to provide a decision-making approach to facilitate the process of evaluating crash risks at a strategic level. However, discovering the detailed reasons behind the high and low speeding crash risks across the counties is not within the scope and can be considered in upcoming studies. A future study may also use an optimization model to optimize the resource allocation of the safety improvement strategies (Chen et al., 2013).

REFERENCES

Aarts, L., & van Schagen, I. (2006). Driving speed and the risk of road crashes: A review. *Accident Analysis & Prevention*, *38*(2), 215–224. https://doi.org/10.1016/j.aap.2005.07.004

Abdulhafedh, A. (2016). Crash Frequency Analysis. *Journal of Transportation Technologies*, *06*(04), 169–180. https://doi.org/10.4236/jtts.2016.64017

Agusdinata, D. B., Zhao, F., Ileleji, K., & Delaurentis, D. (2011). Life Cycle Assessment of Potential Biojet Fuel Production in the United States. *Environ. Sci. Technol*, *45*(21), 9133–9143. https://doi.org/10.1021/es202148g

Ail, S. S., & Dasappa, S. (2016). Biomass to liquid transportation fuel via Fischer Tropsch synthesis – Technology review and current scenario. *Renewable and Sustainable Energy Reviews*, *58*, 267–286. https://doi.org/10.1016/J.RSER.2015.12.143

Al-Kaisy, A., Ewan, L., & Hossain, F. (2019). Identifying Candidate Locations for Safety Improvements on Low-Volume Rural Roads: The Oregon Experience. *Transportation Research Record: Journal of the Transportation Research Board*, *2673*(12), 690–698. https://doi.org/10.1177/0361198119853549

Alam, A., & Dwivedi, P. (2019). Modeling site suitability and production potential of carinata-based sustainable jet fuel in the southeastern United States. *Journal of Cleaner Production*, *239*, 117817. https://doi.org/10.1016/j.jclepro.2019.117817

Alkheder, S., Taamneh, M., & Taamneh, S. (2017). Severity Prediction of Traffic Accident Using an Artificial Neural Network. *Journal of Forecasting*, *36*(1), 100–108. https://doi.org/10.1002/for.2425

Alyami, H., Yang, Z., Riahi, R., Bonsall, S., & Wang, J. (2019). Advanced uncertainty modelling for container port risk analysis. *Accident Analysis and Prevention*, *123*, 411–421. https://doi.org/10.1016/j.aap.2016.08.007

Bacenetti, J., Restuccia, A., Schillaci, G., & Failla, S. (2017). Biodiesel production from unconventional oilseed crops (Linum usitatissimum L. and Camelina sativa L.) in Mediterranean conditions: Environmental sustainability assessment. *Renewable Energy*, *112*, 444–456. https://doi.org/10.1016/j.renene.2017.05.044

Behbahani, H., Amiri, A. M., Imaninasab, R., & Alizamir, M. (2018). Forecasting accident frequency of an urban road network: A comparison of four artificial neural network techniques. *Journal of Forecasting*, *37*(7), 767–780. https://doi.org/10.1002/for.2542

Blanco-Canqui, H., Ruis, S. J., Proctor, C. A., Creech, C. F., Drewnoski, M. E., & Redfearn, D. D. (2020). Harvesting cover crops for biofuel and livestock production: Another ecosystem service? *Agronomy Journal*, *112*(4), 2373–2400. https://doi.org/10.1002/agj2.20165

BTS. (2021). *Airline Fuel Cost and Consumption*. www.bts.gov

Castillo-Manzano, J. I., Castro-Nuño, M., López-Valpuesta, L., & Vassallo, F. V. (2019). The complex relationship between increases to speed limits and traffic fatalities: Evidence from a meta-analysis. In *Safety Science* (Vol. 111, pp. 287–297). Elsevier B.V. https://doi.org/10.1016/j.ssci.2018.08.030

Chen, H., Chen, F., & Anderson, C. (n.d.). *Developing an Intelligent Decision Support System for the Proactive Implementation of Traffic Safety Strategies Final Report*. Retrieved July 11, 2020, from http://www.its.umn.edu/Publications/ResearchReports/

Chu, P. L., Vanderghem, C., MacLean, H. L., & Saville, B. A. (2017). Financial analysis and risk assessment of hydroprocessed renewable jet fuel production from camelina, carinata and used cooking oil. *Applied Energy*, *198*, 401–409. https://doi.org/10.1016/j.apenergy.2016.12.001

Ciani, L., Guidi, G., & Patrizi, G. (2019). A Critical Comparison of Alternative Risk Priority Numbers in Failure Modes, Effects, and Criticality Analysis. *IEEE Access*, *7*, 92398–92409. https://doi.org/10.1109/ACCESS.2019.2928120

Čuček, L., Martín, M., Grossmann, I. E., & Kravanja, Z. (2014). Multi-period synthesis of optimally integrated biomass and bioenergy supply network. *Computers and Chemical Engineering*, *66*, 57–70. https://doi.org/10.1016/j.compchemeng.2014.02.020

Czernakowski, W., & Müller, M. (1993). Misuse mode and effects analysis—An approach to predict and quantify misuse of child restraint systems. *Accident Analysis & Prevention*, *25*(3), 323–333. https://doi.org/10.1016/0001-4575(93)90026-S

de Jong, S., Antonissen, K., Hoefnagels, R., Lonza, L., Wang, M., Faaij, A., & Junginger, M. (2017). Life-cycle analysis of greenhouse gas emissions from renewable jet fuel production. *Biotechnology for Biofuels*, *10*(1), 1–18. https://doi.org/10.1186/s13068-017-0739-7

de Jong, S., Hoefnagels, R., Faaij, A., Slade, R., Mawhood, R., & Junginger, M. (2015). The feasibility of short-term production strategies for renewable jet fuels - a comprehensive techno-economic comparison. *Biofuels, Bioproducts and Biorefining*, *9*(6), 778–800. https://doi.org/10.1002/bbb.1613

Delen, D., Sharda, R., & Bessonov, M. (2006). Identifying significant predictors of injury severity in traffic accidents using a series of artificial neural networks. *Accident Analysis and Prevention*, *38*(3), 434–444. https://doi.org/10.1016/j.aap.2005.06.024

Delen, D., Tomak, L., Topuz, K., & Eryarsoy, E. (2017). Investigating injury severity risk factors in automobile crashes with predictive analytics and sensitivity analysis methods. *Journal of Transport and Health*, *4*, 118–131. https://doi.org/10.1016/j.jth.2017.01.009

DeLonge, M., & Stillerman, K. (2020). Eroding the Future How Soil Loss Threatens Farming and Our Food Supply. *Union of Concerned Scientists*. https://www.jstor.org/stable/pdf/resrep28410.pdf

Diniz, A. P. M. M., Sargeant, R., & Millar, G. J. (2018). Stochastic techno-economic analysis of the production of aviation biofuel from oilseeds. *Biotechnology for Biofuels*, *11*(1), 1–15. https://doi.org/10.1186/s13068-018-1158-0

DOE. (2022). *Sustainable Aviation Fuel Grand Challenge.* https://www.energy.gov/eere/bioenergy/sustainable-aviation-fuel-grand-challenge

DOE. (2021). *Sustainable Aviation Fuels*. https://www.energy.gov/eere/bioenergy/sustainable-aviation-fuels

Duffy, M. (2012). Value of soil erosion to the land owner. *Agr Decision Maker*. *File A1-75 (August 2012). Iowa State University, Extension and Outreach.*

Ebrahimi, S., Haji Esmaeili, S. A., Sobhani, A., & Szmerekovsky, J. (2022). Renewable jet fuel supply chain network design: Application of direct monetary incentives. *Applied Energy*, *310*, 118569. https://doi.org/10.1016/j.apenergy.2022.118569

EIA. (2021). *US Jet Fuel Wholesale/Resale Price by Refiners*. www.eia.gov

FAA. (2021). *Sustainable Alternative Jet Fuels*. www.faa.gov

Fitzpatrick, C. D., Rakasi, S., & Knodler, M. A. (2017). An investigation of the speeding-related crash designation through crash narrative reviews sampled via logistic regression. *Accident Analysis & Prevention*, *98*, 57–63. https://doi.org/10.1016/j.aap.2016.09.017

Geedipally, S. R., Gates, T. J., Stapleton, S., Ingle, A., & Avelar, R. E. (2019). Examining the Safety Performance and Injury Severity Characteristics of Rural County Roadways. *Transportation Research Record*, *2673*(10), 405–415. https://doi.org/10.1177/0361198119850127

Geleynse, S., Brandt, K., Garcia-Perez, M., Wolcott, M., & Zhang, X. (2018). The Alcohol-to-Jet Conversion Pathway for Drop-In Biofuels: Techno-Economic Evaluation. *ChemSusChem*, *11*(21), 3728–3741. https://doi.org/10.1002/CSSC.201801690

Ghaderi, H., Pishvaee, M. S., & Moini, A. (2016). Biomass supply chain network design: An optimization-oriented review and analysis. *Industrial Crops and Products*, *94*, 972–1000. https://doi.org/10.1016/j.indcrop.2016.09.027

Giarola, S., Shah, N., & Bezzo, F. (2012). A comprehensive approach to the design of ethanol supply chains including carbon trading effects. *Bioresource Technology*, *107*, 175–185. https://doi.org/10.1016/j.biortech.2011.11.090

Gonela, V., Zhang, J., & Osmani, A. (2015). Stochastic optimization of sustainable industrial symbiosis based hybrid generation bioethanol supply chains. *Computers & Industrial Engineering*, *87*, 40–65. https://doi.org/10.1016/J.CIE.2015.04.025

Guo, C., Hu, H., Wang, S., Rodriguez, L. F., Ting, K. C., & Lin, T. (2022). Multiperiod stochastic programming for biomass supply chain design under spatiotemporal variability of feedstock supply. *Renewable Energy*, *186*, 378–393. https://doi.org/10.1016/j.renene.2021.12.144

Gutiérrez-Antonio, C., Gómez-Castro, F. I., de Lira-Flores, J. A., & Hernández, S. (2017). A review on the production processes of renewable jet fuel. *Renewable and Sustainable Energy Reviews*, *79*, 709–729. https://doi.org/10.1016/j.rser.2017.05.108

Gutiérrez-Antonio, Claudia, Israel Gómez-Castro, F., Segovia-Hernández, J. G., & Briones-Ramírez, A. (2013). Simulation and optimization of a biojet fuel production process. In *Computer Aided Chemical Engineering* (Vol. 32, pp. 13–18). Elsevier B.V. https://doi.org/10.1016/B978-0-444-63234-0.50003-8

Haji Esmaeili, S. A., Sobhani, A., Szmerekovsky, J., Dybing, A., & Pourhashem, G. (2020). First-generation vs. second-generation: A market incentives analysis for bioethanol supply chains with carbon policies. *Applied Energy*, *277*, 115606. https://doi.org/10.1016/j.apenergy.2020.115606

Haji Esmaeili, S. A., Szmerekovsky, J., Sobhani, A., Dybing, A., & Peterson, T. O. (2020). Sustainable biomass supply chain network design with biomass switching incentives for first-generation bioethanol producers. *Energy Policy*, *138*. https://doi.org/10.1016/j.enpol.2019.111222

Haydary, J. (2019). Chemical process design and simulation: Aspen Plus and Aspen HYSYS applications. *John Wiley & Sons*

Hendricks, A. M., Wagner, J. E., Volk, T. A., Newman, D. H., & Brown, T. R. (2016). A cost-effective evaluation of biomass district heating in rural communities. *Applied Energy*, *162*, 561–569. https://doi.org/10.1016/j.apenergy.2015.10.106

Huang, E., Zhang, X., Rodriguez, L., Khanna, M., de Jong, S., Ting, K. C. C., Ying, Y., & Lin, T. (2019). Multi-objective optimization for sustainable renewable jet fuel production: A case study of corn stover based supply chain system in Midwestern U.S. *Renewable and Sustainable Energy Reviews*, *115*, 109403. https://doi.org/10.1016/j.rser.2019.109403

Huang, H., Zeng, Q., Pei, X., Wong, S. C., & Xu, P. (2016). Predicting crash frequency using an optimised radial basis function neural network model. *Transportmetrica A: Transport Science*, *12*(4), 330–345. https://doi.org/10.1080/23249935.2015.1136008

Huang, J., You, J., Liu, H., & Song, M. (2020). Failure mode and e ff ect analysis improvement : A systematic literature review and future research agenda. *Reliability Engineering and System Safety*, *199*(February), 106885. https://doi.org/10.1016/j.ress.2020.106885

Iragavarapu, V., Carlson, P., & Schertz, G. (2015). Review of Tribal Transportation Safety. *Transportation Research Record: Journal of the Transportation Research Board*, *2531*(1), 153–160. https://doi.org/10.3141/2531-18

Islam, M., & Mannering, F. (2021). The role of gender and temporal instability in driver-injury severities in crashes caused by speeds too fast for conditions. *Accident Analysis & Prevention*, *153*, 106039. https://doi.org/10.1016/j.aap.2021.106039

Kargbo, H., Harris, J. S., & Phan, A. N. (2021). "Drop-in" fuel production from biomass: Critical review on techno-economic feasibility and sustainability. *Renewable and Sustainable Energy Reviews*, *135*(December 2019), 110168. https://doi.org/10.1016/j.rser.2020.110168

Kumar, S., Seepaul, R., Mulvaney, M. J., Colvin, B., George, S., Marois, J. J., Bennett, R., Leon, R., Wright, D. L., & Small, I. M. (2020). Brassica carinata genotypes demonstrate potential as a winter biofuel crop in South East United States. *Industrial Crops and Products*, *150*, 112353. https://doi.org/10.1016/j.indcrop.2020.112353

Leila, M., Whalen, J., & Bergthorson, J. (2018). Strategic spatial and temporal design of renewable diesel and biojet fuel supply chains: Case study of California, USA. *Energy*, *156*, 181–195. https://doi.org/10.1016/j.energy.2018.04.196

Li, X., Mupondwa, E., & Tabil, L. (2018). Technoeconomic analysis of biojet fuel production from camelina at commercial scale: Case of Canadian Prairies. *Bioresource Technology*, *249*, 196–205. https://doi.org/10.1016/j.biortech.2017.09.183

Liu, H.-C., Liu, L., & Liu, N. (2013). Risk evaluation approaches in failure mode and effects analysis: A literature review. *Expert Systems with Applications*, *40*(2), 828–838. https://doi.org/10.1016/J.ESWA.2012.08.010

Malladi, K. T., & Sowlati, T. (2018). Biomass logistics: A review of important features, optimization modeling and the new trends. *Renewable and Sustainable Energy Reviews*, *94*, 587–599. https://doi.org/10.1016/j.rser.2018.06.052

Mandal, S., & Maiti, J. (2014). Risk analysis using FMEA: Fuzzy similarity value and possibility theory based approach. *Expert Systems with Applications*, *41*(7), 3527–3537. https://doi.org/10.1016/j.eswa.2013.10.058

Martinkus, N., Latta, G., Rijkhoff, S. A. M., Mueller, D., Hoard, S., Sasatani, D., Pierobon, F., & Wolcott, M. (2019). A multi-criteria decision support tool for biorefinery siting: Using economic, environmental, and social metrics for a refined siting analysis. *Biomass and Bioenergy*, *128*, 105330. https://doi.org/10.1016/j.biombioe.2019.105330

Mohamed Abdul Ghani, N. M. A., Vogiatzis, C., & Szmerekovsky, J. (2018). Biomass feedstock supply chain network design with biomass conversion incentives. *Energy Policy*, *116*(April 2017), 39–49. https://doi.org/10.1016/j.enpol.2018.01.042

Mohammed, F., Selim, S. Z., Hassan, A., & Syed, M. N. (2017). Multi-period planning of closed-loop supply chain with carbon policies under uncertainty. *Transportation Research Part D: Transport and Environment*, *51*, 146–172. https://doi.org/10.1016/j.trd.2016.10.033

Monsere, C. M., Bertini, R. L., Bosa, P. G., Chi, D., Nolan, C., & El-Seoud, T. A. (2006). *Comparison of Identification and Ranking Methodologies for Speed-Related Crash Locations.* (No. FHWA-OR-RD-06-14). Oregon. Dept. of Transportation.

Mousavi-Avval, S. H., & Shah, A. (2021). Techno-economic analysis of hydroprocessed renewable jet fuel production from pennycress oilseed. *Renewable and Sustainable Energy Reviews*, *149*, 111340. https://doi.org/10.1016/J.RSER.2021.111340

NASS. (2021). *Cropland data*. https://www.nass.usda.gov

Natelson, R. H., Wang, W. C., Roberts, W. L., & Zering, K. D. (2015). Technoeconomic analysis of jet fuel production from hydrolysis, decarboxylation, and reforming of camelina oil. *Biomass and Bioenergy*, *75*, 23–34. https://doi.org/10.1016/j.biombioe.2015.02.001

National Safety Council, & ANSI. (2017). American National Standard: Manual on Classification of Motor Vehicle Traffic Crashes. *Association of Transpotation Safety Information Professionals*. https://www.transportation.gov/sites/dot.gov/files/docs/resources/government/traffic-records/304331/ansid16-2017.pdf

Nocera Alves Junior, P., Costa Melo, I., de Moraes Santos, R., da Rocha, F. V., & Caixeta-Filho, J. V. (2021). How did COVID-19 affect green-fuel supply chain? - A performance analysis of Brazilian ethanol sector. *Research in Transportation Economics*, 101137. https://doi.org/10.1016/J.RETREC.2021.101137

Noh, H. M., Benito, A., & Alonso, G. (2016). Study of the current incentive rules and mechanisms to promote biofuel use in the EU and their possible application to the civil aviation sector. *Transportation Research Part D: Transport and Environment*, *46*(2016), 298–316. https://doi.org/10.1016/j.trd.2016.04.007

Nóia Júnior, R. de S., Fraisse, C. W., Bashyal, M., Mulvaney, M. J., Seepaul, R., Zientarski Karrei, M. A., Iboyi, J. E., Perondi, D., Cerbaro, V. A., & Boote, K. J. (2022). Brassica carinata as an off-season crop in the southeastern USA: Determining optimum sowing dates based on climate risks and potential effects on summer crop yield. *Agricultural Systems*, *196*, 103344. https://doi.org/10.1016/J.AGSY.2021.103344

Okoli, C., & Pawlowski, S. D. (2004). The Delphi method as a research tool: An example, design considerations and applications. *Information and Management*, *42*(1), 15–29. https://doi.org/10.1016/j.im.2003.11.002

Osmani, A., & Zhang, J. (2013). Stochastic optimization of a multi-feedstock lignocellulosic-based bioethanol supply chain under multiple uncertainties. *Energy*, *59*, 157–172. https://doi.org/10.1016/j.energy.2013.07.043

Osmani, A., & Zhang, J. (2014). Economic and environmental optimization of a large scale sustainable dual feedstock lignocellulosic-based bioethanol supply chain in a stochastic environment. *Applied Energy*, *114*, 572–587. https://doi.org/10.1016/j.apenergy.2013.10.024

Park, Y. S. (2018). *THREE ESSAYS ON SUSTAINABILITY OF TRANSPORTATION AND SUPPLY CHAIN North Dakota State University* (Issue March). https://hdl.handle.net/10365/28948

Pearlson, M. N. (2007). *A Techno-Economic and Environmental Assessment of Hydroprocessed Renewable Distillate Fuels*. Massachusetts Institute of Technology. https://dspace.mit.edu/handle/1721.1/65508

Pearlson, M., Wollersheim, C., & Hileman, J. (2013). A techno-economic review of hydroprocessed renewable esters and fatty acids for jet fuel production. *Biofuels, Bioproducts and Biorefining*, *7*(1), 89–96. https://doi.org/10.1002/bbb.1378

Pereira, L. G., MacLean, H. L., & Saville, B. A. (2017). Financial analyses of potential biojet fuel production technologies. *Biofuels, Bioproducts and Biorefining*, *11*(4), 665–681. https://doi.org/10.1002/bbb.1775

Perkis, D. F., & Tyner, W. E. (2018). Developing a cellulosic aviation biofuel industry in Indiana: A market and logistics analysis. *Energy*, *142*, 793–802. https://doi.org/10.1016/j.energy.2017.10.022

Pham, V., Holtzapple, M., & El-Halwagi, M. (2010). Techno-economic analysis of biomass to fuel conversion via the MixAlco process. *Journal of Industrial Microbiology and Biotechnology*, *37*(11), 1157–1168. https://doi.org/10.1007/s10295-010-0763-0

Poiša, L., Adamovičs, A., & Stramkale, V. (2010). Bioethanol outcome from winter rye, triticale and wheat depending on n-fertilizer rate. *Research for Rural Development*, *1*, 28–34.

Qin, X., Wellner, A., Graduate, E., & Assistant, R. (2011). *DEVELOPMENT OF SAFETY SCREENING TOOL FOR HIGH RISK RURAL ROADS IN SOUTH DAKOTA*. Mountain Plains Consortium. https://rosap.ntl.bts.gov/view/dot/39149

Ryder, B., Gahr, B., Egolf, P., Dahlinger, A., & Wortmann, F. (2017). Preventing traffic accidents with in-vehicle decision support systems - The impact of accident hotspot warnings on driver behaviour. *Decision Support Systems*, *99*, 64–74. https://doi.org/10.1016/j.dss.2017.05.004

Sajid, Z. (2021). A dynamic risk assessment model to assess the impact of the coronavirus (COVID-19) on the sustainability of the biomass supply chain: A case study of a U.S. biofuel industry. *Renewable and Sustainable Energy Reviews*, *151*, 111574. https://doi.org/10.1016/J.RSER.2021.111574

Schmidt, J., Leduc, S., Dotzauer, E., & Schmid, E. (2011). Cost-effective policy instruments for greenhouse gas emission reduction and fossil fuel substitution through bioenergy production in Austria. *Energy Policy*, *39*(6), 3261–3280. https://doi.org/10.1016/j.enpol.2011.03.018

Searcy, E., Flynn, P., Ghafoori, E., & Kumar, A. (2007). The relative cost of biomass energy transport. *Applied Biochemistry and Biotechnology*, *137–140*(1–12), 639–652. https://doi.org/10.1007/s12010-007-9085-8

Seepaul, R, Small, I. M., Mulvaney, M. J., George, S., Leon, R. G., Geller, D., & Wright, D. L. (2019). Carinata , the Sustainable Crop for a Bio-based Economy : 2018 – 2019 Production Recommendations for the Southeastern United States. *University of Florida, IFAS Extension*, 1–12. https://edis.ifas.ufl.edu

Seepaul, Ramdeo, Kumar, S., Iboyi, J. E., Bashyal, M., Stansly, T. L., Bennett, R., Boote, K. J., Mulvaney, M. J., Small, I. M., George, S., & Wright, D. L. (2021). Brassica carinata: Biology and agronomy as a biofuel crop. *GCB Bioenergy*, *13*(4), 582–599. https://doi.org/10.1111/GCBB.12804

Shah, S. A. R., & Ahmad, N. (2020). Accident risk analysis based on motorway exposure: an application of benchmarking technique for human safety. *International Journal of Injury Control and Safety Promotion*, 1–11. https://doi.org/10.1080/17457300.2020.1774619

Shah, S., Ahmad, N., Shen, Y., Pirdavani, A., Basheer, M., & Brijs, T. (2018). Road Safety Risk Assessment: An Analysis of Transport Policy and Management for Low-, Middle-, and High-Income Asian Countries. *Sustainability*, *10*(2), 389. https://doi.org/10.3390/su10020389

Shen, Y., Hermans, E., Brijs, T., Wets, G., & Vanhoof, K. (2012). Road safety risk evaluation and target setting using data envelopment analysis and its extensions. *Accident Analysis & Prevention*, *48*, 430–441. https://doi.org/10.1016/j.aap.2012.02.020

Sokhansanj, S., Mani, S., Turhollow, S., Kumar, A., Bransby, D., Lynd, L., & Laser, M. (2009). Large-scale production, harvest and logistics of switchgrass (Panicum virgatum L.) - Current technology and envisioning a mature technology. In *Biofuels, Bioproducts and Biorefining* (Vol. 3, Issue 2, pp. 124–141). https://doi.org/10.1002/bbb.129

Stelle, P., & Pearce, B. (2011). Powering the future of flight: The six easy steps to growing a viable aviation biofuels industry. *Geneva: Air Transport Action Group, March*, 1–20.

Tangtinthai, N., Heidrich, O., & Manning, D. A. C. (2019). Role of policy in managing mined resources for construction in Europe and emerging economies. *Journal of Environmental Management*, *236*, 613–621. https://doi.org/10.1016/j.jenvman.2018.11.141

Tao, L., Milbrandt, A., Zhang, Y., & Wang, W. C. (2017). Techno-economic and resource analysis of hydroprocessed renewable jet fuel. *Biotechnology for Biofuels*, *10*(1), 1–16. https://doi.org/10.1186/s13068-017-0945-3

U.S. Department of Energy. (2011). U.S. Billion-Ton Update: Biomass supply for a bioenergy and bioproducts industry | Department of Energy. *Oak Ridge National Laboratory*.

USDA's National Agricultural Statistics Service. (2021). *Cattle inventory*. https://www.nass.usda.gov

Walther, G., Schatka, A., & Spengler, T. S. (2012). Design of regional production networks for second generation synthetic bio-fuel - A case study in Northern Germany. *European Journal of Operational Research*, *218*(1), 280–292. https://doi.org/10.1016/j.ejor.2011.09.050

Waltho, C., Elhedhli, S., & Gzara, F. (2019). Green supply chain network design: A review focused on policy adoption and emission quantification. *International Journal of Production Economics*, *208*, 305–318. https://doi.org/10.1016/j.ijpe.2018.12.003

Wan, C., Yan, X., Zhang, D., Qu, Z., & Yang, Z. (2019). An advanced fuzzy Bayesian-based FMEA approach for assessing maritime supply chain risks. *Transportation Research Part E: Logistics and Transportation Review*, *125*, 222–240. https://doi.org/10.1016/j.tre.2019.03.011

Wang, W.-C., Tao, L., Markham, J., Zhang, Y., Tan, E., Batan, L., Warner, E., & Biddy, M. (2016). *Review of Biojet Fuel Conversion Technologies*. www.nrel.gov/publications.

Wang, W. C. (2016). Techno-economic analysis of a bio-refinery process for producing Hydro-processed Renewable Jet fuel from Jatropha. *Renewable Energy*, *95*, 63–73. https://doi.org/10.1016/j.renene.2016.03.107

Wei, H., Liu, W., Chen, X., Yang, Q., Li, J., & Chen, H. (2019). Renewable bio-jet fuel production for aviation: A review. In *Fuel* (Vol. 254, p. 115599). Elsevier Ltd. https://doi.org/10.1016/j.fuel.2019.06.007

Wise, M., Muratori, M., & Kyle, P. (2017). Biojet fuels and emissions mitigation in aviation: An integrated assessment modeling analysis. *Transportation Research Part D: Transport and Environment*, *52*, 244–253. https://doi.org/10.1016/j.trd.2017.03.006

Witcover, J., & Williams, R. B. (2020). Comparison of "Advanced" biofuel cost estimates: Trends during rollout of low carbon fuel policies. *Transportation Research Part D: Transport and Environment*, *79*, 102211. https://doi.org/10.1016/j.trd.2019.102211

Xie, Y., Lord, D., & Zhang, Y. (2007). Predicting motor vehicle collisions using Bayesian neural network models: An empirical analysis. *Accident Analysis and Prevention*, *39*(5), 922–933. https://doi.org/10.1016/j.aap.2006.12.014

Xu, Z., Dang, Y., Munro, P., & Wang, Y. (2020). A data-driven approach for constructing the component-failure mode matrix for FMEA. *Journal of Intelligent Manufacturing*, *31*(1), 249–265. https://doi.org/10.1007/s10845-019-01466-z

You, F., & Wang, B. (2011). Life cycle optimization of biomass-to-liquid supply chains with distributedàcentralized processing networks. *Ind. Eng. Chem. Res*, *50*, 10102–10127. https://doi.org/10.1021/ie200850t

Zemanek, D., Champagne, P., & Mabee, W. (2020). Review of life-cycle greenhouse-gas emissions assessments of hydroprocessed renewable fuel (HEFA) from oilseeds. *Biofuels, Bioproducts and Biorefining*, 935–949. https://doi.org/10.1002/bbb.2125

Zetterholm, J., Pettersson, K., Leduc, S., Mesfun, S., Lundgren, J., & Wetterlund, E. (2018). Resource efficiency or economy of scale: Biorefinery supply chain configurations for co-gasification of black liquor and pyrolysis liquids. *Applied Energy*, *230*, 912–924. https://doi.org/10.1016/J.APENERGY.2018.09.018

Zhang, F., Johnson, D. M., & Wang, J. (2015). Life-Cycle Energy and GHG Emissions of Forest Biomass Harvest and Transport for Biofuel Production in Michigan. *Energies 2015, Vol. 8, Pages 3258-3271*, *8*(4), 3258–3271. https://doi.org/10.3390/EN8043258

Zhang, J., Osmani, A., Awudu, I., & Gonela, V. (2013). An integrated optimization model for switchgrass-based bioethanol supply chain. *Applied Energy*, *102*, 1205–1217. https://doi.org/10.1016/j.apenergy.2012.06.054

Zheng, T., Wang, B., Rajaeifar, M. A., Heidrich, O., Zheng, J., Liang, Y., & Zhang, H. (2020). How government policies can make waste cooking oil-to-biodiesel supply chains more efficient and sustainable. *Journal of Cleaner Production*, *263*, 121494. https://doi.org/10.1016/j.jclepro.2020.121494

Zhou, X., Zhang, H., Xin, S., Yan, Y., Long, Y., Yuan, M., & Liang, Y. (2020). Future scenario of China's downstream oil supply chain: Low carbon-oriented optimization for the design of planned multi-product pipelines. *Journal of Cleaner Production*, *244*. https://doi.org/10.1016/j.jclepro.2019.118866

APPENDIX A. SUPPLEMENTAL INFORMATION FOR CHAPTER 2

Table A1. Values of input parameters for the carinata-based RJF supply chain model in Chapter 2

Parameter & Value	Description	Reference
π=1.73	RJF selling price ($/gallon)	(EIA, 2021)
φ=281.23	Carinata coproduct selling price (protein meal) ($/ton)	(Chu et al., 2017)
ψ^{LPG}=0.66	Carinata coproduct selling price (LPG) ($/gallon)	(EIA, 2021)
$\psi^{Naphtha}$=1.37	Carinata coproduct selling price (naphtha) ($/gallon)	(E. Huang et al., 2019)
ψ^{RDF}=1.90	Carinata coproduct selling price (RDF) ($/gallon)	(EIA, 2021)
α=317.52	Selling price of carinata ($/ton)	(Chu et al., 2017)
ρ =29.59	Operational cost to convert carinata oil to renewable fuel products ($/ton)	(Diniz et al., 2018)
γ^c=6.3	Transportation fixed cost of carinata/meal ($/ton)	(Čuček et al., 2014)
η^c=0.113	Transportation variable cost of carinata/meal ($/ton-mile)	(Čuček et al., 2014)
γ^j=0.0124	Transportation fixed cost of liquid fuels ($/gallon)	(Čuček et al., 2014)
η^j=0.00024	Transportation variable cost of liquid fuels ($/gallon-km)	(Čuček et al., 2014)
θ=77.75	RJF conversion rate from carinata (gallons/ton)	(EIA, 2021)
∂^{LPG}=11.44	LPG conversion rate from carinata (gallons/ton)	(EIA, 2021)
$\partial^{Naphtha}$=20.99	Naphtha conversion rate from carinata (gallons/ton)	(E. Huang et al., 2019)
∂^{RDF}=19.11	RDF conversion rate from carinata (gallons/ton)	(EIA, 2021)
σ=0.560	Carinata meal coproduct conversion rate from carinata (ton/ton)	(Chu et al., 2017)
D_e	Demand for RJF at demand zone e (gallons/year)	(BTS, 2021)
D_g^r	Demand for fuel byproduct *r* at demand zone *g* (gallons/year)	Assumed
D_v^m	Demand for carinata meal at demand zone *v* (tons/year)	(NASS, 2021)
d_{ik}	Distance from supplier *i* to biorefinery k (miles)	From GIS
d_{ke}	Distance from biorefinery *k* to demand zone *e* (miles)	From GIS
d_{kg}	Distance from biorefinery *k* to demand zone *g* (miles)	From GIS
d_{kv}	Distance from biorefinery *k* to demand zone *v* (miles)	From GIS
λ	RJF production credit under RPCP ($/gallon)	Variable
β	Discount rate on selling price of carinata under BCAP incentive (%)	Variable
ϕ	Rate of biorefinery cost reduction under BAP (%)	Variable
w=88,000	Annual payment to each work force ($)	(M. Pearlson et al., 2013)
ξ=0.072	Aggregate rate of utility cost (overhead, maintenance, insurance, and taxes)	(Diniz et al., 2018)

Table A2. Available carinata at each ASD in Chapter 2 (NASS, 2021)

ASDs	Carinata seed (Thousand tons)	ASDs	Carinata seed (Thousand tons)
Alabama		Georgia	
0110	555.66	1310	58.33
0120	278.00	1320	13.02
0130	114.14	1330	22.83
0140	205.66	1340	91.85
0150	283.27	1350	327.99
0160	470.54	1360	529.72
Florida		1370	1,304.19
1210	439.28	1380	1,342.45
1230	164.87	1390	321.73
1250	119.84	Total	2,686.85
1280	55.60		

Table A3. Demand for carinata meal at ASDs (NASS, 2021)

States	ASDs	Demand share (%)
Alabama	0110	4.70%
	0120	7.73%
	0130	4.54%
	0140	6.26%
	0150	3.09%
	0160	5.31%
Florida	1210	3.40%
	1230	4.26%
	1250	14.04%
	1280	19.66%
Georgia	1310	2.88%
	1320	2.89%
	1330	4.15%
	1340	2.85%
	1350	3.40%
	1360	2.40%
	1370	3.80%
	1380	3.11%
	1390	1.53%

APPENDIX B. SUPPLEMENTAL INFORMATION FOR CHAPTER 3

Table B1. Values of input parameters for RJF supply chain with corn stover feedstock

Parameter & Value	Description	Reference
$\omega_{naphtha}$ = 0.36	Selling price of naphtha (*$/liter*)	(Ebrahimi et al., 2022)
ω_{RDF} = 0.50	Selling price of RDF (*$/liter*)	(Ebrahimi et al., 2022)
π =0.51	Selling price of RJF (*$/liter*)	(E. Huang et al., 2019)
α_c = 49.61	Selling price of corn stover (*$/tonne*)	(Haji Esmaeili, Sobhani, et al., 2020)
ρ =0.59	Production cost of RJF at biorefinery (*$/liter*)	(Pereira et al., 2017)
θ= 144.38	RJF conversion rate from corn stover (*liter/tonne*)	(Pereira et al., 2017)
$\sigma^{naphtha}$ = 72.25	Fuel coproduct *j* (naphtha) conversion rate from corn stover (*liter/tonne*)	(Pereira et al., 2017)
σ^{RDF} = 72.25	Fuel coproduct *j* (RDF) conversion rate from corn stover (*liter/tonne*)	(Pereira et al., 2017)
γ^b= 6.615	Transportation fixed cost of corn stover via truck (*$/tonne*)	(Sokhansanj et al., 2009)
η^b = 0.0548	Transportation variable cost of corn stover via truck (*$/tonne-km*)	(Sokhansanj et al., 2009)
γ^m= 0.0031	Transportation fixed cost of RJF via truck (*$/liter*)	(Searcy et al., 2007)
η^m = 0.000394	Transportation variable cost of RJF via truck (*$/liter-km*)	(Searcy et al., 2007)
e_c = 0.0756	Emission factor of transporting corn stover (*kg CO2/tonne-km*)	(You & Wang, 2011)
e_j^{truck} = 0.00009235	Emission factor of transporting RJF (*kg CO2/liter-km*)	(F. Zhang et al., 2015)
$e_c^{acquisition}$ = 0.0001654	Emission factor of corn stover acquisition (*kg CO2/tonne*)	(You & Wang, 2011)
$e_F^{production}$ = - 0.343	Emission factor of producing RJF through FT pathway from corn stover (*kg CO2/liter*)	(E. Huang et al., 2019)
f= 45.51	Annual fixed cost of biorefinery (*M $*)	(E. Huang et al., 2019)
ρ =0.59	Production cost of RJF at biorefinery *($/liter*)	(Pereira et al., 2017)

Table B2. Optimal assignment of supply zones and demand nodes to activated biorefineries

Supplier district (share of supply assignment)	Activated biorefinery and its capacity	Demand node (share of demand fulfillment)
S[5]1940 (34.82%), S1950 (38.53%), S1960 (26.65%).	B[6]1710	ORD (100%).
S1710 (34.07%), S1720 (16.16%), S1810 (17.09%), S1930 (5.30%), S1980 (10.40%), S1990 (16.98%).	B1720	MDW (1.11%), ORD (98.89).
S1730 (19.75%), S1740 (29.67%), S1750 (28.36%), S1760 (21.18%), S1810 (1.04%).	B1750	MDW (71.53%), DTW (28.47%).
S1770 (26.67%), S1820 (10.88%), S1840 (12.69%), S1850 (18.06%), S1860 (7.59%), S1870 (12.28%), S1880 (3.09%), S1890 (2.45%), S3790 (5.98%).	B1850	CVG (40.60%), DTW (17.63%), IND (41.77%).
S1820 (3.03%), S1830 (8.21%), S2610 (0.38%), S2620 (1.10%), S2630 (0.83%), S2640 (1.78%), S2650 (5.34%), S2660 (8.19%), S2670 (7.53%), S2680 (12.20%), S2690 (3.76%), S3910 (6.09%), S3920 (7.08%), S3930 (4.12%), S3940 (11.77%), S3950 (13.56%), S3960 (1.67%), S3980 (2.03%), S3990 (1.32%).	B2690	DTW (100%).
S2740 (31.79%), S2750 (29.97%), S2760 (3.18%), S2770 (25.42%) S4630 (3.06%), S5510 (6.58%).	B2750	MSP (100%).
S1920 (40.24%), S2780 (34.29%), S2790 (23.51%), S5540 (1.96%).	B2790	MSP (48.12%), ORD (51.88%).
S1970 (30.36%), S2070 (20.13%), S2080 (8.74%), S2910 (21.21%), S3190 (19.56%).	B2910	OMA (31.73), KCI (68.27%).
S1760 (10.14%), S1780 (12.06%), S1790 (12.14%), S2080 (0.92%), S2920 (9.76%), S2930 (15.18%), S2940 (10.23%), S2950 (11.37%), S2960 (4.62%), S2970 (3.82%), S2980 (0.56%), S2990 (9.21%).	B2960	STL (100%).
S1930 (27.65%), S5520 (6.59%), S5530 (3.97%), S5540 (11.67%), S5550 (8.04%), S5560 (10.36%), S5570 (11.36%), S5580 (16.32%), S5590 (4.06%).	B5590	MKE (30.70%), ORD (69.30%).

[5] The letter "S" in the beginning of the biorefinery node indicates that the supply node is located at ASD 1940.
[6] The letter "B" in the beginning of the biorefinery node indicates that the biorefinery node is located at ASD 1720.

APPENDIX C. SUPPLEMENTAL INFORMATION FOR CHAPTER 4: DELPHI SURVEY ROUND 1

The following is the first round of survey questionnaire distributed to experts.

SPEEDING CRASH RISK FACTORS, EXPERT SURVEY

To Survey Participants:

Please provide your estimation and comments on these metrics based on your experience. Results from our study are provided as context for your response. The extreme limits for each risk factor may be higher or lower than the actual (observed) ND county results that are shared in Tables 1, 2, and 3. Your responses are encouraged even if you are uncertain about values, since you will be able to revise your responses in knowing the 'average response' in a next survey round to move toward consensus.

Introduction

In a study to assess risk of speeding crashes in ND counties, we collected data related to risk factors, including occurrence, severity, and detectability of speeding crashes. Results associated with county-level risk factors are presented in summary tables accompanying each of the following sections (Summary Table 1, Summary Table 2, and Summary Table 3). To have a local assessment of crash risks and prioritize them, we need to know experts' opinions about each risk factor's different severity levels. Reaching consensus on the levels from this survey, we will categorize the level of risk for each risk factor more effectively.

1. Occurrence risk of speeding crashes

Occurrence risk of speeding crashes is defined as how likely speeding crashes are to occur in each county. Actual values from our study for speeding crash occurrence risks, including the 10^{th}, 50^{th}, and 90^{th} percentile for the risk in ND counties, are presented in Summary Table 1. (A percentile is a value below which a given percentage of values in a data set fall)

Summary Table 1. Speeding crashes occurrence, 10^{th}, 50^{th}, and 90^{th} percentile for the observed values

Actual occurrence risk percentiles observed for ND counties	Observed frequency of speeding crashes per 100M VMT
90^{th} percentile for the occurrence risk observed	62*
50^{th} percentile for the occurrence risk observed	14
10^{th} percentile for the occurrence risk observed	7

*90 percent of the speeding crash risk observations in ND counties experienced less than or equal to 62 crashes per 100M VMT.

Based on your experience and the results provided to you, please share your opinions and estimations on different levels of speeding crash occurrence.

Expert table 1. Experts' opinions on the risk level of speeding crash occurrence

Risk of speeding crash occurrence range value (probability of occurrence)		Frequency of speeding crashes per 100M VMT
1.a.	Highest occurrence risk estimate	
1.b.	Lowest occurrence risk estimate	

2. Severity risk of speeding crashes

Severity risk of speeding crashes among counties illustrates event consequences. Severity is evaluated based on proxy financial costs for speeding crashes in injury outcomes of "death", "disabling injury", "evident injury", "possible injury", and "no-injury observed". The severity of speeding crashes is presented by incurred costs illustrated by costs per speeding crash. We obtained the results using the cost estimations for the various injury intensities provided in Complementary data Table 2. Actual values in our study's results for speeding crash severity risks, including 10^{th}, 50^{th}, and 90^{th} percentile for the risks in ND counties, are presented in Summary Table 2.

Complimentary Table 2. Average comprehensive cost of injuries with respect to their intensity[1]

Injury intensity	Cost
Death	$10,855,000
Disabling	$1,187,000
Evident	$327,000
Possible injury	$151,000
No injury observed	$50,000

[1]National Safety Council & ANSI (2017)

Summary Table 2. Speeding crashes severity, 10^{th}, 50^{th}, and 90^{th} percentile for the observed values

Actual severity risk percentiles observed for ND Counties	Cost per crash ($)
90^{th} percentile for the severity risk observed	$616,000
50^{th} percentile for the severity risk observed	$180,000
10^{th} percentile for the severity risk observed	$92,000

Based on your experience and the results provided, please share your opinions and estimations of severity values.

Expert Table 2. Experts' opinions on the level of risk of speeding crash severity

Severity risk of speeding crashes		Cost per crash ($)
2.a.	Highest severity risk estimate	
2.b.	Lowest severity risk estimate	

3. Detectability Risk of Speeding Crashes

This factor shows law enforcement activity related to speeding and crashes before the crash event. The value is defined by dividing the number of speeding tickets cited at crash scenes by the total number of speeding citations either from speeding crashes or only speeding behavior. Therefore, the higher values mean that the higher percentage of citations have been related to speeding crashes. In comparison, lower values imply having more speeding tickets cited for speeding behavior, not including crashes, which means higher detectability of the risk (less detectability risk). The tenth, 50^{th}, and 90^{th} percentiles of observed values for speeding crash detectability risk in ND counties are presented in Summary Table 3.

Summary Table 3. Detectability of speeding crashes, 10^{th}, 50^{th}, and 90^{th} percentile for the observed values

Actual detectability risk percentiles observed for ND Counties	$\frac{Speeding\ citations\ at\ the\ crash\ scene}{Total\ number\ of\ speeding\ citations}\%$
90^{th} percentile for the detectability risk observed	16 %
50^{th} percentile for the detectability risk observed	6 %
10^{th} percentile for the detectability risk observed	2 %

Please share your opinions and estimations of detectability risk values associated with the scoring values.

Table 3. Experts' opinions on the level of risk of speeding crash detectability

Detectability risk of speeding crashes		$\frac{Speeding\ citations\ at\ the\ crash\ scene}{Total\ number\ of\ speeding\ citations}\%$
3.a.	Highest detectability risk estimate**	
3.b.	Lowest detectability risk estimate*	

**Every speeding behavior will certainly be detected by law enforcement.

*Very remote chance that the speeding behavior will be detected by law enforcement.

APPENDIX D. SUPPLEMENTAL INFORMATION FOR CHAPTER 4: DELPHI SURVEY-ROUND 2

The following is the second round of survey questionnaire distributed to experts.

SPEEDING CRASH RISK FACTORS, EXPERT SURVEY (Second round)

To Survey Participants in Round Two:

Results from our study and Round One are provided as context for your response. The extreme limits for each risk factor may be higher or lower than the actual ND county results that are shared in Tables 1, 2, and 3. Your responses are encouraged even if you are uncertain about values.

Introduction

In a study to assess risk of speeding crashes in ND counties, we collected data related to risk factors including occurrence, severity, and detectability of speeding crashes. Results associated with county-level risk factors are presented in summary tables accompanying each of the following sections (Summary Table 1, Summary Table 2, and Summary Table 3). To have a local assessment of crash risks and prioritize them, we need to know experts' opinions about the different severity levels of each risk factor. Reaching consensuson the levels from this survey, we will be able to categorize the level of risk for each risk factor more practically.

1. Occurrence Risk of Speeding crashes

Occurrence risk of speeding crashes is defined as how likely speeding crashes are to occur in each county. Actual values from our study for speeding crash occurrence risks, including the 10^{th}, 50^{th}, and 90^{th} percentile for the risk in ND counties, are presented in Summary Table 1. (A percentile is a value below which a given percentage of values in a data set fall)

Summary Table 1. Speeding crashes occurrence, 10^{th}, 50^{th}, and 90^{th} percentile for the observed values

Actual occurrence risk percentiles observed for ND counties	Observed frequency of speeding crashes per 100M VMT
90^{th} percentile for the occurrence risk observed	62*
50^{th} percentile for the occurrence risk observed	14
10^{th} percentile for the occurrence risk observed	7

*90 percent of the speeding crash risk observations in ND counties experienced less than or equal to 62 crashes per 100M VMT.

Based on your experience and the results provided to you, please share your opinions andestimations on different levels of speeding crash occurrence.

Response 1. Experts' opinions on level of risk of speeding crash occurrence

Risk of speeding crash occurrence range value (probability of occurrence)		Average from the first-round survey	Frequency of speeding crashes per 100M VMT
1.a.	Highest occurrence risk level		
1.b.	Lowest occurrence risk level		

2.Severity Risk of Speeding Crashes

Severity risk of speeding crashes among counties illustrates event consequences. Severity is evaluated based on proxy financial costs for speeding crashes in injury outcomes of "death", "disabling injury", "evident injury", "possible injury", and "no-injury observed". The severity of speeding crashes is presented by incurred costs illustrated by costs per speeding crash. We obtained the results using the cost estimations for the various injury intensities provided in Summary Table 2. Actual values in our study's results for speeding crash severity risks, including 10^{th}, 50^{th}, and 90^{th} percentile for the risks in ND counties, are presented in Summary Table 2.

Complimentary Table 2. Average comprehensive cost of injuries with respect to their intensity[1]

Injury intensity	Cost
Death	$10,855,000
Disabling	$1,187,000
Evident	$327,000
Possible injury	$151,000
No injury observed	$50,000

[1]National Safety Council & ANSI (2017)

Summary Table 2. Speeding crashes severity, 10^{th}, 50^{th}, and 90^{th} percentile for the observed values

Actual severity risk percentiles observed for ND Counties	Cost per crash ($)
90^{th} percentile for the severity risk observed	$616,000
50^{th} percentile for the severity risk observed	$180,000
10^{th} percentile for the severity risk observed	$92,000

Based on your experience and the results provided to you, please share your opinions andestimations of severity values.

Expert Table 2. Experts' opinions on level of risk of speeding crashes severity

	Severity risk of speeding crashes	Average from the first-round survey	Cost per 100M VMT
2.a.	Highest severity risk level		
2.b.	Lowest severity risk level		

3. Detectability Risk of Speeding Crashes

This factor shows law enforcement activity related to speeding and crashes before the crash event. The value is defined by dividing the number of speeding tickets cited at crash scenes by the total number of speeding citations either from speeding crashes or only speeding behavior. Therefore, the higher values mean that the higher percentage of citations have been related to speeding crashes. In comparison, lower values imply having more speeding tickets cited for speeding behavior, not including crashes, which means higher detectability of the risk (less detectability risk). The tenth, 50^{th}, and 90^{th} percentiles of observed values for speeding crash detectability risk in ND counties are presented in Summary Table 3.

Summary Table 3. Detectability of speeding crashes, 10^{th}, 50^{th}, and 90^{th} percentile for the observed values

Actual detectability risk percentiles observed for ND Counties	$\frac{Speeding\ citations\ at\ the\ crash\ scene}{Total\ number\ of\ speeding\ citations}\%$
90^{th} percentile for the detectability risk observed	16 %
50^{th} percentile for the detectability risk observed	6 %
10^{th} percentile for the detectability risk observed	2 %

Please share your opinions and estimations of detectability risk values associated with the scoring values.

Table 3. Experts' opinions on level of risk of speeding crash detectability

	Detectability risk of speeding crashes	Average from the first-round survey	$\frac{Speeding\ citations\ at\ the\ crash\ scene}{Total\ number\ of\ speeding\ citations}\%$
3.a.	Highest detectability risk level *		
3.b.	Lowest detectability risk level **		

* Very remote chance that the speeding behavior will be detected by law enforcement.

** Every speeding behavior will certainly be detected by law enforcement.